Dynamics of formation flying

Jordi Fontdecaba I Baig

Observatoire de Paris
Ecole Doctorale Astronomie et Astrophyisique d'Île de France

PhD THESIS in
ASTRONOMY and ASTROPHYSICS

Dynamics of formation flying

Applications to Earth and Universe observation

Jordi Fontdecaba i Baig

Defended at Observatoire de la Côte d'Azur on October, 24, 2008 in front of the committee :

Pr. Gerard Gómez	Universitat de Barcelona	Reviewer
Pr. Edwin Wnuk	Adam Mickiewicz University	Reviewer
Dr. Nicole Capitaine	Observatoire de Paris	Committee member
Pr. Benedicte Escudier	Institut Supérieur de l'Aéronautique et de l'Espace	Committee member
Pr. Jesús Pelaéz	Universidad Politécnica de Madrid	Committee member
Dr. Pierre Exertier	Observatoire de la Côte d'Azur	PhD advisor

Abstract

Relative motion is a key technology for future missions using formation flying. In my thesis, I have developed three different methods to study it, as function of its representation.
Cartesian coordinates have been the main tool to study the relative motions, even if they present some drawbacks in terms of equations linearisation and introduction of perturbations. These limitations can be overcome using differential orbital elements. A third representation of the relative motion is the local orbital elements. They are very interesting to study relative trajectories.
The use of differential orbital elements enable the introduction of the main perturbations. For low orbits, the dominant perturbation is the gravity field, and in particular, the oblateness of the Earth. For very high orbits, solar radiation pressure plays a main role when satellites do not have the same ratio surface to mass.
The study of relative motion is concluded with the analysis of two missions. First, I have analyzed the interest of formation flying for gravity field determination. In order to do so, I have obtained the sensitivity equations of intersatelllite measurements to geophysical parameters. Second, I have worked on the characteristics of high eccentric orbits (HEO) for formation flying. I have analyzed different aspects of Simbol-X mission.

Résumé

Le mouvement relatif est un élément clé pour le développement des futures missions spatiales qui utiliseront les vols en formation. Dans cet ouvrage je développe trois méthodes différentes pour son étude, utilisant différentes représentations.
Les coordonnées cartésiennes ont été pendant de nombreuses années l'outil principal pour étudier le mouvement relatif, même si elles présentent des limitations en terme de linéarisation des équations ou des perturbations. Ces limitations peuvent être dépassées grace à l'utilisation d'une représentation alternative: les différences d'éléments orbitaux.
Une troisième représentation qui s'avère très intéressante pour l'étude des trajectoires utilise les éléments orbitaux locaux.
L'utilisation des différences d'éléments orbitaux nous a permis d'étudier l'influence des perturbations les plus importantes. Pour les orbites basses, la perturbation dominante est le champ de gravité, et en particularier le second harmonique zonal lié l'aplatissement de la Terre. Pour les orbites très hautes, la pression de radiation solaire joue un rle dominant quand les satellites ne présentent pas le même rapport surface sur masse.
J'ai développé des études concretes du mouvement relatif pour deux missions particulières. D'abord je me suis intéressé à l'intérêt des vols en formation pour l'étude du champ de gravité. Pour cela, j'ai obtenu les équations de sensibilité des mesures intersatellitaires aux paramètres géophysiques. Je me suis également intéressé aux difficultés liées aux orbites très excentriques (HEO) pour les vols en formation en étudiant une mission du type SIMBOL-X.

Contents

Chapter 1

Introduction

1.1 History of relative motion and formation flying

The epicyclus of Apollonius of Perga Even if it seems to be a paradox, first pre-Keplerian attempts on astronomy were not far from the right description of the relative motion. Apollonius of Perga (262 BC - 190 BC) introduced the concepts of deferent and epicycle that were used by Claudius Ptolemaeus (83-161 AD) later on to describe the motion of the planets around the Earth. Ptolemaeus is well-known as one of the greatest astronomers of the Antiquity because of his book 'Almagest'. In the 'Almagest' he describes the geocentric theory for the motion of the planets.
Geocentric theory describes the motion of the planets around the Earth as a perfect circle (deferent) perturbed by smaller circles described at the same orbital frequency around the deferent (epicycle). As we will see, this kind of motion matches well with the classical description of the relative motion, the Hill equations. Geocentric theory had to add a huge number of epicycles in order to match with the improving quality of astronomical observations. It was finally abandoned for Copernicus model during 16th century.

The Hill's Moon theory George William Hill (1838-1914) is one of the greatest American mathematicians of 19th century. Since the beginning of his studies, he was especially interested in the work of Lacroix, Lagrange, Laplace and Legendre. His work treated basically on astronomical mathematics. In 1878 he published *Researches in Lunar Theory* in American Journal of Mathematics. This publication contains important new ideas on the three-body problem. In particular, he presented the so famous 'Hill equations' for the relative motion.
He spent the biggest part of his life in his family farm in West Nyack working in the theory of the orbit of the Moon, but also of Jupiter and Saturn.

The first space rendezvous It was until the race to the Moon between USA and USSR that the space rendezvous became a key technologies and theories of relative motion were deeply developed. The space rendezvous was an intermediary step towards the big goal: the Moon. But lunar missions included a lunar rendezvous between the lunar lander and the orbiter. That's the reason why Gemini missions in USA, and Vostok missions in USSR, included tests of space rendezvous around Earth.
On August 12, 1962 two Vostok spacecrafts, Vostok 3 and Vostok 4, were placed into nearby orbits, separated just by some kilometers. But spacecrafts had not the capability to do final

Figure 1.1: *On the left side, Apollonius of Perga. On the right side Claudius Ptolemaeus*

approach maneuvers. The first space rendezvous took place on December 15, 1965, when Gemini 6A maneuvered within 30 cm of the passive Gemini 7. The first docking took place on March 16, 1966 when Gemini 8, under the command of Neil Armstrong, docked with uncrewed Agena 8 vehicle.
Lunar missions boosted the development of the equations of the relative motion. Probably the most important development was obtained through Lawden's equations. Good knowledge of relative motion was also a key point to become an astronaut, as it is shown by the Ph. D. degree of the astronaut Buzz Aldrin specialized in relative motions.
Since then, space rendezvous has been used largely in space missions. They are particularly important for resupply functions in Mir and ISS stations. Recent achievements took place on April 3, 2008 with the first ATV rendezvous with ISS.

The irruption of formation flying After the end of lunar missions, space rendezvous was a well-known subject. But, new concepts including groups of spacecrafts flying in close formation required a deeper knowledge of the relative motion. While in rendezvous the duration of the relative motion is short (just some hours), in formation flying the configuration must be kept during all the length of the mission (up to several years).
The first paper that I have found using a formation flying is the Labeyrie concept of a space interferometer using several satellites published in 1982 [46]. This first concept, called Trio, consisted in three satellites, two mirrors and a combiner, to do space interferometry. At the same epoch, the European mission Cluster was proposed. It consisted in four satellites flying in a tetrahedral formation to study the magnetosphere. This mission was finally launched in 2000. This mission exemplifies the interest of multisatellite missions, even if it cannot be considered as a formation flying mission because the satellites are controlled independently.
In recent years, main space agencies have developed important programs to acquire required

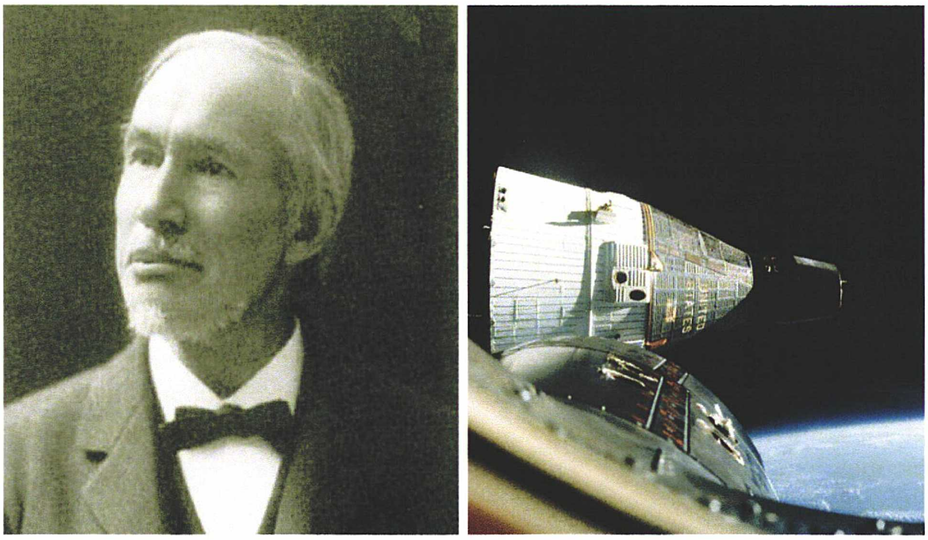

Figure 1.2: *On the left, George William Hill. On the right, Gemini 7 photographed from Gemini 6*

technologies for formation flying, as Spheres program at NASA, or Proba serie at ESA. At the same time, several formation flying missions have been launched, like A-Train or Grace mission dedicated to the study of the Earth.
For the future, a new generation of very challenging missions are currently being prepared. Formation flying could help to develop many fields of astronomy, fundamental physics, or Earth sciences. Darwin, Lisa or Simbol-X are just some examples of future missions.
These new missions present new challenges in different engineering fields. They will need autonomous navigation, very precise knowledge of their relative positions (less than the micrometer) and also autonomous relative control algorithms. Moreover, each mission presents its own difficulties. At the sight of all these new projects, there is still a lot of research to do on relative motion.

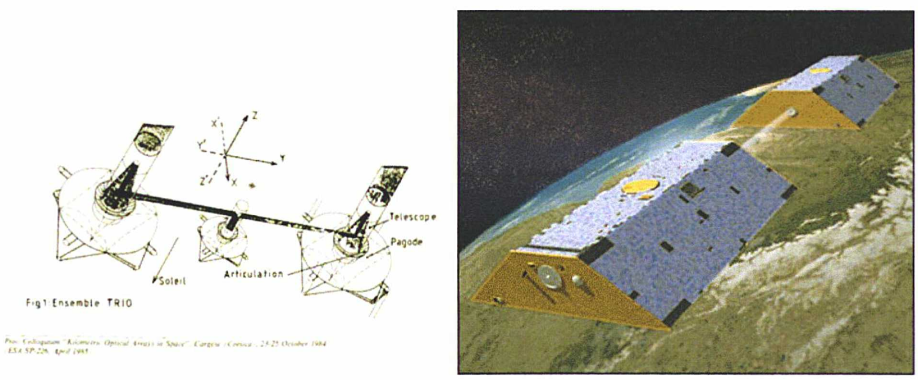

Figure 1.3: *Trio concept from Labeyrie on the left side. Artist view of Grace mission on the right side.*

1.2 Definition of formation flying

Space missions that use a certain number of satellites to accomplish the same goal are constellations of satellites (GPS, Galileo) and formation flying missions. Two criteria are usually used to differentiate between them: (i) the GNC (Guidance, Navigation, Control) system of the mission, and (ii) the relative dynamics between the satellites.

From a GNC point of view, a formation flying is controlled through the relative positions and relative velocities between satellites, while in constellations each satellite is controlled individually through its absolute position and velocity. In formation flying, relative position is important for the success of the mission. For example, in interferometry missions, relative position must be known with great accuracy in order to determine the path of the light of different telescopes.

From a dynamical point of view, in formation flying, satellites are *near* one from each other, while in constellations they are *far*. Of course, *near* and *far*, are not precise terms. We try to define them in the following lines.
First of all, the relative distance (ρ) must not be considered in absolute, but with respect to the semi-major axis of the orbit of the satellites (a). It is not the same a relative distance between satellites of 1000 km when they are orbiting the Earth than when they are orbiting the Sun.
All along the document, I consider that two satellites are near when: *The dynamics of one satellite with respect to another can be studied using the Taylor's development of the dynamics around the second one and this development is convergent.* In most of cases, the linear term is enough for a good accuracy. In these conditions, the precision is given by the parameter $(\frac{\rho}{a})$.

1.2.1 Classification of missions from a dynamical point of view

Formation flying can be classified with different criteria. In [9], they are classified following three criteria: the dynamics, the guidance, and the geometry. For our purposes, we are interested only in the dynamics criteria.
We adopt the same dynamical classification as in [9] adding a second division. It is, we separate formation flying in (i) missions around Lagrange points, and (ii) missions around a central body. The missions around a central body can be also separated in (ii.a) small intersatellite distance, and (ii.b) large intersatellite distance. This classification is schematized in figure 1.4
The dynamics around the Lagrange points is a restricted three-body problem, where the gravitational attractions of two attractive bodies are equal. The dynamics around these points is completely different from a central body dynamics; that is why the two problems must be studied separately. The study of Lagrange points is beyond the scoop of this thesis and I focus only on the central body dynamics.
The difference of relative motions around a central body with a big intersatellite distance or a small one, is not so relevant. It deals with the accuracy of the linear model and the interest of introducing no linear effects.

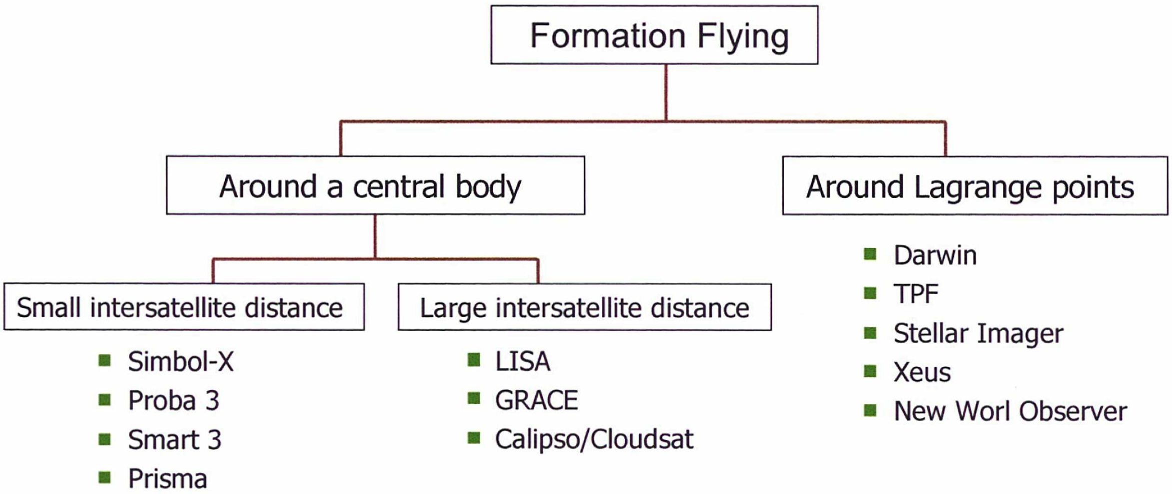

Figure 1.4: *Classification of formation flying from a dynamical point of view*

1.3 Present status of formation flying

1.3.1 Current missions

Thereafter, we give a short description of some of the most significant present and planned formation flying missions. Each mission is followed by a link to the official website of the mission.

GRACE: It is a mission dedicated to the detection of the gravity field and the magnetic field. It focuses on the temporal variations of the gravity field. It has been realised thanks to the collaboration between JPL and DLR. The satellites were launched in March 2002 and it has been providing data for six years.
Two twin satellites flying in a leader-follower configuration compose the mission. The intersatellite distance changes over time from 40 km to 200 km. The satellites are equipped with a laser link that measures with a high frequency and high precision ($10\mu m$) their relative distance. Satellites are placed in a near polar orbit ($i = 89°$), with a very low altitude ($a = 6683\ km$), and very low eccentricity ($e = 0.0022$).

http://www.csr.utexas.edu/grace/

DARWIN: It is an ESA project scheduled for 2012. The project is made up by an uncertain number of satellites, varying between three and six. One of them is placed on the centre of the formation and combines the light coming from the other satellites. The centre satellite is also in charge of telecommunications. Telescopes that collect the light coming from stars are placed in a symmetric configuration around the central satellite. The central satellite, using nulling interferometry detects the presence of exoplanets around studied stars and their chemical composition.
Satellites will be sent to a Lagrange point (L2), one and half million kilometres from the Earth, in order to avoid Earth pollution and perturbations. Once placed, there relative distances will be of about some hundreds of metres. The interelative distance must be controlled

with a precision of the micrometer, and known with a precision of the nanometer. These specifications come from the interferometer technology.

http://darwin.esa.int/science-e/www/area/index.cfm?fareaid=28

LISA: It is a future mission issued from a collaboration between NASA and ESA composed of a three satellites interferometer. The orbits of the satellites will be similar to the Earth's, but will trail behind our planet at distances of around 50 million kilometres, equivalent to 20 degrees. Launching date is about 2018 with a mission lifetime of 5 years. The three satellites form an equilateral triangle (5 million km. between satellites) facing the Sun, slanting at 60 degrees to the plane of the Earth's orbit and revolving with the Earth around the Sun.
The main goal of the mission is the detection of gravitational waves. They are predicted by Einstein theory but they have never been directly detected in spite of very performing experiments. The tiny size of the waves, and the number of perturbations on Earth are the two factors that have prevented their detection. Their detection would certainly open another door for the exploration of the Universe. Nowadays, natural relative motion of the formation is not adapted for the goal of the mission. For interferometer purposes, satellites should keep constant interdistance and angle, but natural motion of the satellites introduces a kind of 'breathing' of the configuration all along the orbit.

http://lisa.esa.int/science-e/www/area/index.cfm?fareaid=27

CALIPSO / CLOUDSAT: Calipso and Cloudsat are two Earth observation satellites launched on April 28, 2006. Cloudsat is dedicated to the study of the clouds and Calipso is dedicated to study the role of aerosols in climate changing. Each of the satellites has its own vital systems, but they are designed to have the same ground path with a small distance between them (100 km). That is why they are considered as a formation flying. The formation is completed with several others satellites dedicated to Earth observation, it is the so-called 'A-train'.
Satellites Calipso and Cloudsat have a length life of about three years, they have a heliosynchronous retrograde orbit, with a semi-major axis of 705 km and an inclination of 98.2 degrees.

http://www.nasa.gov/mission_pages/cloudsat/main/index.html
http://www.nasa.gov/mission_pages/calipso/main/index.html

SIMBOL-X: It is an Italian(ASI) - French(CNES) mission composed by two satellites flying in very close formation (25 metres). The two satellites compose a telescope that will observe in the X band. So, it will observe the very energetic elements as black holes. The lifetime of the mission would be between three and five years.
Satellites will be placed in very eccentric ($e = 0.75$) high ($a = 100000km$) orbits (HEO) around the Earth. These orbits represent an alternative to Lagrange points in terms of perturbations. Observations are taken beyond the Van Allen radiation belt. Simbol-X represents one of the most challenging future projects because of the high eccentricity of the orbit and the major role of the solar radiation pressure on the relative motion.

http://www.cnes.fr/web/5848-simbol-x.php

TERRESTRIAL PLANET FINDER: It is the NASA mission equivalent to the European DARWIN mission. It will be composed of two observatories: a visible light coronagraph, and an infrared interferometer. They would also flight to L2 points and the main goal of the mission is exoplanet detection.

http://planetquest.jpl.nasa.gov/TPF/tpf_index.cfm

TechSat 21: It is a mission conducted by the US Air Force Research Laboratory to prove the capabilities of formation flying to operate in different tasks as radio frequency sparse aperture imaging, precision geolocation or ground moving target indication. The mission is a technological demonstrator composed by three satellites of about hundred kilos each one. Mission should have been launched in June 2004.

PROBA 3: It is the third satellite of the European Technological Demonstrators PROBA. There is still no date for its launch but this will not be before 2010. Two satellites will compose the formation with a varying separation between 5 meters and 8 kilometers, and an accuracy on the determination of the relative motion of a few centimetres.
It will be used to verify the metrology, the actuation techniques and the GNC strategies for future formation flying. Both satellites will fly in very eccentric orbits and will be controlled only far from the perigee, where the fuel consumption is smaller.

http://www.esa.int/techresources/ESTEC-Article-fullArticle_par-28_1153128123055.html

TANDEM-X/TERRASAR-X: It is a DLR mission consisting of two companion SAR satellites flying in close formation with the main goal to provide operational, bi-static single pass interferometry products of new quality with tunable interferometric baselines. The along track distance between the satellites varies between thirty and fifty kilometres, and there is also a small across track variation to avoid collision risk.

http://www.dlr.de/hr/desktopdefault.aspx/tabid-2317//3669_read-5488/

PRISMA: It is a Swedish-French technological demonstrator to prepare future missions like Simbol-X. Prisma is scheduled to be launched in spring 2009. The estimated lifetime for Prisma is around ten months. Prisma will be launched into a low, sun-synchronous, dawn/dusk orbit at an altitude of $600km$. The mission will be carried out as a long series of experiments, including both manoeuvring and sensor/motor experiments. A certain number of days will be allocated to each party.

http://www.prismasatellites.se/?id=9036

STELLAR IMAGER: It is a NASA mission to enable an understanding of solar/stellar magnetic activity and its impact on the Universe. The mission would be composed by a large number (20-30) of primary mirror elements focusing on beam combining hub with a baseline between 100 and 1000 metres. The lifetime of the mission is about ten years. Satellites would be launched in L2 point.

http://hires.gsfc.nasa.gov/si/

XEUS: Selected for Cosmic Vision ESA program, with a possible launch in 2018. XEUS is the potential successor to XMM-Newton, ESA's current X-ray observatory. With $5m^2$ of collecting area at 1 keV and $2m^2$ at 7 keV, an imaging resolution of 5" half-energy width (HEW) and a goal of 2" HEW, XEUS will have a limiting sensitivity around 200 times deeper than XMM-Newton. XEUS requires a focal length of around $35m$ to reach a collecting area of $5m^2$ at 1 keV. Given this long focal length, a dual spacecraft configuration is favoured. A Halo orbit around the second Lagrangian point of the Sun-Earth system (L2) provides optimal conditions. The chosen orbit can be reached in about one month with an almost full-year launch window. L2 provides the necessary low gravity-gradient environment for economical formation flying, long observing windows and optimal cooling for the instruments.

http://sci.esa.int/science-e/www/object/index.cfm?fobjectid=42271

New Worlds Observer: The New Worlds Mission is a project funded by NASA Institute for Advanced Concepts (NIAC), headed by Dr. Webster Cash of the University of Colorado at Boulder in conjunction with Ball Aerospace & Technologies Corp., Northrop Grumman, Southwest Research Institute and others. The project plans to build a large occulter in space designed to block the light of nearby stars, in order to observe their orbiting planets. The observations could be taken with an existing space telescope, possibly the James Webb Space Telescope when it launches, or a dedicated visible light telescope optimally designed for the task of finding exoplanets. New World Observer is one of the possible configurations for the mission. New Worlds Observer would use two spacecraft and two starshades increase the angular resolution and allow better analysis of the exoplanet's composition.

http://newworlds.colorado.edu/

1.3.2 Major areas of development

The domains for which we note the most intense activity are the followings:

- *Modelling relative motions*: Even if important progress have been recently done in this direction, some aspects remain unresolved. Modellisation of non-conservative perturbations, or simplified expressions for non-linear effects are two of them. First part of this thesis is dedicated to this modellisation.

- *Control laws*: The control of the formation can be done using different control laws. They must be evaluated in terms of efficiency, precision, and propellant consumption. This problem has two different approaches when we consider continuous thrust or isolated maneuvers.

- *Optimal reconfiguration*: The problem consists in changing relative positions or deploying the formation after the insertion by consuming the minimum of energy. This is a very complex optimization problem because of the number of parameters: time, number of manoeuvres, initial and final positions. Particular techniques exist to deal with it. In some cases, the problem can be simplified into a two maneuvers strategy.

- *Non-drift orbits*: When satellites are not in operation for a while, they remain in a low-energy state. During this period, in a general configuration, natural forces could drift away satellites. This could be a problem for posterior recovery of the mission. That is the reason why satellites are placed in non-drift orbits. The determination of non-drift orbits is a current problem for formation flying missions.

- *Navigation techniques*: Navigation in formation flying is specific because it is not always easy to have measurements of the distance between satellites with precision. The two main techniques are laser link between satellites and radar measurements. Problem of both of them is that they are very directional. The challenge is to obtain a completely on-board navigation system. Determination of absolute and relative motions at the same time could present advantages for the accuracy of the determination, but at the same time, it could present instabilities.

This different problems involve different scientific areas: orbital mechanics, automatics, optimal control or filtering are just some of them.

1.4 Plan of the thesis

The origin of the interest for formation flying within the team *Géodésie et Mécanique Céleste* of the *Observatoire de la Côte d'Azur* is linked with space geodesy. At the sight of the success of GRACE mission, and considering future needs of space geodesy, it seems reasonable to start preparing future GRACE 'follow-on' missions. The first fundamental question about this hypothetical missions is the configuration of the formation flying. GRACE configuration presents several technological advantages (same orientation of the satellites, same drag effects,..), but, are there other configurations more sensitive to the gravity field?
In order to answer this question, we wanted to sweep all the possible configurations. Analytical models seem to be the most suited for fast numerical sweeping. I realized that a in-depth study of relative motion was necessary to get an accurate analytical model standing for gravity field effects. So, I started doing an exhaustive research of analytical models for relative motion. In some cases, when I considered that the model was not accurate enough, I did necessary improvements. In a second time, I studied geodesy missions.
Thanks to my contacts with the French space agency (CNES) and Thales Alenia Space, I discovered a very challenging formation flying: Simbol-X. I also collaborate with them in the mission analysis.

The document is divided into three parts, the two first are devoted to the relative motion (first part to the Keplerian motion, and second part to the perturbations), and the third part is dedicated to formation flying missions.
In the first part, I present three different representations of the relative motion. The first one is the cartesian coordinates. It is the most usual one. The second one is the differential orbital elements. This representation is quite recent, and is very well adapted for the introduction of the perturbations. The last representation is local orbital elements. Local orbital elements are interesting for circular reference orbit case. They are particularly well suited to get a good insight on the relative trajectory.
In the second part I study two perturbations: the central gravity field and the solar radiation pressure. Gravity field is split in two chapters. The first one is dedicated to the J_2 effects while the second one is dedicated to the rest of the gravity field. The effects of the solar radiation pressure are studied because they are the main perturbation of high eccentric orbits

(HEO).
The last part is dedicated to space missions using formation flying technology. I study an Earth observation mission for the determination of the Earth gravity field, and a Universe observation mission composed of a telescope distributed over two satellites in HEO orbit.

Part I

The relative motion

Chapter 2

Generalities

2.1 The statement of the problem

We want to study the relative motion of a body b with respect to a body a, both a and b being in orbit around the central body c. By convention, the orbit of a is designed as the reference orbit and we suppose that b is close to a. The notion of proximity is given by the convergence of the Taylor's development around a reference orbit.

Moreover, we suppose these two conditions:

$$m_c >> m_a, m_b \tag{2.1}$$

so as to neglect gravitational interaction between bodies a and b. The second condition is:

$$|\vec{r}_a - \vec{r}_b| << |\vec{r}_a - \vec{r}_c|, |\vec{r}_b - \vec{r}_c| \tag{2.2}$$

Second condition will be used to assume the convergence of a polynomial development.

We consider that bodies describe a keplerian motion around a central body. Later on, we will introduce perturbations on the motion.

Notations In the whole text, we use the well-known keplerian elements: the semi-major axis a, the eccentricity e, the inclination i, the right ascension of ascending node Ω, the argument of perigee ω, and the mean anomaly M. We also use the true anomaly f, an intermediary variable $\eta = \sqrt{1-e^2}$, and the sum of the perigee and the anomaly: $u = \omega + f$. $\overrightarrow{EO}$ stands for:

$$\overrightarrow{EO} = (a, e, i, \Omega, \omega, M)^T \tag{2.3}$$

For low or null eccentricities we will use the non-singular keplerian elements, $\overrightarrow{ENS} = (a, C, i, \Omega, S, M)^T$, defined as function of keplerian elements:

$$\begin{aligned} C &= e\cos\omega \\ S &= e\sin\omega \\ \lambda &= \omega + M \end{aligned} \tag{2.4}$$

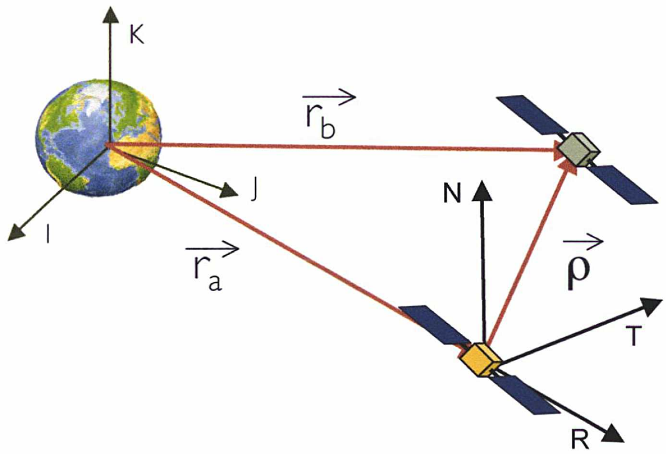

Figure 2.1: *Local reference frame and local cartesian coordinates*

We will also use in chapter[7] Delaunay variables (L, G, H, l, g, h) defined as follows:

$$\begin{array}{ccc} h = \Omega - \theta & g = \omega & l = M \\ L = \sqrt{\mu a} & G = \sqrt{\mu a(1-e^2)} & H = G\cos i \end{array}$$

where θ is the sidereal Greenwhich time. The motion, studied in an inertial reference frame denoted IJK, is described through temporal series of keplerian elements as well as of positions $\overrightarrow{r}|_{IJK}$ and velocities $\overrightarrow{v}|_{IJK}$. We use the following notations:

$$\overrightarrow{x}|_{IJK} = \begin{pmatrix} \overrightarrow{r}|_{IJK} \\ \overrightarrow{v}|_{IJK} \end{pmatrix}$$

We will consider a reference orbit which will be described by its orbital elements or by its position and velocity. This reference orbit can be the orbit of one of the satellites of the formation $(\overrightarrow{r}_a)$ or it can correspond to a fictitious point. For clarity, we will name it the reference satellite indicated by the subscript $_{ref}$. Inertial position and velocity can also be projected in the orbital local frame (RTN) (Radial $\overrightarrow{e}_R$, Transverse $\overrightarrow{e}_T$, Normal $\overrightarrow{e}_N$) defined by a given reference orbit. Relations between the two projections are given by matrix $\mathcal{R}(\overrightarrow{EO})$:

$$\overrightarrow{r}|_{RTN} = \mathcal{R}(\overrightarrow{EO}_{ref})\overrightarrow{r}|_{IJK} \tag{2.5}$$

$$\mathcal{R}(\overrightarrow{EO}) = \begin{pmatrix} \cos\Omega\cos u - \sin\Omega\sin u\cos i & -\cos\Omega\sin u - \sin\Omega\cos u\cos i & \sin\Omega\sin i \\ \sin\Omega\cos u + \cos\Omega\sin u\cos i & -\sin\Omega\sin u + \cos\Omega\cos u\cos i & -\cos\Omega\sin i \\ \sin u\sin i & \cos u\sin i & \cos i \end{pmatrix} \tag{2.6}$$

The relative motion between a satellite and the reference satellite can be described by the difference of absolute position and velocity projected in the orbital frame of the reference orbit:

$$\Delta\vec{x}|_{RTN} = \vec{x}|_{RTN} - \vec{x}_{ref}|_{RTN} = \begin{pmatrix} \Delta\vec{r}|_{RTN} \\ \Delta\vec{v}|_{RTN} \end{pmatrix} \tag{2.7}$$

or by the differences of orbitals elements between the two orbits:

$$\Delta\overrightarrow{EO} = \overrightarrow{EO} - \overrightarrow{EO}_{ref} \tag{2.8}$$

We will also use the following notation:

$$\begin{aligned} \Delta\vec{r}|_{RTN} &\equiv (\Delta R, \Delta T, \Delta N)^T \\ \Delta\vec{v}|_{RTN} &\equiv (\Delta V_R, \Delta V_T, \Delta V_N)^T \end{aligned}$$

Relative motion can also be described by the position and the velocity relatives to the reference orbit $(\vec{\rho}, \dot{\vec{\rho}})$ or their coordinates:

$$\begin{aligned} \vec{\rho} &\equiv (\rho_R, \rho_T, \rho_N)^T \\ \dot{\vec{\rho}} &\equiv (\dot{\rho}_R, \dot{\rho}_T, \dot{\rho}_N)^T \end{aligned}$$

2.1.1 Different cases of relative motion

Previous conditions can be accomplished in different cases in space missions:

- *Formation Flying:* two or more satellites flying together with the same mission around a central body. As I explained in the introduction, formation flying can also be placed on Lagrange points. This case is not treated in this thesis.
- *Space rendezvous:* one spacecraft maneuvering to dock into a second spacecraft. It was at the origin of the interest in formation flying.
- *Asteroids:* In asteroid belts, there may be groups of bodies flying in close positions. Their motions can be studied independently or as a relative motion.
- *Space debris:* After a collision or the explosion of an spacecraft, a certain number of pieces may rest in similar orbits. Equations of relative motion may be interesting in order to describe the evolution of the population.

2.2 The various representations

I have divided our study as function of the different representations of the relative motion. Here, we describe the three possible representations:

- *cartesian coordinates:* Their temporal evolution is driven by classical Hill equations and Lawden equations, the classical one.
- *Differential orbital elements:* It is very useful to introduce perturbations thanks to precedent experience on orbital mechanics.
- *Local orbital elements:* It is useful only for circular or low eccentric orbits. It enables a better understanding of the trajectory.

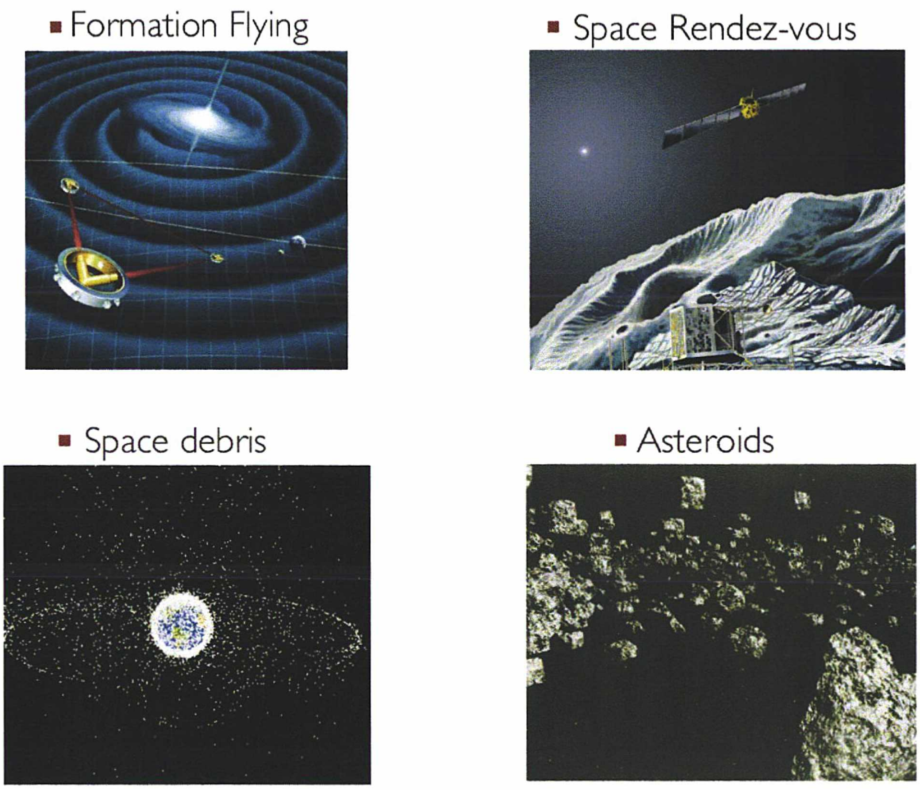

Figure 2.2: *Different cases of relative motion*

2.3 Linearization of the equations

The use of exact expressions of the relative motion leads to very complicated analytical expressions which are not well-adapted for analytical manipulations. In order to simplify them, we linearize these equations with respect to the distance as follows:
The motion of two points around a central body is given by generic expressions:

$$\begin{aligned} \overrightarrow{x}_a(t) &= \overrightarrow{f}\left(\overrightarrow{x}_a(t_0), t\right) \\ \overrightarrow{x}_b(t) &= \overrightarrow{f}\left(\overrightarrow{x}_b(t_0), t\right) \end{aligned} \tag{2.9}$$

where the subscript 0 stands for initial conditions. Here, the first body plays the role of the reference orbit and the second is the satellite that we analyze. The relative position is:

$$\overrightarrow{\rho}(t) = \overrightarrow{x}_b(t) - \overrightarrow{x}_a(t) \tag{2.10}$$

We can rewrite the motion of the second body as:

$$\overrightarrow{x}_b(t) = \overrightarrow{f}\left(\overrightarrow{x}_a(t_0) + \overrightarrow{\rho}(t_0), t\right) \tag{2.11}$$

Moreover, assuming:

$$\overrightarrow{\rho} \ll \overrightarrow{x}_a, \overrightarrow{x}_b \tag{2.12}$$

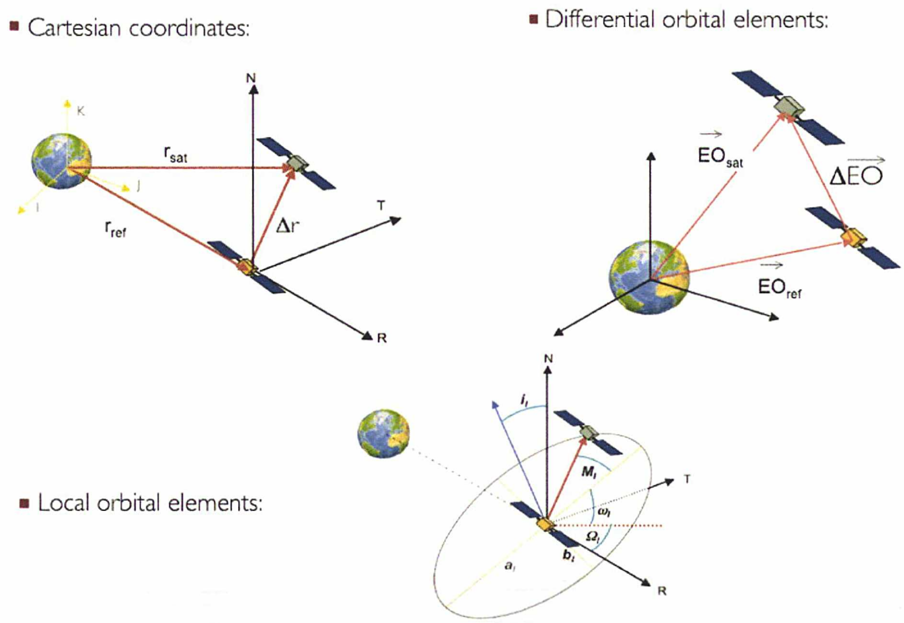

Figure 2.3: *The three different representations*

We can do the Taylor expansion of the function supposed to be convergent:

$$\overrightarrow{\rho}(t) = \frac{\partial \overrightarrow{f}}{\partial \overrightarrow{x}(t_0)}|_{\overrightarrow{x}_a(t_0)} \overrightarrow{\rho}(t_0) + \frac{\partial^2 \overrightarrow{f}}{\partial \overrightarrow{x}(t_0)^2}|_{\overrightarrow{x}_a(t_0)} (\overrightarrow{\rho}(t_0))^2 + \mathcal{O}(\rho^3) \tag{2.13}$$

Usually, first terms of the development are sufficient to obtain a good precision. In table 2.1 we give the error of the linear approach for different missions. The parameter which determines the precision of the linear approach is $\frac{\rho}{a_r}$, where a_r is the semi-major axis of the reference orbit. In certain cases, second order might be interesting. Some efforts have been done in this direction in [61].
Next chapters are devoted to different methods used to study the relative motions. We present a linear approach, but for all representations it would be possible to introduce second order effects.
The approach in terms of a polynomial development is a very deep change in the structure of the motion. The nature of the keplerian motion is periodical, and a polynomial development is not well-adapted for periodical motions. It implies that polynomial developments cannot take into account long-term secular drifts.

	ρ (km)	a_r(Km)	error (%)
GRACE	200	6900	10
LISA	5 M	150 M	0,1
SIMBOL-X	0,02	106 K	10^{-12}

Table 2.1: *Linearisation errors for different formation flying missions*

2.3.1 The choice of the reference orbit

The choice of the reference orbit determines the interest of the relative motion. The precision of the reference orbit plays a role on the precision of obtained results. Hereafter, we present the most common reference orbits:

- *The real orbit of one of the satellites*: This orbit should be used in order to obtain the exact relative motion. But this orbit is quite complicated to describe analytically and it is usually given numerically, that is not well suited for analytical use. It is necessary to obtain high precision variations of distance, but the effects of neglecting some variations on the reference orbit are really small. We will not use it.

- *The non-perturbed orbit of a satellite:* It is the most current choice. This has the advantage of an easy analytical representation and a level of precision usually high enough for mission analysis. It can also be interesting to study the effects of perturbations on a single satellite mission.

- *The orbit of a fictitious point:* It can be useful when the choice of a reference satellite might be problematic. In general no gain in precision should be obtained by changing the reference orbit since the gain in one side should be lost in the other side. An example of such a reference orbit is [7]

Chapter 3

The classical approach

In this chapter we present classical developments about relative motion. They are based on the cartesian representation of the formation flying. The most well-known are Hill equations [35] for the circular reference orbit case (also known as Clohessy-Wilthsire equations [20]), and Lawden equations [47] for the eccentric reference orbit case. In both cases, two simplifications are done: equations are linearized, and the motion is purely keplerian.
In the first section, we present the general equations of relative motion in the framework of classical non-relativistic mechanics. Two following sections are dedicated to Hill and Lawden equations respectively. We finish the chapter with some notes on further developments of precedent equations in order to take into account perturbations or non-linear effects.

3.1 The equations of the relative motion

Classical mechanics gives the expression of the relative acceleration with respect to a non-inertial frame (see figure 3.1) with an angular velocity $\overrightarrow{\omega}$ and an acceleration $\overrightarrow{a}_{ref}$.

Using previous notions, the equations of the relative motion in a rotating reference frame become:

$$\ddot{\overrightarrow{\rho}} = \overrightarrow{a}_{sat} - \overrightarrow{a}_{ref} - 2\overrightarrow{\omega} \times \dot{\overrightarrow{\rho}} - \dot{\overrightarrow{\omega}} \times \overrightarrow{\rho} - \overrightarrow{\omega} \times (\overrightarrow{\omega} \times \overrightarrow{\rho}) \tag{3.1}$$

where $\overrightarrow{a}_{sat}$ is the absolute acceleration of the body and the dot stands for the derivatives with respect to time. These equations use three variables: (i) the relative position and its derivatives, (ii) the difference of accelerations between the two satellites, and (iii) the rotation of the reference frame, also with its derivatives. Relative position is the unknown, and the other two variables can be modeled in different ways. Both of them depend on the reference orbit. The easiest way for modeling them, is to take a non-perturbed circular reference orbit. This choice leads to the well-known Hill or Clohessy-Wiltshire equations. They are described as follows. The use of a non-perturbed elliptical reference orbit leads to Lawden equations. At the end of the chapter we will introduce the effects of perturbations.

3.2 Hill equations

We particularise precedent equations to the case of two satellites orbiting around a central body following non-perturbed keplerian motions. We place the non-inertial reference frame

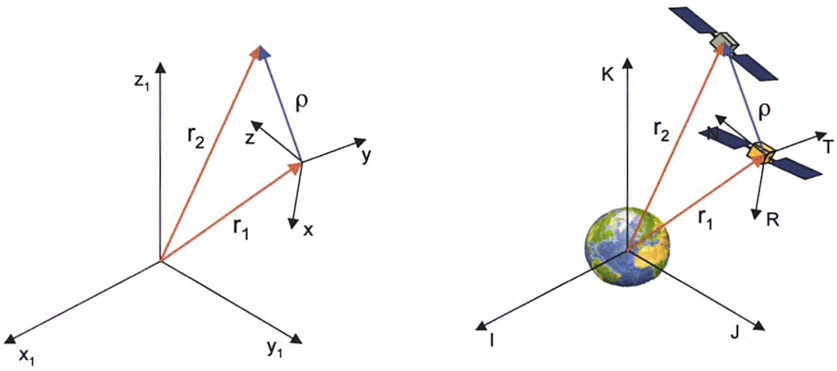

Figure 3.1: *At the left side, general inertial and non-inertial reference frames. At the right side, particularisation for a two-satellite formation flying*

in the orbit of one satellite and we suppose the orbit to be circular. The non-inertial reference frame is orientated as follows: first axe follows radial direction ($\vec{e}_R$), the third one follows the direction normal to the motion ($\vec{e}_N$), and the second one completes an orthogonal system ($\vec{e}_T$). In the circular case the second axis coincides with the direction of the velocity, but this is not the general case.

In the non-perturbed circular motion the rotation of the reference frame reads:

$$\vec{\omega} = n\vec{e}_N \tag{3.2}$$

with $n = \sqrt{\frac{\mu}{a_{ref}^3}}$, and μ is the product between the gravitational constant and the mass of the central body. The differential acceleration has a simple expression:

$$\vec{a}_{sat} - \vec{a}_{ref} = -\frac{\mu}{|\vec{r}_{ref} + \vec{\rho}|^3}(\vec{r}_{ref} + \vec{\rho}) + \frac{\mu}{|\vec{r}_{ref}|^3}\vec{r}_{ref} \tag{3.3}$$

Supposing that the distance between satellites is small, we can linearize precedent equations to obtain:

$$\vec{a}_{sat} - \vec{a}_{ref} = \frac{\mu}{r_{ref}^3}\begin{pmatrix} 2\rho_R \\ -\rho_T \\ -\rho_N \end{pmatrix} \tag{3.4}$$

Introducing (3.2) and (3.4) in (3.1), we obtain the well-known Hill equations:

$$\boxed{\begin{aligned} \ddot{\rho}_R &= 3n^2\rho_R + 2n\dot{\rho}_T \\ \ddot{\rho}_T &= -2n\dot{\rho}_R \\ \ddot{\rho}_N &= -n^2\delta_N \end{aligned}} \tag{3.5}$$

The integration of these equations is immediate:

$$
\begin{aligned}
\rho_R(t) &= \frac{\dot{\rho}_R(t_0)}{n}\sin nt - \left(2\frac{\dot{\rho}_T(t_0)}{n} + 3\delta_R(t_0)\right)\cos nt \\
&+ \left(2\frac{\dot{\rho}_T(t_0)}{n} + 4\rho_R(t_0)\right) \\
\rho_T(t) &= 2\frac{\dot{\rho}_R(t_0)}{n}\cos nt + \left(4\frac{\dot{\rho}_T(t_0)}{n_0} + 6\rho_R(t_0)\right)\sin nt \\
&+ \left(-2\frac{\dot{\rho}_R(t_0)}{n} + \rho_T(t_0)\right) - \left(3\dot{\rho}_T(t_0) + 6n\rho_R(t_0)\right)t \\
\rho_N(t) &= \rho_N(t_0)\cos nt + \frac{\dot{\rho}_N(t_0)}{n}\sin nt
\end{aligned}
$$

3.3 Lawden equations

In [47], Lawden introduced the solution for the relative motion with eccentric non-perturbed reference orbit. Hereafter, we summarize and comment his results.
When working with eccentric reference orbits, the orbital rotation is no more constant:

$$\vec{\omega} = \frac{n}{(1-e^2)^{3/2}}\left(1 + e\cos f\right)^2 \vec{e}_N \tag{3.6}$$

$$\dot{\vec{\omega}} = -2n^2 e \sin f \left(\frac{1+e\cos f}{1-e^2}\right)^3 \vec{e}_N \tag{3.7}$$

where all the orbital elements correspond to the reference orbit. It leads to a new set of differential equations:

$$\boxed{\begin{aligned}
\ddot{\rho}_R &= 2\frac{\mu}{r^3}\rho_R + 2\omega\dot{\rho}_T + \dot{\omega}\rho_T + \omega^2\rho_R \\
\ddot{\rho}_T &= -\frac{\mu}{r^3}\rho_T - 2\omega\dot{\rho}_R - \dot{\omega}\rho_R + \omega^2\rho_T \\
\ddot{\rho}_N &= -\frac{\mu}{r^3}\rho_N
\end{aligned}}$$

These equations do not have an exact explicit solution, Lawden gives an implicit one ([47], pag 85):

$$
\begin{aligned}
\rho_R(t) &= A\cos f + Be\sin f + CI_2 \\
\rho_T(t) &= -A\sin f + B(1+e\cos f) + \frac{D - A\sin f}{1+e\cos f} + CI_2 \\
\rho_N(t) &= \frac{1}{1+e\cos f}\left(E\cos f + F\sin f\right)
\end{aligned} \tag{3.8}
$$

with:

$$
\begin{aligned}
I_2 &= \frac{\cot f}{e(1+e\cos f)} + \frac{1+e\cos f}{e\sin f}I_1 \\
I_1 &= \sin f\int\frac{df}{\sin^2 f(1+e\cos f)^2}
\end{aligned} \tag{3.9}
$$

Integral I_1 has been the object of a reference [14] where I_1 is decomposed as a sum of elementary functions. Lawden also gives a closed form of the solution, but does not give parameters A, B, C, D, E, F as function of initial conditions. Lawden's solution has been used in some papers to study the control of formations [13], [36].
Lawden solution, to our point of view, has two weak points: first, the parameters of his solution (A, B, C, D, E, F) are not expressed as function of initial conditions; second, his solution is not convenient because of the integral I_1.

3.4 Relative velocity versus differences of velocity

A determining choice is the coordinates that we use for the motion. Since we use a local reference frame, we can project the relative motion in this reference frame, or we can study the relative motion with respect to the reference frame. The difference between projection and derivation has later effects on the relations between the cartesian representation and the other ones. Each possibility has some advantages and drawbacks:

- *Relative position and velocity:* represented by $\overrightarrow{\rho}$ or $(\rho_R, \rho_T, \rho_N)^T$. Hill and Lawden equations are written using these coordinates. For GNC purposes, these equations are also well adapted because what we need for GNC is the expression of the derivatives of the variables: the velocity.

- *Projection of differences of position and velocity:* represented by $\Delta\overrightarrow{r}|_{RTN}, \Delta\overrightarrow{v}|_{RTN}$, or also as:

$$\begin{aligned}\Delta\overrightarrow{r}|_{RTN} &\equiv (\Delta R, \Delta T, \Delta N)^T \\ \Delta\overrightarrow{v}|_{RTN} &\equiv (\Delta V_R, \Delta V_T, \Delta V_N)^T\end{aligned}$$

The advantage of these coordinates is their physical meaning, which enables a direct use for the observable, while the other coordinates must be transformed before. The main disadvantage is that they cannot be used for GNC since the difference of the projection of the velocity is not the derivative of the projection of the difference of positions:

$$\Delta\overrightarrow{v}|_{RTN} \neq \frac{d}{dt}(\Delta\overrightarrow{r}|_{RTN}) \tag{3.10}$$

The relations between both coordinates are quite easy to be derived:

$$\begin{aligned}\Delta\overrightarrow{r}|_{RTN} &= \overrightarrow{\delta} \\ \Delta\overrightarrow{v}|_{RTN} &= \dot{\overrightarrow{\delta}} + \overrightarrow{\omega} \wedge \overrightarrow{\delta}\end{aligned} \tag{3.11}$$

3.4.1 Hill equations using differences of velocity

In the circular case, equations (3.11) become:

$$\begin{aligned} \Delta\vec{r}|_{RTN} &= \vec{\delta} \\ \Delta\vec{v}|_{RTN} &= \dot{\vec{\delta}} + n\,(-\delta_T, \delta_R, 0)^T \end{aligned} \tag{3.12}$$

Using these relations, we can rewrite the solution of Hill equations in terms of differences of velocities:

$$\begin{aligned} \Delta R(t) &= \left(\Delta T_0 + \frac{\Delta V_{R0}}{n}\right)\sin nt - \left(2\frac{\Delta V_{T0}}{n} + \Delta R_0\right)\cos nt + \left(2\frac{\Delta V_{T0}}{n} + 2\Delta R_0\right) \\ \Delta T(t) &= \left(2\Delta T_0 + 2\frac{\Delta V_{R0}}{n}\right)\cos nt + \left(4\frac{\Delta V_T}{n} + 2\Delta R_0\right)\sin nt \\ &\quad + \left(-2\frac{\Delta V_{R0}}{n} - \Delta T_0\right) - (3\Delta V_{T0} + 3n\Delta R_0)\,t \\ \Delta N(t) &= \Delta N_0 \cos nt + \frac{\Delta V_{N0}}{n}\sin nt \end{aligned} \tag{3.13}$$

3.5 Further developments

Lawden's equations present a double drawback: (i) they ignore non-linear effects, and (ii) they ignore perturbations of the keplerian motion. Several authors have worked in order to improve the equations considering the effects that have been neglected.

3.5.1 Perturbations

Cartesian coordinates are not well suited for the introduction of perturbations because they must be taken into account in two different ways. First, perturbations must be introduced in the difference of accelerations, and second in the rotation of the reference frame. This double action of perturbations leads to complex differential equations which usually do not have an analytical solution. If we are interested in obtaining simplified expressions, we could think to use a simplified non-perturbed reference orbit. To do so, we should neglect the effects of the perturbation on $\vec{\omega}$, but the difference of acceleration must always consider the perturbations.

J2 effects In [59], the author presents a method to introduce J_2 perturbations on the relative motion. He uses local spherical coordinates instead of cartesian coordinates in order to improve the precision of his solution. He modelizes the force due to J_2 in the local orbital frame as follows:

$$\vec{J}_2 = -\frac{3}{2}\frac{J_2 \mu R}{r^4}\begin{pmatrix} 1 - 3\sin^2 i \sin^2 u \\ 2\sin^2 i \sin u \cos u \\ 2\sin i \cos i \sin u \end{pmatrix} \tag{3.14}$$

The motion of the reference orbit perturbed with the mean J2 effects reads:

$$\ddot{\vec{r}}_{ref} = \frac{-\mu}{r_{ref}^3}\vec{r}_{ref} + \frac{1}{2\pi}\int_0^{2\pi} \vec{J}_2(\vec{r}_{ref})du \tag{3.15}$$

This motion leads to a new mean rotational velocity which is computed as follows:

$$\vec{\omega} \wedge (\vec{\omega} \wedge \vec{r}_{ref}) = \frac{\mu}{r_{ref}^3}\vec{r}_{ref} + \frac{1}{2\pi}\int_0^{2\pi} \vec{J}_2(\vec{r}_{ref})du \tag{3.16}$$

This first equation enables to introduce J_2 perturbation on the rotation of the reference frame. The second effect of the perturbation must be introduced in the differential acceleration:

$$\vec{a}_{sat} - \vec{a}_{ref} = \left(\frac{-\mu}{r_{sat}^3}\vec{r}_{sat} + \frac{\mu}{r_{ref}^3}\vec{r}_{ref}\right) + \vec{J}_2(\vec{r}_{sat}) - \frac{1}{2\pi}\int_0^{2\pi} \vec{J}_2(\vec{r}_{ref})du \tag{3.17}$$

The first two terms correspond to the keplerian motion. The third term corresponds to the J_2 effects on the satellite orbit, and the last terms are the mean J_2 effects on the reference orbit. As usual, the author linearizes previous equation:

$$\vec{J}_2(\vec{r}_{sat}) = \vec{J}_2(\vec{r}_{ref}) + \frac{\partial \vec{J}_2}{\partial \vec{r}}(\vec{r}_{ref})\vec{\delta} + \mathcal{O}\left(\frac{\delta}{r}\right)^2 \tag{3.18}$$

He also averages the differential effects of J_2 :

$$\vec{a}_{sat} - \vec{a}_{ref} = \left(\frac{-\mu}{r_{sat}^3}\vec{r}_{sat} + \frac{\mu}{r_{ref}^3}\vec{r}_{ref}\right) + \vec{J}_2(\vec{r}_{ref}) + \frac{1}{2\pi}\int_0^{2\pi} \frac{\partial \vec{J}_2}{\partial \vec{r}}(\vec{r}_{ref})\vec{\delta}\,du - \frac{1}{2\pi}\int_0^{2\pi} \vec{J}_2(\vec{r}_{ref})du \tag{3.19}$$

The detailed solution of this equation can be found in [59]. Another interesting work that has been with J_2 is [78]

.

Gravity field effects Also a very interesting development to introduce perturbations is presented in [50]. First, the author finds an analytical solution for Hill equations perturbed with a general periodic perturbation:

$$\begin{aligned} \ddot{\rho}_R &= 3n_0^2\rho_R + 2n_0\dot{\rho}_T + A_R\cos ft + B_R\sin ft \\ \ddot{\rho}_T &= -2n_0\dot{\rho}_R + A_T\cos ft + B_T\sin ft \\ \ddot{\rho}_N &= -n^2\rho_N + A_N\cos ft + B_N\sin ft \end{aligned} \tag{3.20}$$

where $A_R, B_R, A_T, B_T, A_N, B_N$ are the coefficients describing the perturbative force. He finds following solution:

$$\rho_R(t) = \frac{n}{f(n^2-f^2)}(R_0 + R_{Cf}\cos ft + R_{Sf}\sin ft + R_{Cn}\cos nt + R_{Sn}\sin nt) \tag{3.21}$$

$$\rho_T(t) = \frac{n^2}{f^2(n^2-f^2)}(T_0 + T_t t + T_{Cf}\cos ft + T_{Sf}\sin ft + T_{Cn}\cos nt + T_{Sn}\sin nt)$$

$$\rho_N(t) = \frac{1}{n^2-f^2}(N_{Cf}\cos ft + N_{Sf}\sin ft + N_{Cn}\cos nt + N_{Sn}\sin nt) \tag{3.22}$$

where the coefficients are given as function of initial conditions and perturbing forces. The second step consists in introducing differential gravitational perturbations as periodic perturbations. For sake of brevity I do not reproduce the results that can be found in [50]. The author do not introduce perturbations on the reference frame. It means that the angular velocity of the reference frame is the keplerian one. Certainly, this simplification does not affect precision for short periods of time, but it might be an important source of error for long extrapolations.

3.5.2 The non-linear effects

The most interesting work developing non-linear effects using cartesian coordinates are [31], [52], and [39]. In [31], the authors present a semi-analytical method to consider the whole non-linear effects on Hill equations. This is the generalization of paper [52], where only second and third order effects are considered.
The departure point in [31] are the non-linearized Hill equations:

$$
\begin{aligned}
\ddot{\rho}_R &= -\frac{\mu}{r+\rho}^{3}(\rho_R + r) + 2n\dot{\rho}_T + n^2(\rho_R + r) \\
\ddot{\rho}_T &= -\frac{\mu}{r+\rho}^{3}\rho_T - 2n\dot{\rho}_R + n^2\rho_T \\
\ddot{\rho}_N &= -\frac{\mu}{r+\rho}^{3}\rho_N
\end{aligned}
\tag{3.23}
$$

Their technique consists in expanding the non-linear terms, which in their dimensionless form can be written as the derivatives of the function:

$$
\Omega(x, y, z) = \frac{(x+1)^2 + y^2}{2} + \frac{1}{\sqrt{(x+1)^2 + y^2 + z^2}} \tag{3.24}
$$

This function is expanded as a series using Legendre polynoms and is solved using Lindstedt-Poincaré Procedure.

In [39], the author obtain only the second order terms of circular problem using spherical coordinates.

3.6 Conclusions

In this chapter we have presented the classical equations of the relative motion, their advantages and their disadvantages. At the end of the chapter we can conclude that, even if they are very useful, they are not well-adapted for the introduction of perturbations. The method presented in the next chapter is very complementary because it is specially developed for the introduction of perturbations.

Chapter 4

An alternative approach

4.1 Introduction

In this chapter we present an alternative method to study the dynamics of formation flying. The principle of the method is simple. The representation of the motion is done in a local orbital frame, but the extrapolation is done using the equivalent differences of orbital elements. To use this method it is necessary to have transformations between the two representations: the difference of orbital elements and the local orbital frame. Historically, the first article that presented these transformations was [15], but the author did not use them for relative motion. Other transformations were used by Garrison et al. [28] to obtain the equations of the relative motion for an eccentric reference orbit. Alfriend proposed another way to obtain the transformations and introduced another set of orbital elements in [3]. Using Alfriend's method, also called 'geometric method', Gim [29] introduced J_2 perturbations and Sengupta introduced second order effects [61]. This solution has none of the drawbacks of Hill and Lawden equations. It can take into account second order effects, eccentric reference orbit, and perturbations. This solution is very well-adapted for control and navigation.
Our method presents some differences with respect to previous work. First, we use classical orbital elements with mean anomaly. This set of orbital elements keeps simple analytical expressions, but has a double singularity for zero eccentricity and zero inclination. A second difference is the use of the difference of absolute velocities instead of relative velocities. These variables are better adapted for mission analysis because Doppler effect measures this difference of velocities, while relative velocities are well-adapted for control and navigation. Third, we present an analytical procedure to inverse the transformation matrix, when this was done numerically in other articles. Moreover, in following chapters we use this method to introduce not only the effects of the gravity field, but also the perturbation produced by the solar radiation pressure.
This chapter is organized with the following structure. In the second section, we present our general strategy to propagate relative motions by combining the differences of orbital elements and the rectangular coordinates. The third section is dedicated to linear transformations using the Poisson brackets. In section four, we apply our method to the linear, keplerian case. We finish by particularizing the equations for the circular case.

4.2 Propagation method for relative motions

Principles of the method The principle of our approach consists in using the differences of orbital elements to study the dynamics of the motion, while rectangular coordinates are used to give a better insight of the formation. Our goal is to obtain final expressions:

$$\Delta\vec{x}(t) = f(\Delta\vec{x}(t_0), \overrightarrow{EO}_{ref}(t), t) \tag{4.1}$$

The method consists in a double transformation. The initial difference of orbital elements is deduced from the initial conditions given as a difference of position and velocity at the epoch t_0:

$$\Delta\vec{x}(t_0)|_{RTN} \rightarrow \Delta\overrightarrow{EO}(t_0) \tag{4.2}$$

This transformation does not imply the dynamics of the problem; consequently, the perturbations do not change these relations. Once the initial conditions are known as differences of orbital elements, we propagate the reference orbit and the relative motion. The extrapolation of reference orbit can be done with one of the various analytical theories available in orbital elements. Lagrange equations, Gauss equations or Kaula's method are some tools that can be used:

$$\overrightarrow{EO}_{ref}(t) = f(\overrightarrow{EO}_{ref}(t_0), t) \tag{4.3}$$

The same analytical theories can be used to express the difference of orbital elements :

$$\Delta\overrightarrow{EO}(t) = f(\overrightarrow{EO}_{sat}(t_0), t) - f(\overrightarrow{EO}_{ref}(t_0), t) \tag{4.4}$$

In most of cases we can use the differentiated form:

$$\Delta\overrightarrow{EO}(t) = g\left(\Delta\overrightarrow{EO}(t_0), \overrightarrow{EO}_{ref}(t), t\right) \tag{4.5}$$

Such an expression separates the effects of a perturbation on the reference orbit and on the relative motion. It is also possible to choose different perturbations for the reference orbit and the formation.

Finally, once the temporal evolution of the differences of orbital elements is known, these differences can be reprojected in terms of differences of position and velocity:

$$\Delta\overrightarrow{EO}(t) \rightarrow \Delta\vec{x}|_{RTN}(t) \tag{4.6}$$

As a result, the evolution of the relative motion can be described in the local reference frame defined by the reference orbit. The combination of these three steps gives the expression:

$$\Delta\vec{x}(t) = f(\Delta\vec{x}(t_0), \overrightarrow{EO}_{ref}(t), t) \tag{4.7}$$

These transformations have a general form and they can account for non linear effects, even if in this study we present only the linear case. Perturbations are included in two different ways. Perturbations on the formation are introduced through the transformation (4.5). Perturbations on the reference orbit are given through the temporal evolution of $\overrightarrow{EO}_{ref}$ in equation (4.3).

Linearization Because of the differences, the exact explicit form of the transformations (4.2) and (4.6) seems unreachable. It is convenient to use simplified relations when differences are small enough. The quality of the approximation determines the precision and the range of validity of resulting equations. In this document we use the linear transformations. This writes:

$$\begin{aligned} \Delta\overrightarrow{EO}(t_0) &= \left[\mathcal{M}^{-1}(\overrightarrow{EO}_{ref})\right]\Delta\overrightarrow{x}(t_0)|_{RTN} \\ \Delta\overrightarrow{EO}(t) &= \left[\mathcal{L}(\overrightarrow{EO}_{ref}(t_0))\right]\Delta\overrightarrow{EO}(t_0) \\ \Delta\overrightarrow{x}(t)|_{RTN} &= \left[\mathcal{M}(\overrightarrow{EO}_{ref})\right]\Delta\overrightarrow{EO}(t) \end{aligned} \tag{4.8}$$

where the matrices $\mathcal{M}$ and $\mathcal{M}^{-1}$ are:

$$\mathcal{M}(\overrightarrow{EO}_{ref}) = \frac{\partial\overrightarrow{x}|_{RTN}}{\partial\overrightarrow{EO}} \qquad \mathcal{M}^{-1}(\overrightarrow{EO}_{ref}) = \frac{\partial\overrightarrow{EO}}{\partial\overrightarrow{x}|_{RTN}} \tag{4.9}$$

and the matrix $\mathcal{L}$ gives the linearised temporal evolution of initial differences of orbital elements. For the linear case, the final result given by the combination of three matrices reads:

$$\Delta\overrightarrow{x}(t)|_{RTN} = \left[\mathcal{M}(\overrightarrow{EO}_{ref}(t))\cdot\mathcal{L}(\overrightarrow{EO}_{ref}(t))\cdot\mathcal{M}^{-1}(\overrightarrow{EO}_{ref}(t_0))|_{RTN}\right]\Delta\overrightarrow{x}(t_0) \tag{4.10}$$

The matrix $\mathcal{L}$ depends on the perturbations, but not the matrices $\mathcal{M}$ and $\mathcal{M}^{-1}$. The matrix $\mathcal{M}$ corresponding to the direct transformation can be found in the literature [15], but not the matrix $\mathcal{M}^{-1}$ corresponding to the inverse transformation. Next section explains how both matrices can be obtained. The only non-linear approach that we have found actually is [61].

4.3 Transformations between representations

The aim of this section is to find direct and inverse transformations between the two representations, $\Delta\overrightarrow{x}|_{RTN}$ and $\Delta\overrightarrow{EO}$, through explicit expressions of matrices $\mathcal{M}$ and $\mathcal{M}^{-1}$.

4.3.1 Direct transformation

The differences of position and velocity in terms of differences of orbital elements is detailed by Casotto in [15]. Here, we just quote it to link his approach with ours. To compute $\mathcal{M}$, Casotto follows a schema made up in two steps. First, he differentiates explicit relations between the position-velocity and the orbital elements $\overrightarrow{x}|_{IJK} = f(\overrightarrow{EO})$ to obtain:

$$\Delta\overrightarrow{x}|_{IJK} = J_f(\overrightarrow{EO})\Delta\overrightarrow{EO} \tag{4.11}$$

where J_f is the jacobian matrix associated to $\frac{d\overrightarrow{x}}{d\overrightarrow{EO}}\frac{d\overrightarrow{f}(EO)}{d\overrightarrow{EO}}$. Secondly, he projects the resulting relations in the orbital frame (RTN):

$$\Delta\overrightarrow{x}|_{RTN} = \mathcal{R}^{-1}J_f\Delta\overrightarrow{EO} \tag{4.12}$$

where $\mathcal{R}$ is defined in (2.6). So, he finds:

$$\Delta\overrightarrow{x}|_{RTN} = [\mathcal{M}(\overrightarrow{EO})]\Delta\overrightarrow{EO} \tag{4.13}$$

with the matrix $\mathcal{M}(\overrightarrow{EO}) = \mathcal{R}^{-1}J_f$:

$$\mathcal{M} = \begin{pmatrix} \frac{r}{a} & -a\cos f & 0 & 0 & 0 & \frac{ae}{\eta}\sin f \\ 0 & a\left(1+\frac{1}{\eta^2}\frac{r}{a}\right)\sin f & 0 & r\cos i & r & \frac{a^2\eta}{r} \\ 0 & 0 & r\sin u & -r\sin i\cos u & 0 & 0 \\ -\frac{na\sin f}{\eta}\frac{e}{2a} & -\frac{na\sin f}{\eta}\frac{a}{r} & 0 & -\frac{na^2\eta}{r}\cos i & -\frac{na^2\eta}{r} & -\frac{na^3}{r^2} \\ -\frac{na}{\eta}\frac{\eta^2}{2r} & \frac{na}{\eta}\frac{e+\cos f}{\eta^2} & 0 & \frac{na}{\eta}e\cos i\sin f & \frac{na}{\eta}e\sin f & 0 \\ 0 & 0 & \frac{na}{\eta}(\cos u + e\cos\omega) & \frac{na}{\eta}\sin i(\sin u + e\sin\omega) & 0 & 0 \end{pmatrix} \tag{4.14}$$

4.3.2 The inverse transformation using Poisson brackets

Different possibilities can be investigated to obtain the inverse transformation. The first idea is the direct inversion of the matrix $\mathcal{M}$. Even if possible, this method leads to complex results, very difficult to simplify. Another method could be a direct differentiation of expressions $\overrightarrow{EO} = f^{-1}(\overrightarrow{x})$ with later projection in orbital frame, using the same schema as Casotto. But, since equations $\overrightarrow{EO} = f^{-1}(\overrightarrow{x})$ are not explicit, this is very complex to achieve. There, we propose to take advantage of the properties of canonical variables, using Poisson brackets.

The Poisson bracket of two functions f, g is defined by:

$$\{f,g\}_{q,p} = \sum_{j=1}^{s}\left[\frac{\partial f}{\partial q_j}\frac{\partial g}{\partial p_j} - \frac{\partial f}{\partial p_j}\frac{\partial g}{\partial q_j}\right] \tag{4.15}$$

where q_j, p_j $(j = 1...s)$ are canonical conjugated variables. Using the theorem that proves that a transformation, $(p_j, q_j) \rightarrow (P_j, Q_j)$, is canonical, if, and only if it keeps the Poisson bracket [30], it is well-known that for two sets of canonical variables $(q;p) = (q_1, q_2, ..., q_s; p_1, p_2, ..., p_s)$, and $(Q;P) = (Q_1, Q_2, ..., Q_s; P_1, P_2, ..., P_s)$:

$$\begin{aligned} \frac{\partial Q_i}{\partial q_j} &= \frac{\partial p_j}{\partial P_i} & \frac{-\partial P_i}{\partial q_j} &= \frac{\partial p_j}{\partial Q_i} & \forall j, i = (1, ..., s) \\ \frac{\partial Q_i}{\partial p_j} &= \frac{-\partial q_j}{\partial P_i} & \frac{\partial P_i}{\partial p_j} &= \frac{\partial q_j}{\partial Q_i} \end{aligned} \tag{4.16}$$

With such a property, and a function V defined as a function of (p, q) and seen as a function of (P, Q) it is possible to deduce:

$$\begin{aligned} \frac{dV}{dq_j} &= \sum_{i=1}^{s} \frac{\partial V}{\partial Q_i}\frac{dQ_i}{dq_j} + \frac{\partial V}{\partial P_i}\frac{dP_i}{dq_j} \\ &= \sum_{i=1}^{s} \frac{\partial V}{\partial Q_i}\frac{dp_j}{dP_i} - \frac{\partial V}{\partial P_i}\frac{dp_j}{dQ_i} = \{V, p_j\} \end{aligned} \tag{4.17}$$

If we suppose moreover that the canonical variables p_α, q_α, $\alpha = 1..3$, are functions of orbital elements $\overrightarrow{EO} = (EO_1, ..., EO_6)^T$:

$$\begin{aligned}
\frac{dV}{dq_j} &= \sum_{i=1}^{3}\left(\frac{\partial V}{\partial Q_i}\frac{dp_j}{dP_i} - \frac{\partial V}{\partial P_i}\frac{dp_j}{dQ_i}\right) \\
&= \sum_{i=1}^{3}\left(\frac{\partial V}{\partial Q_i}\sum_{k=1}^{6}\frac{dp_j}{dEO_k}\frac{dEO_k}{dP_i} - \frac{\partial V}{\partial P_i}\sum_{k=1}^{6}\frac{dp_j}{dEO_k}\frac{dEO_k}{dQ_i}\right) \\
&= \sum_{k=1}^{6}\frac{dp_j}{dEO_k}\{V, EO_k\}
\end{aligned} \tag{4.18}$$

Applying this relation to an orbital element EO_i, we get:

$$\frac{dEO_i}{dq_j} = \sum_{k=1}^{6}\frac{dp_j}{dEO_k}\{EO_i, EO_k\} \tag{4.19}$$

With a completely equivalent proof we can also deduce:

$$\frac{dEO_i}{dp_j} = -\sum_{k=1}^{6}\frac{dq_j}{dEO_k}\{EO_i, EO_k\} \tag{4.20}$$

The interest of these equations lies in the possibility to compute the derivatives of each orbital element with respect to canonical variables using the derivatives of these canonical variables with respect to orbital elements. Poisson brackets of orbital elements are well-known [25]:

$$\{a, M\} = -\tfrac{2}{na} \qquad \{e, M\} = -\tfrac{1-e^2}{na^2 e} \qquad \{i, \omega\} = -\tfrac{1}{\sqrt{1-e^2}na^2}\tfrac{\cos i}{\sin i}$$
$$\{e, \omega\} = \tfrac{\sqrt{1-e^2}}{na^2 e} \quad \{i, \Omega\} = \tfrac{1}{\sqrt{1-e^2}na^2}\tfrac{1}{\sin i}$$

All other brackets are equal to zero. Since the position and the velocity in the inertial frame form a set of canonical variables [30] we can use them in equations (7.12), (7.27) and we obtain:

$$\begin{aligned}
\frac{dEO_i}{d\vec{r}|_{IJK}} &= \sum_k \frac{d\vec{v}|_{IJK}}{dEO_k}\{EO_i, EO_k\} \\
\frac{dEO_i}{d\vec{v}|_{IJK}} &= -\sum_k \frac{d\vec{r}|_{IJK}}{dEO_k}\{EO_i, EO_k\}
\end{aligned} \tag{4.21}$$

As we are interested in the derivatives with respect to inertial position and velocity, projected in the orbital frame, we can keep the previous expressions just projected in the orbital frame (the canonicity is preserved under a rotation):

$$\begin{aligned}
\frac{dEO_i}{d\vec{r}|_{RTN}} &= \sum_k \frac{d\vec{v}|_{RTN}}{dEO_k}\{EO_i, EO_k\} \\
\frac{dEO_i}{d\vec{v}|_{RTN}} &= -\sum_k \frac{d\vec{r}|_{RTN}}{dEO_k}\{EO_i, EO_k\}
\end{aligned} \tag{4.22}$$

Previous formula does not apply to relative position $\overrightarrow{\rho}$ and velocity $\dot{\overrightarrow{\rho}}$ because they do not form a set of canonical variables.

The derivatives of position and velocity computed in section 4.3.1 (4.14) can be used in equation (4.22) to obtain following results:

$$\mathcal{M}^{-1} = \begin{pmatrix} 2\left(\frac{a}{r}\right)^2 & 0 & 0 & 2\frac{e}{n\eta}\sin f & 2\frac{\eta}{n}\frac{a}{r} & 0 \\ \frac{\eta^2}{re}\left(\frac{a}{r}-1\right) & \frac{\sin f}{a} & 0 & \frac{\eta}{na}\sin f & \frac{\eta}{en}\left(\frac{\eta^2}{r}-\frac{r}{a^2}\right) & 0 \\ 0 & 0 & \frac{\sin u + e\sin\omega}{\eta^2}\frac{1}{a} & 0 & 0 & \frac{r\cos u}{\eta n a^2} \\ 0 & 0 & -\frac{\cos u + e\cos\omega}{\eta^2 a\sin i} & 0 & 0 & \frac{r}{na^2}\frac{\sin u}{\eta\sin i} \\ \frac{\sin f}{re} & -\frac{e+\cos f}{\eta^2 ae} & \frac{\cos u + e\cos\omega}{\eta^2 a\tan i} & -\frac{\cos f\eta}{nae} & \left(1+\frac{1}{\eta^2}\frac{r}{a}\right)\frac{\sin f\eta}{nae} & -\frac{r\sin u}{\eta n a^2\tan i} \\ -\frac{\sin f}{\eta}\left(\frac{\eta^2}{re}+\frac{e}{a}\right) & \frac{1}{\eta}\left(\frac{e+\cos f}{ea}-\frac{\eta^2}{r}\right) & 0 & \frac{1}{na}\left(\frac{\eta^2\cos f}{e}-2\frac{r}{a}\right) & -\frac{\sin f}{nae}\left(\frac{r}{a}+\eta^2\right) & 0 \end{pmatrix} \tag{4.23}$$

4.4 Application to the keplerian case

First, we apply our method to the description of relative motion in the case of the non-perturbed linear keplerian motion described by equation (4.10). Since matrices $\mathcal{M}$ and $\mathcal{M}^{-1}$ are known, only the temporal evolution of orbital elements and the matrix $\mathcal{L}_{kep}$ remain to be expressed. For the keplerian case, all elements keep constant values except the mean anomaly which is linear with time.

$$\begin{aligned} EO_i(t) &= EO_i(t_0) \qquad i = 1....5 \\ M(t) &= M(t_0) + n_0(t - t_0) \end{aligned} \tag{4.24}$$

Initial orbital elements at initial time (t_0) are referenced by the subscript $_0$. Differential orbital elements $(\Delta\overrightarrow{EO})$ evolve exactly in the same way: all differences keep constant values except the difference of mean anomalies which evolves linearly:

$$\begin{aligned} \Delta EO_i(t) &= \Delta EO_i(t_0) \qquad i = 1....5 \\ \Delta M(t) &= \Delta M(t_0) + \Delta n_0(t - t_0) \end{aligned} \tag{4.25}$$

with:

$$\Delta n_0 = n(t_0) - n_{ref}(t_0) = \sqrt{\frac{\mu}{(a_{ref} + \Delta a)^3(t_0)}} - \sqrt{\frac{\mu}{a^3_{ref}(t_0)}} \tag{4.26}$$

The variation of the differential mean anomaly ΔM is linear with respect to the differences of orbital frequencies Δn_0, but not with respect to the initial difference of semi-major axis (Δa_0). In the framework of a linear approach, it is consistent to use:

$$\Delta n = -\frac{3}{2}\frac{n}{a}\Delta a \tag{4.27}$$

Finally, the matrix $\mathcal{L}_{kep}$ reads:

$$
\mathcal{L}_{kep} = \begin{pmatrix} 1 & 0 & 0 & 0 & 0 & 0 \\ 0 & 1 & 0 & 0 & 0 & 0 \\ 0 & 0 & 1 & 0 & 0 & 0 \\ 0 & 0 & 0 & 1 & 0 & 0 \\ 0 & 0 & 0 & 0 & 1 & 0 \\ -\frac{3}{2}\frac{n}{a}(t-t_0) & 0 & 0 & 0 & 0 & 1 \end{pmatrix} \tag{4.28}
$$

Inserting $\mathcal{M}$ (4.14), $\mathcal{L}$ (4.28), and $\mathcal{M}^{-1}$ (4.23) in equation (4.10), we get:

$$
\begin{aligned}
\Delta R(t) &= K_1\frac{r}{a} - K_2\cos f + K_3\sin f - \frac{3}{2}\frac{ne}{\eta}K_1\sin f(t-t_0) \\
\Delta T(t) &= K_2\sin f + \frac{1}{\eta^2}K_2\frac{r}{a}\sin f + \frac{\eta^2}{e}K_3\frac{a}{r} - \frac{3}{2}n\eta K_1\frac{a}{r}(t-t_0) + K_4\frac{r}{a} \\
\Delta N(t) &= K_5\frac{r}{a}\cos f + K_6\frac{r}{a}\sin f
\end{aligned} \tag{4.29}
$$

with the coefficients:

$$
\begin{aligned}
K_1 &= 2\left(\frac{a}{r_0}\right)^2\Delta R_0 + 2\frac{e}{n\eta}\sin f_0\Delta V_{R0} + 2\frac{\eta}{n}\frac{a}{r_0}\Delta V_{T0} \\
K_2 &= \frac{a\eta^2}{r_0 e}\left(\frac{a}{r_0}-1\right)\Delta R_0 + \sin f_0\Delta T_0 + \frac{\eta}{n}\sin f_0\Delta V_{R0} + \frac{\eta}{en}\left(\frac{a\eta^2}{r_0} - \frac{r_0}{a}\right)\Delta V_{T0} \\
K_3 &= \frac{ae}{\eta}\Big[-\frac{\sin f_0}{\eta}\left(\frac{\eta^2}{r_0 e}+\frac{e}{a}\right)\Delta R_0 + \frac{1}{\eta}\left(\frac{e+\cos f_0}{ea} - \frac{\eta^2}{r_0}\right)\Delta T_0 \\
&\quad + \frac{1}{na}\left(\frac{\eta^2\cos f_0}{e} - 2\frac{r_0}{a}\right)\Delta V_{R0} - \frac{\sin f_0}{nae}\left(\frac{r_0}{a}+\eta^2\right)\Delta V_{T0}\Big] \\
K_4 &= \frac{a\sin f_0}{r_0 e}\Delta R_0 - \frac{e+\cos f_0}{\eta^2 e}\Delta T_0 - \frac{\cos f_0\eta}{ne}\Delta V_{R0} + \left(1+\frac{1}{\eta^2}\frac{r_0}{a}\right)\frac{\sin f_0\eta}{ne}\Delta V_{T0} \\
K_5 &= \frac{1}{\eta^2}\left(\cos f_0 + e\right)\Delta N_0 - \sin f_0\frac{r_0}{a\eta n}\Delta V_{N0} \\
K_6 &= \frac{1}{\eta^2}\Delta N_0\sin f_0 + \frac{r_0}{\eta na}\Delta V_{N0}\cos f_0
\end{aligned} \tag{4.30}
$$

These equations are equivalent to Lawden's equations [47] that we have presented in the precedent chapter. We can see the advantage of this second method because we have obtained the constants as function of initial conditions and we have avoid the introduction of the integrals as in Lawden [47].

4.5 The circular reference orbit

The matrix $\mathcal{M}^{-1}$ is singular in case of circular orbit. Since the perigee is not defined in the circular case, it is necessary to use the non-singular elements defined in (2.4). Linear relations between the differences of non-singular and orbital elements can be obtained by differentiation:

$$
\begin{aligned}
\Delta e &= \Delta C \cos\omega_r + \Delta S \sin\omega_r \\
e_r \Delta\omega &= \Delta S \cos\omega_r - \Delta C \sin\omega_r \\
\Delta\omega + \Delta M &= \Delta\lambda
\end{aligned}
\tag{4.31}
$$

With these elements, in circular case, linear approach leads to:

$$
\begin{aligned}
\Delta\overrightarrow{ENS}(t_0) &= [\mathcal{N}^{-1}(\overrightarrow{ENS}_{ref})]\Delta\overrightarrow{x}(t_0)|_{RTN} \\
\Delta\overrightarrow{ENS}(t) &= [\mathcal{L}(\overrightarrow{ENS}_{ref}(t))]\Delta\overrightarrow{ENS}(t_0) \\
\Delta\overrightarrow{x}(t)|_{RTN} &= [\mathcal{N}(\overrightarrow{ENS}_{ref})]\Delta\overrightarrow{ENS}(t)
\end{aligned}
\tag{4.32}
$$

with matrices $\mathcal{N}$ and $\mathcal{N}^{-1}$:

$$
\mathcal{N}|_{e=0} = \begin{pmatrix}
1 & -a\cos\lambda & 0 & 0 & -a\sin\lambda & 0 \\
0 & 2a\sin\lambda & 0 & a\cos i & -2a\cos\lambda & a \\
0 & 0 & a\sin\lambda & -a\sin i\cos\lambda & 0 & 0 \\
0 & -na\sin\lambda & 0 & -na\cos i & na\cos\lambda & -na \\
-\frac{n}{2} & na\cos\lambda & 0 & 0 & na\sin\lambda & 0 \\
0 & 0 & na\cos\lambda & na\sin i\sin\lambda & 0 & 0
\end{pmatrix}
$$

$$
\mathcal{N}^{-1}|_{e=0} = \begin{pmatrix}
2 & 0 & 0 & \frac{2}{n} & 0 & 0 \\
\frac{\cos\lambda}{a} & \frac{\sin\lambda}{a} & 0 & \frac{\sin\lambda}{na} & \frac{2\cos\lambda}{na} & 0 \\
0 & 0 & \frac{\sin\lambda}{a} & 0 & 0 & \frac{\cos\lambda}{na} \\
0 & 0 & -\frac{\cos\lambda}{a\sin i} & 0 & 0 & \frac{\sin\lambda}{na\sin i} \\
\frac{\sin\lambda}{a} & -\frac{\cos\lambda}{a} & 0 & -\frac{\cos\lambda}{na} & \frac{2\sin\lambda}{na} & 0 \\
0 & \frac{-1}{a} & \frac{\cos\lambda}{a\tan i} & -\frac{2}{na} & 0 & -\frac{\sin\lambda}{na\tan i}
\end{pmatrix}
$$

The matrix $\mathcal{L}$ is not modified. Applying the same composition of matrices as in the eccentric case (4.10) we obtain the linear non-perturbed equations for the circular reference orbit:

$$
\begin{aligned}
\Delta R(t) &= \left(\Delta T_0 + \frac{\Delta V_{R0}}{n_0}\right)\sin n_0(t-t_0) - \left(2\frac{\Delta V_{T0}}{n_0} + \Delta R_0\right)\cos n_0(t-t_0) + \left(2\frac{\Delta V_{T0}}{n_0} + 2\Delta R_0\right) \\
\Delta T(t) &= 2\left(\Delta T_0 + \frac{\Delta V_{R0}}{n_0}\right)\cos n_0(t-t_0) + \left(4\frac{\Delta V_{T0}}{n_0} + 2\Delta R_0\right)\sin n_0(t-t_0) \\
&\quad - \left(2\frac{\Delta V_{R0}}{n_0} + \Delta T_0\right) - 3\left(\Delta V_{T0} + n_0\Delta R_0\right)(t-t_0) \\
\Delta N(t) &= \Delta N_0 \cos n_0(t-t_0) + \frac{\Delta V_{N0}}{n_0}\sin n_0(t-t_0)
\end{aligned}
\tag{4.33}
$$

These equations are equivalent to Hill solution introduced in chapter 3 but expressed in terms of differences of velocity (3.13).

4.6 Conclusions

In this chapter we have presented a new method to obtain analytical expressions of relative motion expressed in cartesian coordinates as function of initial conditions and time, $\Delta\overrightarrow{x}(t) = f\left(\Delta\overrightarrow{x}(t_0), \overrightarrow{EO}_{ref}(t), t\right)$. This method can be applied to different kind of perturbations, for eccentric reference orbit. In order to apply this method, we have first used the properties of Poisson brackets to derive linear relations between two representations of relative motion, differences of position and velocity ($\Delta\overrightarrow{x}|_{RTN}$) and differences of orbital elements ($\Delta\overrightarrow{EO}$).

This work follows the direction marked by precedent works of Casotto, Garrison, and Alfriend. It is, the use of differences of orbital elements for orbit extrapolation, and transformations between different representations to project the results in the local orbital frame. The orbital elements have been chosen because they are well suited for the introduction of the gravity field, and to keep simple analytical expressions. The use of differences of velocities ($\Delta\overrightarrow{v}|_{RTN}$) instead of relative velocities is determined by the further utilisation of equations, since these variables are better adapted for mission analysis.

In the second part of the thesis, differential orbital elements will be used extensively in order to obtain the effects of different perturbations. It will be applied to the gravity field and to the solar radiation pressure. This method can be applied to all kind of perturbations with the only condition that perturbative force must be conservative.

Chapter 5

The local orbital elements

5.1 Introduction

Two precedent chapters were devoted to the derivation of the equations of the relative motion. But, the resulting equations do not enable an insight of the relative trajectories. That is why we have worked in obtaining an alternative representation with a better physical meaning.
Inspired by the two-body problem, we propose an alternative representation of the relative motion. Under certain conditions, it is possible to define an adapted set of orbital elements with respect to the local reference frame that we name local orbital elements. The local orbital elements are well suited when the relative motion describes a trajectory close to an ellipse. In this chapter we present the necessary conditions for having elliptical motions and the relations between other representations and local orbital elements for the unperturbed case.
Section two is devoted to the relative motion in the case of circular reference orbit and to the definition of the local orbital elements. In section three, we study the case of the non-circular reference orbit.

5.1.1 The equations of the relative motion

As we explained in precedent chapter, we can obtain the equations of motion combining matrices $[\mathcal{M}][\mathcal{L}][\mathcal{M}]^{-1}$. When we combine only two of them $[\mathcal{M}][\mathcal{L}]$, in the keplerian case, we get the following equations:

$$\begin{aligned}
\Delta R(t) &= \frac{r_r}{a_r}\Delta a_0 - a_r \cos f_r \Delta e_0 + \frac{a_r e_r}{\eta_r}\sin f_r \Delta M_0 - \frac{3}{2}\frac{n_r e_r}{\eta_r}\sin f_r (t-t_0)\Delta a_0 \\
\Delta T(t) &= a_r\left(1+\frac{1}{\eta_r^2}\frac{r_r}{a_r}\right)\sin f_r \Delta e_0 + r_r \cos i_r \Delta\Omega_0 + r_r\Delta\omega_0 + \frac{a_r^2\eta_r}{r_r}\Delta M_0 \\
&\quad - \frac{3}{2}\frac{a_r n_r \eta_r}{r_r}(t-t_0)\Delta a_0 \\
\Delta N(t) &= r_r \sin u_r \Delta i_0 - r_r \sin i_r \cos u_r \Delta\Omega_0
\end{aligned} \tag{5.1}$$

For clarity's sake, the subscript for the reference orbit is $_r$ instead of $_{ref}$. These equations give temporal evolution of relative position projected in the local orbital frame as function of six parameters: $\Delta\overrightarrow{EO}(t_0)$. Thereafter, we will describe resulting motion in two cases: (i) when the reference orbit is circular, (ii) when the reference orbit is eccentric.

5.2 The circular reference orbit case

Direct particularization of equations (5.1) is not correct because of the singularity of orbital elements in circular case. It is necessary to introduce non-singular elements (defined in 2.4) in equations (5.1) to particularize to the circular case. We finally obtain:

$$\begin{aligned}
\Delta R(t) &= \Delta a_0 - a_r\left(\cos\lambda\Delta C_0 + \sin\lambda\Delta S_0\right) \\
\Delta T(t) &= a_r\left(2\sin\lambda\Delta C_0 - 2\cos\lambda\Delta S_0 + \Delta\lambda_0 + \cos i_r\Delta\Omega_0 - \frac{3}{2}n(t-t_0)\Delta a_0\right) \\
\Delta N(t) &= a_r\left(\sin\lambda\Delta i_0 - \sin i_r\cos\lambda\Delta\Omega_0\right)
\end{aligned} \tag{5.2}$$

Thereafter, we analyze the resulting motion described by equations (5.2). We note that they correspond to the standard parametrical equation of an ellipse centered on the origin of the local frame except for two kind of terms:

- *terms providing from a difference of semi-major axis*: a difference of semi-major axis leads to different orbital frequencies which produce a secular growth of the ΔT term. As this effect destroys the formation in a short period of time, we impose: $\Delta a_0 = 0$. This hypothesis may not be true for docking or rendezvous operations, but it is always fulfilled in Keplerian formation flying.

- *constant term on the T axis*: this term, $(\Delta\lambda_0 + \cos i_r\Delta\Omega_0)$, can be removed just by a shift on the origin of the axis. That is why we ignore it.

Disgarding foregoing terms, equations (5.2) rewrite:

$$\begin{aligned}
\Delta R &= -a_r\Delta C_0\cos\lambda - a_r\Delta S_0\sin\lambda \\
\Delta T &= -2a_r\Delta S_0\cos\lambda + 2a_r\Delta C_0\sin\lambda \\
\Delta N &= -a_r\Delta\Omega_0\cos\lambda + a_r\Delta i_0\sin\lambda
\end{aligned} \tag{5.3}$$

which correspond to the elliptical trajectory. As it is usually done in the two-body problem, the elliptical motion will be parametrized through a set of orbital elements called *local orbital elements* ($\overrightarrow{eo_l}$): semi-major axis (a_l), eccentricity (e_l), inclination (i_l), longitude of ascending node (Ω_l), longitude of perigee (ω_l) and anomaly (M_l).

There are two main differences with respect to classical keplerian elliptical motion (i) the origin of the axis does not correspond to a focus of the ellipse, but to the center. This leads to an ambiguity on the definition of the longitude of the perigee which is solved by imposing that $\omega \in [0, \pi]$ (ii) the angular velocity is not dependent on the distance to the origin, but is constant and equal to the angular velocity of the reference frame. That is, the period of any local orbit corresponds to the period of the reference frame.

Thereafter, we derive the analytical relations between the initial conditions expressed in terms of $\Delta\overrightarrow{ENS}$ and the local orbital elements.

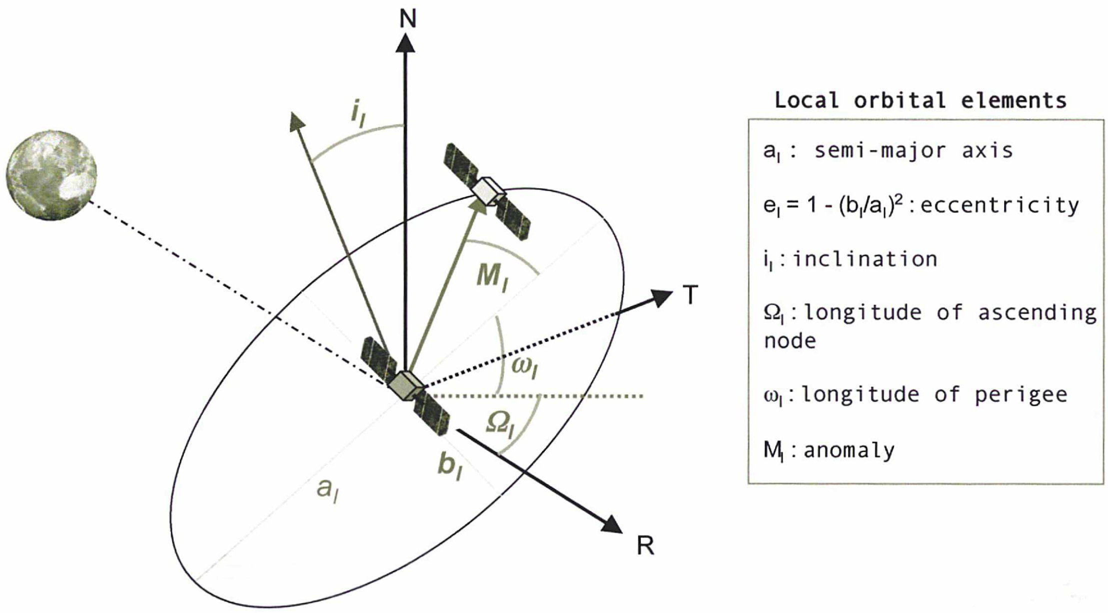

Figure 5.1: *definition of local orbital elements*

5.2.1 The local orbital elements as function of initial conditions

In a first stage, we will find the relations between a generic ellipse defined by its constants $\overrightarrow{P} = (A, B, C, D, E, F)^T$ such as:

$$\begin{aligned} \Delta R &= A\cos\lambda + B\sin\lambda \\ \Delta T &= C\cos\lambda + D\sin\lambda \\ \Delta N &= E\cos\lambda + F\sin\lambda \end{aligned} \tag{5.4}$$

and the local orbital elements. The second stage will consist in replacing the constants $\overrightarrow{P}$ by the differences of non-singular elements $\Delta\overrightarrow{ENS}$.

The elliptical motion expressed in the frame defined by the principal axis of the ellipse in terms of local orbital elements writes:

$$\begin{aligned} x_{PA} &= a_l \cos\left(M_l(t)\right) \\ y_{PA} &= a_l \eta_l \sin\left(M_l(t)\right) \\ z_{PA} &= 0 \end{aligned} \tag{5.5}$$

The transformation between the axis defined by the principal axis of the ellipse and the RTN frame is done through the matrix $\mathcal{R}$:

$$(\Delta R, \Delta T, \Delta N)^T = [\mathcal{R}]\left(x_{PA}, y_{PA}, z_{PA}\right)^T \tag{5.6}$$

with:

$$\mathcal{R} = \begin{pmatrix} \cos\Omega_l\cos\omega_l - \sin\Omega_l\sin\omega_l\cos i_l & -\cos\Omega_l\sin\omega_l - \sin\Omega_l\cos\omega_l\cos i_l & \sin\Omega_l\sin i_l \\ \sin\Omega_l\cos\omega_l + \cos\Omega_l\sin\omega_l\cos i_l & -\sin\Omega_l\sin\omega_l + \cos\Omega_l\cos\omega_l\cos i_l & -\cos\Omega_l\sin i_l \\ \sin\omega_l\sin i_l & \cos\omega_l\sin i_l & \cos i_l \end{pmatrix}$$

As temporal evolution of the motion is described by the angle λ in equations (5.4) and by the angle M_l in equations (5.5), both angles must be equal up to a constant phase: $M_l = \lambda - \varphi_l$. In order to obtain the relations between $\overrightarrow{P}$ and $\overrightarrow{eo}_l$, we do the following operations. First, we identify the vector $\overrightarrow{h} = (h_x, h_y, h_z)^T$ normal to the plan of the ellipse, expressed as function of local orbital elements on the one hand, and expressed as function of $\overrightarrow{P}$ on the other hand:

$$\begin{aligned} h_x &= h\sin i_l\sin\Omega_l = CF - DE \\ h_y &= -h\sin i_l\cos\Omega_l = BE - AF \\ h_z &= h\cos i_l = AD - BC \end{aligned} \tag{5.7}$$

with:

$$h = \sqrt{h_x^2 + h_y^2 + h_z^2} \tag{5.8}$$

This leads to:

$$\begin{aligned} \sin\Omega_l &= \frac{h_x}{\sqrt{h_x^2 + h_y^2}} \\ \cos\Omega_l &= \frac{-h_y}{\sqrt{h_x^2 + h_y^2}} \\ \cos i_l &= \frac{h_z}{\sqrt{h_x^2 + h_y^2 + h_z^2}} \end{aligned} \tag{5.9}$$

Second, we write the expressions of the distance to the center of an ellipse expressed through its parametric form, and through its local orbital elements. According to (5.4), the distance expressed in terms of $\overrightarrow{P}$ is:

$$\begin{aligned} d^2 = {} & \left(A^2 + C^2 + E^2\right)\cos^2\lambda + \left(B^2 + D^2 + F^2\right)\sin^2\lambda + \\ & + (AB + CD + EF)\sin 2\lambda \end{aligned} \tag{5.10}$$

The distance, using equation (5.5) is:

$$\begin{aligned} d^2 = {} & \left(a^2\cos^2\varphi + a^2\eta^2\sin^2\varphi\right)\cos^2\lambda + \left(a^2\sin^2\varphi + a^2\eta^2\cos^2\varphi\right)\sin^2\lambda + \\ & + \left(a^2\eta^2 - a^2\right)\sin\varphi\cos\varphi\sin 2\lambda \end{aligned} \tag{5.11}$$

The identification of the coefficients of $\cos^2\lambda$, $\sin^2\lambda$ and $\sin 2\lambda$ in equations (5.10) and (5.11) yields:

$$\begin{aligned} a_l^2 \sin 2\varphi_l \left(1 - \eta_l^2\right) &= K_3 \\ a_l^2 \left(1 + \eta_l^2\right) &= K_1 + K_2 \\ a_l^2 \cos 2\varphi_l \left(1 - \eta_l^2\right) &= K_1 - K_2 \end{aligned} \tag{5.12}$$

where:

$$K_1 = A^2 + C^2 + E^2 \qquad K_2 = B^2 + D^2 + F^2 \qquad K_3 = 2(AB + CD + EF) \tag{5.13}$$

The resolution of the system (5.13) gives:

$$2a_l^2 = K_1 + K_2 + \sqrt{(K_1 - K_2)^2 + K_3^2} \tag{5.14}$$

$$1 - \eta_l^2 = e_l^2 = 2 - \frac{K_1 + K_2}{a_l^2} \tag{5.15}$$

$$\sin 2\varphi_l = \frac{K_3}{a_l^2 e_l^2} \qquad \cos 2\varphi_l = \frac{K_1 - K_2}{a_l^2 e_l^2} \tag{5.16}$$

To compute the longitude of the local perigee, we identify the expression of ΔN given by equation (5.4) and by equation (5.6)

$$E \cos\lambda + F \sin\lambda = a_l \cos\lambda - \varphi_l \sin\omega_l \sin i_l + a_l \eta_l \sin\lambda - \varphi_l \cos\omega_l \sin i_l \tag{5.17}$$

which leads to:

$$\begin{aligned} E &= a \sin i \cos\omega \cos\varphi_l (\tan\omega - \eta \tan\varphi_l) \\ F &= a \sin i \cos\omega \cos\varphi_l (\tan\omega \tan\Omega_0 + \eta) \end{aligned} \tag{5.18}$$

The solution for ω_l writes:

$$\cos\omega_l = \frac{1}{a_r \eta_r \sin i_r} (F \cos\varphi_l - E \sin\varphi_l) \qquad \sin\omega_l = \frac{1}{a_r \sin i_r} (F \sin\varphi_l + E \cos\varphi_l) \tag{5.19}$$

Once we have obtained the relations between $\overrightarrow{P}$ and $\overrightarrow{eo}_l$, we express $\overrightarrow{P}$ as function of $\Delta\overrightarrow{ENS}$ using equations (5.3) and (5.4):

$$\begin{aligned} A &= -a_r \Delta C_0 & B &= -a_r \Delta S_0 \\ C &= -2a_r \Delta S_0 & D &= 2a_r \Delta C_0 \\ E &= -a_r \sin i_r \Delta\Omega_0 & F &= a_r \Delta i_0 \end{aligned}$$

We summarize final relations between $\Delta\overrightarrow{ENS}$ and $\overrightarrow{eo}_l$:

$$
\begin{array}{|l|}
\hline
\vec{h} = (2(\Delta C_0 \Delta \Omega_0 - \Delta S_0 \Delta i_0), \Delta C_0 \Delta i_0 + \Delta S_0 \Delta \Omega_0, -2(\Delta C_0^2 + \Delta S_0^2))^T \\
\sin \Omega_l = \dfrac{h_x}{\sqrt{h_x^2 + h_y^2}} \qquad \cos \Omega_l = \dfrac{-h_y}{\sqrt{h_x^2 + h_y^2}} \\
\cos i_l = \dfrac{h_z}{\sqrt{h_x^2 + h_y^2 + h_z^2}} \\
K_1 = a_r^2(\Delta C_0^2 + 4\Delta S_0^2 + \sin^2 i_r \Delta \Omega_0^2) \qquad K_2 = a_r^2(\Delta S_0^2 + 4\Delta C_0^2 + \Delta i_0^2) \\
K_3 = 2a_r^2(-3\Delta C_0 \Delta S_0 - \sin i_r \Delta \Omega_0 \Delta i_0) \\
2a_l^2 = K_1 + K_2 + \sqrt{(K_1 - K_2)^2 + K_3^2} \qquad e_l^2 = 2 - \dfrac{K_1 + K_2}{a_l^2} \\
\sin 2\varphi = \dfrac{K_3}{a_l^2 e_l^2} \qquad \cos 2\varphi = \dfrac{K_1 - K_2}{a_l^2 e_l^2} \\
\cos \omega_l = \dfrac{a_r}{a_l \eta_l \sin i_l} (\Delta i \cos \varphi_l + \Delta \Omega \sin i_r \sin \varphi_l) \\
\sin \omega_l = \dfrac{a_r}{a_l \sin i_l} (\Delta i \sin \varphi_l - \Delta \Omega \sin i_r \cos \varphi_l) \\
\hline
\end{array}
\tag{5.20}
$$

5.2.2 Topology of the relative motion

Only four differences of non-singular elements contribute to the determination of the six local orbital elements defined above. Indeed, Δa_0 has been fixed to zero in order not to spread the formation and $\Delta\lambda_0$ only contributes to shift the center of the local ellipse along the T axis. Consequently, only four local orbital elements are independent.

The size (a_l) and the constant phase (φ_l) can always be chosen to our convenience. The other four parameters may be separated in two groups: the elements which give the form of the local orbit (e_l, ω_l), and the elements which give the orientation of the plan of the local orbit (i_l, Ω_l). One group determines the other. We have decided to express the local eccentricity and the local perigee as function of other variables (i_l, Ω_l). Tedious, but simple, algebraic manipulations yield:

$$
\frac{e_l^4}{(2 - e_l^2)^2} = \frac{\left[9 + 6\tan^2 i_l (4\cos^2 \Omega_l - \sin^2 \Omega_l) + \tan^4 i_l (4\cos^2 \Omega_l + \sin^2 \Omega_l)^2\right]}{\left(5 + \tan^2 i_l (4\cos^2 \Omega_l + \sin^2 \Omega_l)\right)^2} \tag{5.21}
$$

and:

$$
\tan^2 \omega_l - \frac{3(\cos^2 \Omega_l - \sin^2 \Omega_l) + \sin^2 i_l (\cos^2 \Omega_l + 4\sin^2 \Omega_l)}{3\cos i_l \cos \Omega_l \sin \Omega_l} \tan \omega_l - 1 = 0 \tag{5.22}
$$

Equation (5.21) is plotted in figure 5.2 while equation (5.22) is plotted in figure 5.3.

5.2.3 Particular local orbits

Figure (5.2) presents two particular motions: (i) null local eccentricity (invariant plans), and (ii) local eccentricity equal to one (non-elliptical motion)

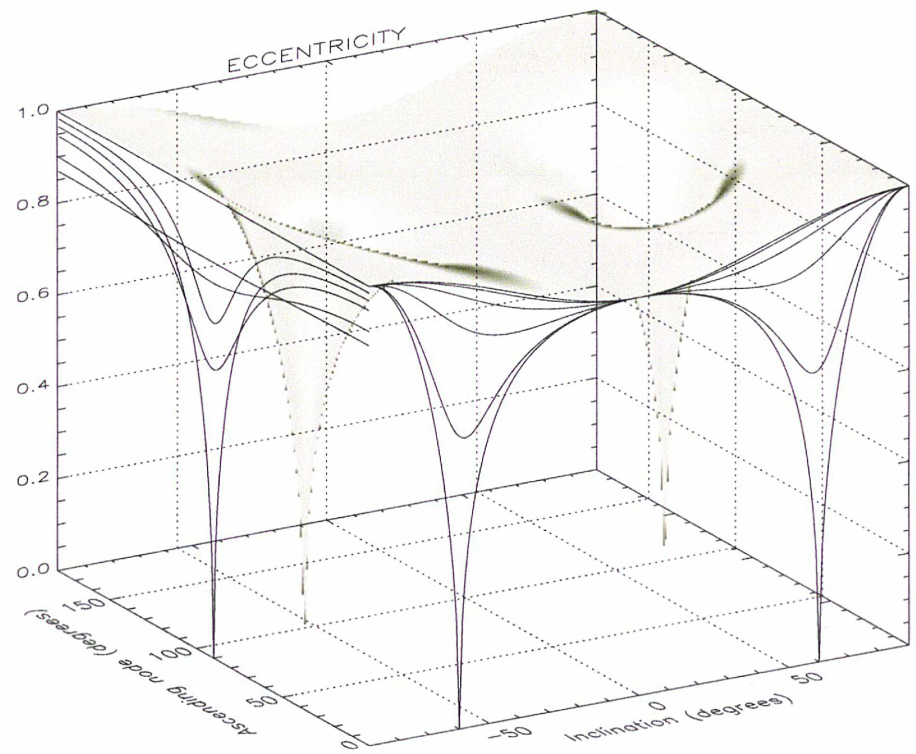

Figure 5.2: *Local eccentricity as function of the local inclination and the local longitude of the ascending node*

Invariant plans

There are two points in figure (5.2) where local eccentricity is zero. Using equation (5.21), it is possible to determine their local plan:

$$\begin{aligned} i_{l1} &= 60^\circ \qquad \Omega_{l1} = 90^\circ \\ i_{l2} &= -60^\circ \qquad \Omega_{l2} = 90^\circ \end{aligned} \tag{5.23}$$

And, using equations (5.20), we can find their corresponding initial conditions:

$$\begin{aligned} \Delta\overrightarrow{ENS}_1 &= (0, \Delta C, -\sqrt{3}\Delta S, \frac{\sqrt{3}\Delta C}{\sin_r}, \Delta S, \Delta\lambda)^T \\ \Delta\overrightarrow{ENS}_2 &= (0, \Delta C, \sqrt{3}\Delta S, -\frac{\sqrt{3}\Delta C}{\sin_r}, \Delta S, \Delta\lambda)^T \end{aligned} \tag{5.24}$$

According to (5.20), ΔC and ΔS determine the size (a_l) and the constant phase of the ellipse (φ_l).
These two particular local plans where the local motion is circular, have a very interesting

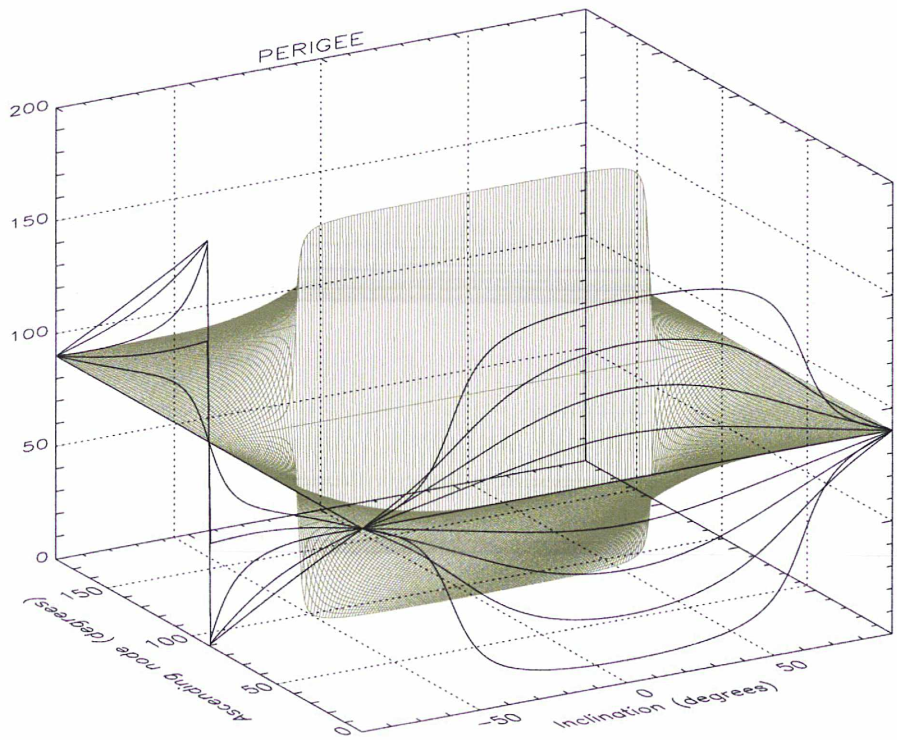

Figure 5.3: *Local perigee as function of the local inclination and the local longitude of the ascending node*

property: due to the fact that the local orbital frequency is independent of the distance to the origin, all the satellites rotate at the same angular velocity around the center of the ellipse and their relative distances do not change. As a consequence, all initial configurations remain invariant all along the trajectory. These plans represent very interesting possibilities for formation flying where it is necessary to keep inter-relative distances constant, as in interferometry missions or future LISA. Residual variations of the distance will be produced by perturbations and non-linear effects that have been neglected.

Non-elliptical motions

Second particular case corresponds to the eccentricity equal to one. If we impose $e = 1$ in equation (5.15), we find the following conditions for the initial differences of non-singular elements: $\Delta C = 0$, $\Delta S = 0$, corresponding to $\overrightarrow{h} = \overrightarrow{0}$. As a consequence, the local inclination and the longitude of the local ascending node are no more defined. In fact, using third equation of (5.9), we can compute:

$$\lim_{\Delta C, \Delta S \to 0} \left(\cos \frac{h_z}{\sqrt{h_x^2 + h_y^2}} \right) \to 0 \tag{5.25}$$

So, the value of the local inclination is $i_l = 90°$ as can be checked in figure (5.2). Setting $\Delta C = \Delta S = 0$ in the equations of motion (5.3) gives:

$$\begin{aligned}
\Delta R(t) &= 0 \\
\Delta T(t) &= 0 \\
\Delta N(t) &= a_r \left(\sin \lambda \Delta i_0 - \sin i_r \cos \lambda \Delta \Omega_0\right)
\end{aligned} \tag{5.26}$$

This particular case is not a parabolic motion as expected in the two-body problem when $e = 1$, but a periodic motion in the N axis. The combination of this motion with a constant term in the T axis ($\Delta\lambda_0 - \cos i_r \Delta\Omega_0$) gives very interesting configurations for flight formations: the second satellite follows the first one with a constant offset on the T axis and a variable term on the N axis. Thus, choosing the adequate values for the N axis term, it is possible to obtain formations with the same ground track for all the satellites. This characteristic is fundamental for Earth observation missions. Some examples are A-TRAIN and TOPEX-JASON satellites.

5.3 The eccentric reference orbit case

5.3.1 Low eccentric reference orbit case

When the reference orbit is sligthly eccentric, we simplify equations (5.1) by means of an expansion of $\frac{r_r}{a_r}, \frac{a_r}{r_r}, \cos f_r, \sin f_r$ in powers of the eccentricity up to first order:

$$\begin{aligned}
\frac{\Delta R}{a_r} &= -\cos\lambda\left(\Delta C_0 + S_r \Delta\lambda_0\right) - \sin\lambda\left(\Delta S_0 - C_r \Delta\lambda_0\right) + \mathcal{O}(e^2) \\
\frac{\Delta T}{a_r} &= \sin\lambda\left[2\Delta C_0 + S_r\left(\Delta\lambda_0 - \Delta\Omega_0 \cos i_r\right)\right] + \cos\lambda\left[-2\Delta S_0 + C_r\left(\Delta\lambda_0 - \Delta\Omega_0 \cos i_r\right)\right] \\
&\quad + \left(\Delta\lambda_0 - \Delta\Omega_0 \cos i_r\right) - \Delta e_0 \frac{e_r}{2}\left(\sin 2\lambda \cos 2\omega_r - \cos 2\lambda \sin 2\omega_r\right) + \mathcal{O}(e^2) \\
\frac{\Delta N}{a_r} &= \sin\lambda \Delta i_0 - \cos\lambda \sin i_r \Delta\Omega_0 + \frac{e_r}{2}\left(\cos\omega \sin i_r \Delta\Omega_0 - \sin\omega_r \Delta i_0\right) \\
&\quad + \frac{e_r}{2}\cos 2\lambda\left(\cos\omega_r \sin i_r \Delta\Omega_0 + \sin\omega_r \Delta i_0\right) + \frac{e_r}{2}\sin 2\lambda\left(\sin\omega_r \sin i_r \Delta\Omega_0 - \cos\omega_r \Delta i_0\right) \\
&\quad + \mathcal{O}(e^2)
\end{aligned} \tag{5.27}$$

In these equations we identify different terms:

- *constant terms*: There are constant terms not only along the T axis (as in the circular case) but also along the N axis. Once again, they can be cancelled by changing the origin of the axis.

- *elliptical terms* $\cos\lambda$ *and* $\sin\lambda$: Their coefficients differ from the coefficients of the circular reference orbit case. The local orbital elements can be computed using equations (5.7-5.19) already used in the circular reference orbit case, but setting parameters $\overrightarrow{P}$:

$$
\begin{aligned}
A &= -a_r\left(\Delta C_0 + S_r \Delta\lambda_0\right) \\
B &= -a_r\left(\Delta S_0 - C_r \Delta\lambda_0\right) \\
C &= a_r\left(-2\Delta S_0 + C_r\left(\Delta\lambda_0 - \Delta\Omega_0 \cos i_r\right)\right) \\
D &= a_r\left(2\Delta C_0 - S_r\left(\Delta\lambda_0 - \Delta\Omega_0 \cos i_r\right)\right) \\
E &= -a_r \sin i_r \Delta\Omega_0 \\
F &= a_r \Delta i_0
\end{aligned}
\tag{5.28}
$$

- *double orbital frequency terms*: due to these terms, the trajectory is no longer an ellipse.

Mean and osculating local orbital elements

As non-elliptic terms are proportional to the eccentricity, they are small compared to the elliptical terms. Consequently, the motion is near-elliptical and we can still use the local orbital elements. We define the mean local orbital elements and the instantaneous osculating local orbital elements.
Mean orbital elements are defined as the local elements corresponding to the relative motion without double orbital frequency terms. They can be computed using equations (5.20). Instantaneous osculating local orbital elements are defined as the local orbital elements corresponding to an ellipse that would have the same position and velocity at the same moment. Mean orbital elements do not correspond with the mean value of the osculating orbital elements.
To compute the osculating local orbital elements, it is necessary to use the relative position and velocity following the steps:

1. compute the relative position using equations (5.27) and the relative velocity using the derivatives of equations (5.27).

2. compute the parameters $\overrightarrow{P}$ corresponding to the instantaneous ellipse using following equations:

$$
\begin{aligned}
A &= x(1)\cos\lambda - \frac{v(1)}{n}\sin\lambda & B &= x(1)\sin\lambda + \frac{v(1)}{n}\cos\lambda \\
C &= x(2)\cos\lambda - \frac{v(2)}{n}\sin\lambda & D &= x(2)\sin\lambda + \frac{v(2)}{n}\cos\lambda \\
E &= x(3)\cos\lambda - \frac{v(3)}{n}\sin\lambda & F &= x(3)\sin\lambda + \frac{v(3)}{n}\cos\lambda
\end{aligned}
$$

3. use equations (5.9), (5.14), (5.15), (5.16), and (5.19) to find corresponding $\overrightarrow{eo_l}$

Figure (5.4) shows the variation along the orbit of the osculating local eccentricity and its mean value, for different eccentricities of the reference orbit. We have used the following reference orbit: $a_r = 7.10^6, i_r = 45°, \Omega_r = 0°, \omega_r = 45°, M_r(t_0) = 0°$ and the following differences of non-singular elements: $\Delta a = 0, \Delta C = 10^{-5}, \Delta S = 2.10^{-5}, \Delta i = -\sqrt{3}\Delta S, \Delta\Omega = \sqrt{3}\Delta C/\sin i_r, \Delta\lambda = 0$ (which corresponds to an invariant plan when the reference orbit is

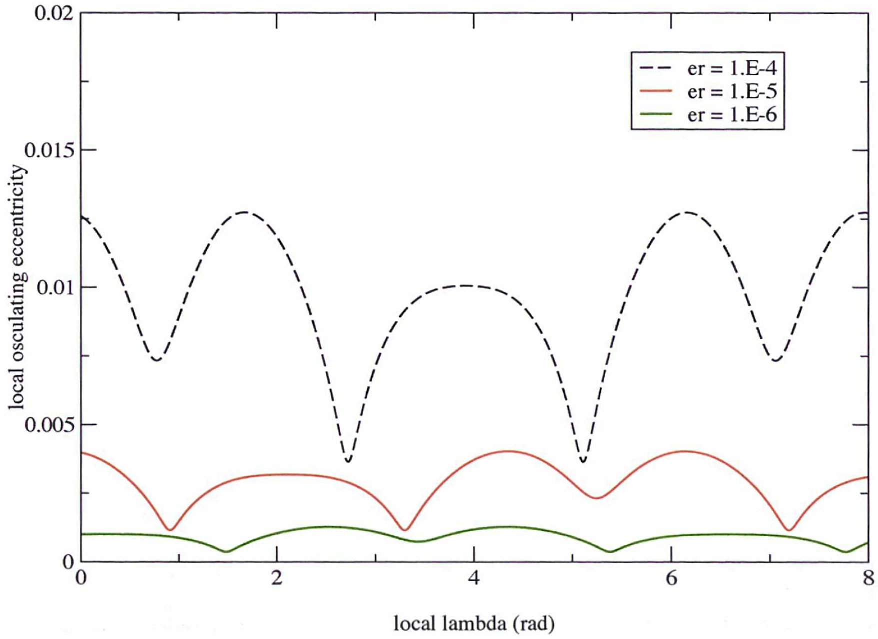

Figure 5.4: *Osculating local eccentricity for different values of the eccentricity of the reference orbit*

circular). The figure shows that the variations of the local eccentricity stay very moderate ($\delta e_l \ll 1$) for values of the eccentricity orbit lower than 10^{-4}.

The main modification with respect to the circular reference orbit case is the new role of $\Delta\lambda$. While in the circular case $\Delta\lambda$ determines only a constant, in the low eccentricity reference orbit case it has an impact on the mean local orbital elements and on the perturbations (double orbital frequency terms). But, as all these effects are proportional to the eccentricity of the reference orbit, they are only corrections of main contributions. So, the topology of the motion will be only slightly modified with respect to the circular reference orbit case.

5.3.2 The high eccentric reference orbit case

When the reference orbit is highly eccentric, relative motion is far from being an ellipse. In order to analyze it, we have rearranged the equations of the relative motion. We have minimized the number of the parameters of the motion, and we have decomposed their effect on inplane and out-of-plane motion.

Our departure point is equations (5.1). For the same precedent reasons, we impose $\Delta a = 0$, obtaining equations:

$$\begin{aligned}
\Delta R(t) &= -a_r \cos f_r \Delta e_0 + \frac{a_r e_r}{\eta_r} \sin f_r \Delta M_0 \\
\Delta T(t) &= a_r \left(1 + \frac{1}{\eta_r^2} \frac{r_r}{a_r}\right) \sin f_r \Delta e_0 + r_r \cos i_r \Delta \Omega_0 + r_r \Delta \omega_0 + \frac{a_r^2 \eta_r}{r_r} \Delta M_0 \\
\Delta N(t) &= r_r \sin u_r \Delta i_0 - r_r \sin i_r \cos u_r \Delta \Omega_0
\end{aligned} \tag{5.29}$$

The in-plane and out-of-plane motions can be decoupled doing the following change of variables:

$$\begin{aligned}
\Delta \omega' &= \Delta \omega + \Delta \Omega \cos i_r \\
\Delta \Omega' &= \Delta \Omega \sin i_r
\end{aligned} \tag{5.30}$$

After, we break down the variable $u = \omega + f$ into its components:

$$\begin{aligned}
\Delta i' &= \sin \omega_r \Delta i - \cos \omega_r \Delta \Omega' \\
\Delta \Omega'' &= \cos \omega_r \Delta i + \sin \omega_r \Delta \Omega'
\end{aligned} \tag{5.31}$$

Finally, we obtain:

$$\begin{aligned}
x &= \frac{\Delta R}{a_r \Delta e} = -\cos f_r + e K_1 \sin f_r \\
y &= \frac{\Delta T}{a_r \Delta e} = \frac{2 + e \cos f_r}{1 + e \cos f_r} \sin f_r + K_1 (1 + e \cos f_r) + \frac{K_2}{1 + e \cos f_r} \\
z &= \frac{\Delta N}{a_r \Delta e} = \frac{1}{1 + e \cos f_r} (K_3 \cos f_r + K_4 \sin f_r)
\end{aligned} \tag{5.32}$$

with the coefficients:

$$\begin{aligned}
K_1 &= \frac{\Delta M}{\eta_r} \\
K_2 &= \eta^2 (\Delta \omega + \cos i_r \Delta \Omega) \\
K_3 &= \eta_r^2 (\sin \omega_r \Delta i - \cos \omega_r \sin i_r \Delta \Omega) \\
K_4 &= \eta_r^2 (\cos \omega_r \Delta i + \sin \omega_r \sin i_r \Delta \Omega)
\end{aligned} \tag{5.33}$$

These equations express all the possible relative trajectories as function of four parameters. K_1, K_2 parameterize the in-plane motion and K_3, K_4 the out-of-plane motion. The out-of-plane motion is given by the sum of a sinus and a cosinus functions divided by $(1 + e \cos f_r)$. The in-plane motion is more complicated. K_1 produces a circular motion:

$$\begin{aligned}
x &= -\cos f_r + e K_1 \sin f_r \\
y - K_1 &= e K_1 \cos f_r + \sin f_r
\end{aligned} \tag{5.34}$$

and K_2 produces a motion only on the y axis:

$$y - K_2 = \frac{-eK_2 \cos f_r}{1 + e \cos f_r}$$

The values of these constants determine the form of the in-plane motion. In figure (5.5) we plot the form of the in-plane motion for different values of K_1, K_2, when the reference orbit eccentricity is 0.6. We verify that for high values of K_1 the motion is circular while K_2 gives linear motions on the T axis.

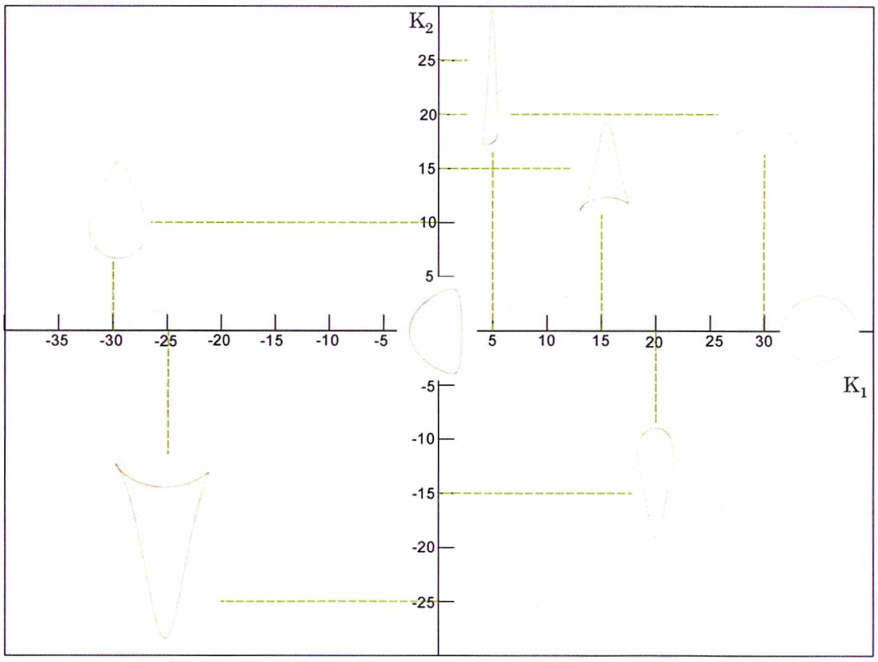

Figure 5.5: *In-plane motion as function of K_1 and K_2*

5.3.3 Looking for circular motions

When the reference orbit is slightly eccentric

When the reference orbit is not circular, the set of equations (5.27) reveals that it is not possible to find perfect circular local motions. But, our analysis of these equations enables to establish the necessary conditions to provide local motions as close as possible to a circle. When changing the parameterization (5.27) by using differential orbital elements we obtain:

$$\begin{aligned}
\frac{\Delta R}{a_r} &= -\cos f_r \Delta e + e_r \sin f_r \Delta M \qquad (5.35)\\
\frac{\Delta T}{a_r} &= 2 \sin f_r \Delta e - e_r \cos f_r \sin f_r \Delta e + (\Delta M + \Delta\omega') + e_r \cos f_r (\Delta M - \Delta\omega')\\
\frac{\Delta N}{a_r} &= (\Delta i' \cos f_r + \Delta\Omega'' \sin f_r) - e_r \cos f_r (\Delta i' \cos f_r + \Delta\Omega'' \sin f_r)
\end{aligned}$$

Considering only elliptical terms, the following initial conditions enable to obtain the same circular motion as in the circular reference orbit case (same local inclination and ascending node):

- *SET 1*

$$\Delta a = 0 \qquad \Delta e = \Delta e \qquad \Delta i = \sqrt{3}\sin\omega_r \Delta e$$
$$\Delta\Omega = -\sqrt{3}\frac{\cos\omega_r}{\sin i_r}\Delta e \qquad \Delta\omega = \sqrt{3}\frac{\cos\omega_r}{\tan i_r}\Delta e \qquad \Delta M = 0$$

- *SET 2*

$$\Delta a = 0 \qquad \Delta e = 0 \qquad \Delta i = \sqrt{3}e_r\cos\omega_r \Delta M$$
$$\Delta\Omega = \sqrt{3}e_r\frac{\sin\omega_r}{\sin i_r}\Delta M \qquad \Delta\omega = -\left(1+\sqrt{3}e_r\frac{\sin\omega_r}{\tan i_r}\right)\Delta M \qquad \Delta M = \Delta M$$

The first set of initial conditions is parameterized by a difference of eccentricity, while the second set is parameterized by a difference of anomaly. Thereafter, we refer to the set 1 as "difference of eccentricity" and to set 1 as "difference of anomaly". Resulting motion is not circular because of double orbital frequency terms. In figure (5.6) we compare the variation of the distance from the origin for each set of initial conditions. Both sets of conditions produce double orbital frequency terms in the N axis, but, Δe produces also these terms in the T axis. That is why the variations are more important in the left part of the figure (5.6).

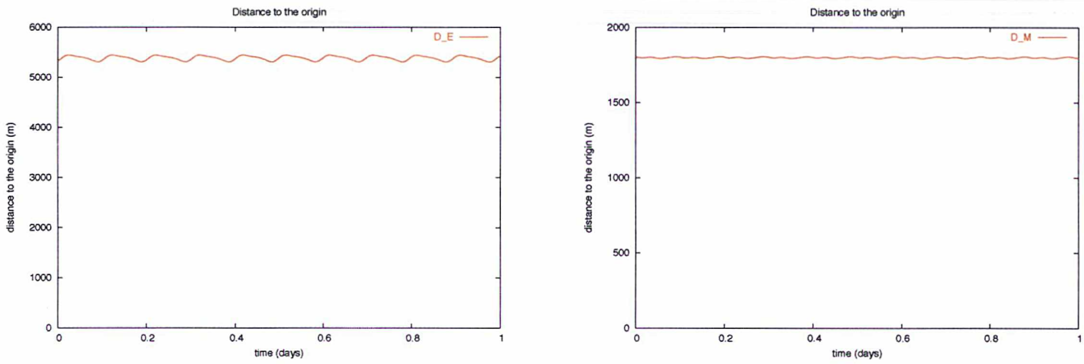

Figure 5.6: *Distance to the origin for different initial conditions (left: difference of eccentricity, right: difference of anomaly)*

When the reference orbit is highly eccentric

It is possible to arrange equations (5.29) to obtain the following form:

$$
\begin{aligned}
\frac{\Delta R}{a_r} &= -\cos f \Delta e + \frac{e}{\eta} \sin f \Delta M \\
\frac{\Delta T}{a_r} &= 2\sin f \Delta e + e\cos f \left(\frac{\Delta M}{\eta} - \frac{\eta^2 \Delta\omega'}{1+e\cos f} \right) + \left(\eta^2 \Delta\omega' + \frac{\Delta M}{\eta} \right) - e\frac{\cos f \sin f}{1+e\cos f} \Delta e \\
\frac{\Delta N}{a_r} &= \frac{\eta^2}{1+e\cos f} \left(\Delta i' \cos f + \Delta\Omega'' \sin f \right)
\end{aligned}
\tag{5.36}
$$

This arrangement allows the comparison with the low eccentric form of the equations (5.35). Comparing the two sets, we identify the transformation of elliptical terms when the eccentricity of the reference orbit grows. We identify the following terms:

$$
\begin{aligned}
-\cos f + e\sin f &\rightarrow -\cos f + \frac{e}{\eta} \sin f \\
2\sin f \Delta e + e\cos f \left(\Delta M - \Delta\omega' \right) &\rightarrow 2\sin f \Delta e + \left(\frac{\Delta M}{\eta} - \eta^2 \Delta\omega' \right) e\cos f \\
\left(\Delta i' \cos f + \Delta\Omega'' \sin f \right) &\rightarrow \eta^2 \left(\Delta i' \cos f + \Delta\Omega'' \sin f \right)
\end{aligned}
$$

We impose the same previous conditions to new terms. Resulting motions are not circular because of double orbital frequency terms and non linear terms in eccentricity, that become very important. Anyway, these initial conditions produce a class of relative motions that is as close as possible to a circle.

- *SET 1*

$$
\Delta a = 0 \qquad \Delta e = \Delta e \qquad \Delta i = \frac{\sqrt{3}}{\eta^2} \sin\omega \Delta e
$$

$$
\Delta\Omega = -\frac{\sqrt{3}}{\eta^2} \frac{\cos\omega}{\sin i} \Delta e \qquad \Delta\omega = \frac{\sqrt{3}}{\eta^2} \frac{\cos\omega}{\tan i} \Delta e \qquad \Delta M = 0
$$

- *SET 2*

$$
\Delta a = 0 \qquad \Delta e = 0 \qquad \Delta i = \sqrt{3} \frac{e_r}{\eta^3} \cos\omega_r \Delta M
$$

$$
\Delta\Omega = \sqrt{3} \frac{e_r}{\eta^3} \frac{\sin\omega_r}{\sin i_r} \Delta M \quad \Delta\omega = -\frac{1}{\eta^3} \left(1 + \sqrt{3} e_r \frac{\sin\omega}{\tan i_r} \right) \Delta M \quad \Delta M = \Delta M
$$

In the following figures (5.7) and (5.8) we have drawn the evolution of the circular motion when the eccentricity of the reference orbit grows. The other parameters of the reference orbit play no role on the form of the trajectory (for the keplerian case). Figures (5.7) and (5.8) show how, for very big reference orbit eccentricities, motion is far from being circular.

5.4 Conclusions

This chapter presents an alternative representation of the relative motion for the circular and the low eccentric reference cases. A parallelism between the two body problem and the relative motion can be done since the relative trajectory is, under certain conditions, an ellipse. This argumentation has lead us to the definition of the local orbital elements. They enable a better understanding of the motion because we are familiar with orbital elements.
We also have found conditions for obtaining local circular motions for circular reference orbit. In the eccentric reference orbit case, local circular orbits do not exist, and we have found the conditions leading to local near circular motions.

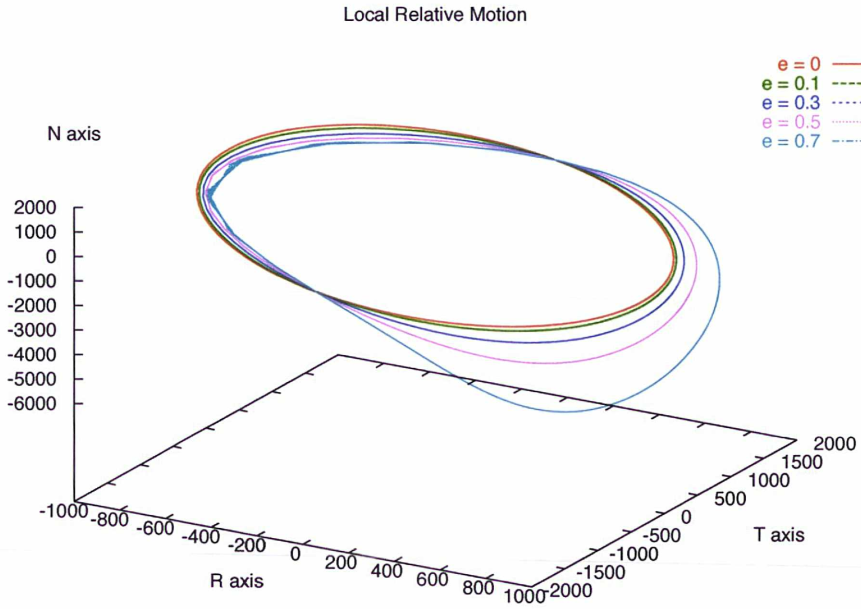

Figure 5.7: *Evolution of the local circular motion produced by a difference of eccentricity when the eccentricity of the reference orbit grows*

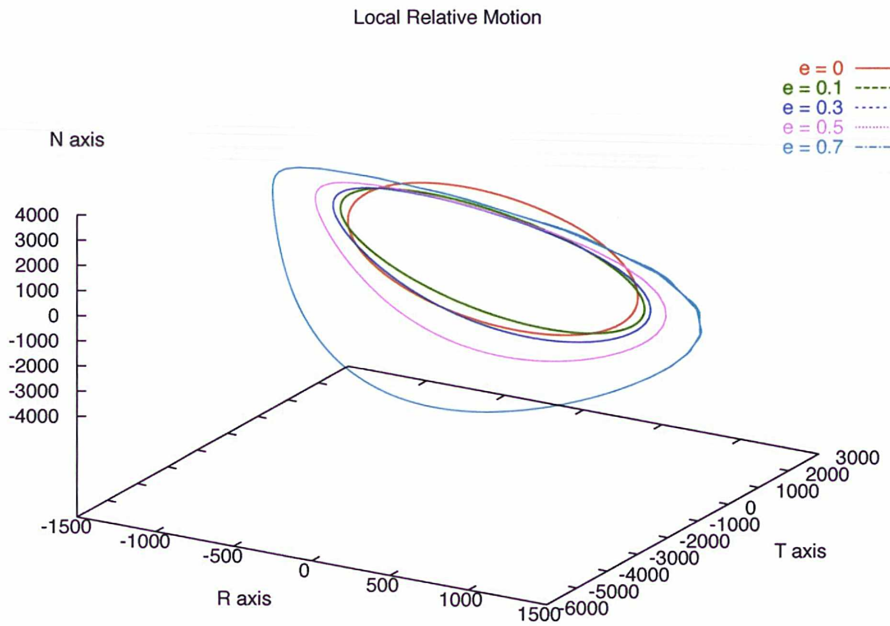

Figure 5.8: *Evolution of the local circular motion produced by a difference of anomaly when the eccentricity of the reference orbit grows*

Part II

Effects of perturbations on formation flying

Chapter 6

The J_2 effects

6.1 Introduction

The most important perturbation acting on a satellite in orbit around the Earth is the oblateness of the Earth represented by the corresponding coefficient in spherical harmonics, J_2. The effects of this perturbation on the absolute orbit are well-known and they are given by several theories [10], [40]. These effects are usually divided in secular, short period and long period effects. In this chapter we focus only on secular effects because they can be particularly harmful for formation flying. If all the satellites do not undergo the same secular effects, they tend naturally to scatter. Large amounts of propellant are necessary to avoid this effect. That is why formations are usually designed to avoid this differential effect. Periodic effects are studied in following chapter with the rest of the gravity field.

The effects of J_2 on formation flying have been largely studied in the literature. A particular interest is given to the research of invariant configurations. In order to do so, different methods are used. Some authors use the differential orbital elements [34], [51], [56],[78], other authors use a hamiltonian approach [42], [8], while others use the cartesian coordinates [60]. Here, we use the differential orbital elements. We focus on circular reference orbits and local circular orbits. We also use the local orbital elements in order to enlarge the comprehension of the trajectory.

In the first section of the chapter, we compute the secular effects of J_2 in terms of differential orbital elements. Derivation of differential effects in terms of differential orbital elements was done before in [56]. We have enlarged its solution by including the effects on circular reference orbits. As we explain, J_2 effects on circular orbits are particular because of the non-definition of the perigee.

In second section, we derive necessary conditions for avoiding drift between satellites. Obtained general conditions agree with precedent results in [56]. We particularize this conditions to the circular relative motions. We prove that there is a particular local circular motion for which the drift is minimized.

Third section is devoted to the computation of the effects of J_2 in terms of local orbital elements. As we show, J_2 effects always increase the local semi-major axis and the perigee.

6.2 The transition matrix

6.2.1 The eccentric case

In this section, we apply the methodology described in chapter 4 to obtain the transition matrix of the J_2 secular effects noted $\mathcal{L}_{J2}$. Methods consists in (i) writing the potential of the force, (ii) using Lagrange planetary equations to obtain the differential equations of the effects on the orbital elements, (iii) integrating the precedent equations, (iv) deriving the obtained equations with respect to the orbital elements.

The potential of the secular part of J_2 is obtained by averaging on the orbit the angular variables. It writes:

$$U_{J_2} = -\frac{1}{4}\frac{\mu}{a}\left(\frac{R}{a}\right)^2 \frac{(1-3\cos^2 i)}{(1-e^2)^{3/2}} J_2 \tag{6.1}$$

where μ is the product between the gravitational constant (G) and the mass of the central body (M) R stands for the radius of the central body. Using Lagrange planetary equations we get the differential effects (keplerian effects non included) on the orbital elements:

$$\begin{aligned}
\frac{da}{dt} &= 0 \qquad (6.2)\\
\frac{de}{dt} &= 0\\
\frac{di}{dt} &= 0\\
\frac{d\Omega}{dt} &= -\frac{3}{2}\left(\frac{R}{a}\right)^2 nJ_2\frac{\cos i}{(1-e^2)^2}\\
\frac{d\omega}{dt} &= -\frac{3}{4}\left(\frac{R}{a}\right)^2 nJ_2\frac{1-5\cos^2 i}{(1-e^2)^2}\\
\frac{dM}{dt} &= -\frac{3}{4}\left(\frac{R}{a}\right)^2 nJ_2\frac{1-3\cos^2 i}{(1-e^2)^{\frac{3}{2}}} + n
\end{aligned}$$

Supposing constant a, e, i, the integration of this set of differential equations is immediate and gives the secular perturbation of J_2:

$$\begin{aligned}
\delta a(t) &= a(t_0) \qquad (6.3)\\
\delta e(t) &= e(t_0)\\
\delta i(t) &= i(t_0)\\
\delta\Omega(t) &= \Omega(t_0) - \left[\frac{3}{2}\left(\frac{R}{a}\right)^2 nJ_2\frac{\cos i}{(1-e^2)^2}\right](t-t_0) \qquad (6.4)\\
\delta\omega(t) &= \omega(t_0) - \left[\frac{3}{4}\left(\frac{R}{a}\right)^2 nJ_2\frac{1-5\cos^2 i}{(1-e^2)^2}\right](t-t_0)\\
\delta M(t) &= M(t_0) - \left[\frac{3}{4}\left(\frac{R}{a}\right)^2 nJ_2\frac{1-3\cos^2 i}{(1-e^2)^{\frac{3}{2}}}\right](t-t_0)
\end{aligned}$$

Linearization of precedent equations give final $\mathcal{L}_{J_2}$ matrix:

$$\mathcal{L}_{J2} = K_{J_2} \begin{pmatrix} 0 & 0 & 0 & 0 & 0 & 0 \\ 0 & 0 & 0 & 0 & 0 & 0 \\ 0 & 0 & 0 & 0 & 0 & 0 \\ -\frac{7}{a}\cos i & \frac{8e}{\eta^2}\cos i & -2\sin i & 0 & 0 & 0 \\ -\frac{7}{2a}\left(1-5\cos^2 i\right) & \frac{4e}{\eta^2}\left(1-5\cos^2 i\right) & 10\cos i \sin i & 0 & 0 & 0 \\ -\frac{7}{2a}\eta\left(1-3\cos^2 i\right) & \frac{6e}{\eta}\left(1-3\cos^2 i\right) & 6\eta\cos i\sin i & 0 & 0 & 0 \end{pmatrix} \tag{6.5}$$

with the constant:

$$K_{J_2} = -\frac{3}{4}\left(\frac{R}{a}\right)^2 n J_2 \frac{1}{\eta^4} \tag{6.6}$$

Combination of J_2 effects matrix $\mathcal{L}_{J_2}$ with keplerian effects matrix $\mathcal{L}_{kep}$, with the matrix $\mathcal{M}$ gives the temporal evolution of relative motion as function of initial reference orbit and initial differences of orbital elements:

$$\Delta\vec{x}(t) = [\mathcal{M}]\left[\mathcal{L}_{kep} + \mathcal{L}_{J_2}\right] = f\left(\overrightarrow{EO}_{ref}, \Delta\overrightarrow{EO}(t_0), t\right) \tag{6.7}$$

The development of these equations reads:

$$\begin{aligned} \Delta R(t) = {} & \frac{r}{a}\Delta a_0 - a\cos f \Delta e_0 + \frac{ae}{\eta}\sin f \Delta M_0 \\ & + \left[3a\Delta i_0 \sin 2i K_{J_2} + \frac{6ae}{\eta^2}\Delta e_0 (1-3\cos^2 i) K_{J_2} - \frac{\Delta a_0}{2}\left(\frac{3n}{\eta} + 7(1-3\cos^2 i)K_{J_2}\right)\right] e \sin f\,(t-t_0) \end{aligned} \tag{6.8}$$

$$\begin{aligned} \Delta T(t) = {} & a\left(1+\frac{r}{\eta^2 a}\right)\sin f \Delta e_0 + r\left(\cos i \Delta\Omega_0 + \Delta\omega_0\right) + \frac{a^2\eta}{r}\Delta M_0 \\ & + r\Big[\frac{-7}{2}\frac{\Delta a_0}{a}\left((1-7\cos^2 i) + \left(\frac{a\eta}{r}\right)^2(1-3\cos^2 i)\right) + \Delta e_0 \sin 2i\left(4+3\left(\frac{a\eta}{r}\right)^2\right) \\ & + 2\Delta i_0 \frac{e}{\eta^2}\left(1-3\cos^2 i\right)\left(1+\left(\frac{a\eta}{r}\right)^2\right)\Big] K_{J_2}(t-t_0) \end{aligned} \tag{6.9}$$

$$\begin{aligned} \Delta N(t) = {} & r\sin u \Delta i_0 - r\sin i\cos u \Delta\Omega_0 \\ & + r\sin i \cos u\left[-\frac{7}{a}\cos i \Delta a_0 - 2\sin i \Delta e_0 + \frac{8e}{\eta^2}\cos i \Delta i_0\right] K_{J_2}(t-t_0) \end{aligned} \tag{6.10}$$

These equations give a closed form of the temporal evolution of the relative position with the true anomaly and the time as independent variables. Parametrization of the motion is done through initial differences of orbital elements.
Neglected periodic terms have also an effect on secular terms through the initial conditions. Computed secular effects are not exact because we use the osculating initial conditions instead

of using mean initial conditions. In the relative motion these effects are small. They can be taken into account but resulting equations become cumbersome. We prefer to keep a simple model.

6.2.2 Circular reference orbit

As we do all along the document, the circular reference orbit case is studied through the non-singular elements defined in equations (2.4). We transform equations (6.2) in terms of non-singular elements:

$$\begin{aligned}
\frac{da}{dt} &= 0 \\
\frac{dC}{dt} &= \frac{3}{4}\left(\frac{Re}{a}\right)^2 nJ_2\frac{1-5\cos^2 i}{\eta^4}S \\
\frac{di}{dt} &= 0 \\
\frac{d\Omega}{dt} &= -\frac{3}{2}\left(\frac{Re}{a}\right)^2 nJ_2\frac{\cos i}{\eta^4} \\
\frac{dS}{dt} &= -\frac{3}{4}\left(\frac{Re}{a}\right)^2 nJ_2\frac{1-5\cos^2 i}{\eta^4}C \\
\frac{d\lambda}{dt} &= -\frac{3}{4}\left(\frac{Re}{a}\right)^2 \frac{nJ_2}{\eta^4}\left[\left(1-5\cos^2 i\right)+\eta\left(2-6\cos^2 i\right)\right]
\end{aligned} \tag{6.11}$$

C and S elements do not have anymore secular perturbations in circular (or near-circular) orbits. They are excited in an equivalent way to the harmonic oscillator.
Since perturbations in C and S are linear, and C and S are very small or null, J_2 perturbations on C and S become neglectable with respect to J_3. The phenomenology of the perigee for very low eccentricities is completely detailed in [21], and [22]. We do not consider these effects because they are not secular.

$\mathcal{L}$ matrix As indicated in 6.2.1, we must calculate the derivatives of $\frac{d\Omega}{dt}$ and $\frac{d\lambda}{dt}$ with respect to a, C, i, S in order to obtain the $\mathcal{L}_{\mathcal{J}_\in}$ matrix. First derivatives of the secular effects with respect to C and S are zero in circular orbits since their relations are of second order. A possible solution is to use Delaunay variable η as it is done in [56]. Mapping between $\delta\eta$ and δC, δS shows how the first terms in C and S are second order ones:

$$\delta\eta = -\left(C(\delta C)+S(\delta S)\right)-\frac{1}{2}\left((\delta C)^2+(\delta S)^2\right)$$

So, for circular orbits:

$$\Delta\eta_0 = -\frac{1}{2}\left(\Delta C_0^2+\Delta S_0^2\right) \tag{6.12}$$

We can no more use matrix formulation because we have introduced second order terms. If we want to keep this formulation, we should use tensors. Instead of doing so, we prefer to obtain general expressions of the perturbed motion. We write the derivatives of the secular terms with respect to the metric variables:

$$\begin{aligned}
\frac{\partial}{\partial a}\left(\frac{d\Omega}{dt}\right) &= -7K_{J2}\frac{\cos i}{a} \\
\frac{\partial}{\partial a}\left(\frac{d\lambda}{dt}\right) &= -\frac{7}{2}\frac{1}{a}K_{J2}\left[(1-5\cos^2 i)+\eta\left(2-6\cos^2 i\right)\right]-\frac{3}{2}\frac{n}{a} \\
\frac{\partial}{\partial \eta}\left(\frac{d\Omega}{dt}\right) &= -8\frac{\cos i}{\eta}K_{J2} \\
\frac{\partial}{\partial \eta}\left(\frac{d\lambda}{dt}\right) &= \frac{K_{J2}}{\eta}\left[4\left(1-5\cos^2 i\right)+3\eta\left(2-6\cos^2 i\right)\right] \\
\frac{\partial}{\partial i}\left(\frac{d\Omega}{dt}\right) &= -2\sin i K_{J2} \\
\frac{\partial}{\partial i}\left(\frac{d\lambda}{dt}\right) &= 2K_{J2}\cos i\sin i\left(6\eta+5\right)
\end{aligned} \tag{6.13}$$

Thanks to these derivatives, we obtain temporal evolution of motion as function of reference orbits, initial differential orbital elements, and time:

$$\begin{aligned}
\Delta R(t) &= \Delta a_0 - a\cos\lambda\Delta C_0 - a\sin\lambda\Delta S_0 \\
\Delta T(t) &= 2a\sin\lambda\Delta C_0 - 2a\cos\lambda\Delta S_0 + a\left(\cos i\Delta\Omega_0+\Delta\lambda_0\right) \\
&\quad + aK_{J_2}\left[-\frac{21}{2}\left(1-3\cos^2 i\right)\frac{\Delta a_0}{a}-\left(5-18\cos^2 i\right)\left(\Delta C_0^2+\Delta S_0^2\right)+9\sin 2i\Delta i_0-\frac{3}{2}\frac{n}{a}\frac{1}{K_{J_2}}\Delta a_0\right](t-t_0) \\
\Delta N(t) &= a\sin\lambda\Delta i_0 - a\sin i\cos\lambda\Delta\Omega_0 \\
&\quad + a\sin i\cos\lambda K_{J_2}(t-t_0)\left[7\cos i\frac{\Delta a_0}{a}-4\cos i\left(\Delta C_0^2+\Delta S_0^2\right)+2\sin i\Delta i_0\right]
\end{aligned} \tag{6.14}$$

6.3 Looking for no drift configurations

6.3.1 The eccentric case

This section is devoted to the research of no drift orbits. This research has been done before in [56]. Here, we take up again his results and we particularize for the circular case. We also focus on the combination of no drifts and local circular orbits. As it is proved, no drift orbits exist only for the circular case.
Secular drift is given by secular terms in equations (6.8), (6.9) and (6.10). The no drift condition implies cancelling drift on the three angular variables (Ω,ω,M):

$$\begin{aligned}
0 &= -7\cos i\frac{\Delta a_0}{a}-2\sin i\Delta i_0+\frac{8e}{\eta^2}\cos i\Delta e_0 \\
0 &= -\frac{7}{2}(1-5\cos^2 i)\frac{\Delta a_0}{a}+5\sin 2i\Delta i_0+\frac{4e}{\eta^2}(1-5\cos^2 i)\Delta e_0 \\
0 &= -\frac{7}{2}(1-3\cos^2 i)\eta\frac{\Delta a_0}{a}+3\eta\sin 2i\Delta i_0+\frac{6e}{\eta}(1-3\cos^2 i)\Delta e_0-\frac{3}{2}\frac{n}{a}\frac{1}{K_{J_2}}\Delta a_0
\end{aligned} \tag{6.15}$$

All the terms in these expressions, except the Keplerian term $-\frac{3}{2}\frac{n}{a}\frac{1}{K_{J_2}}\Delta a_0$, are linear with J_2. Since J_2 is very small for the Earth ($J_2 = 1,083.\ 10^{-3}$), Keplerian term is dominant in N axis. As a consequence, we can neglect the term $-\frac{7}{2}(1-3\cos^2 i)\eta\frac{\Delta a_0}{a}$, and, as a consequence $\Delta a_0 \ll (\Delta e_0, \Delta i_0)$. So, we can also neglect the terms $-7\cos i\frac{\Delta a_0}{a}$ and $\frac{7}{2}(1-5\cos^2 i)\frac{\Delta a_0}{a}$. We obtain simplified equations:

$$\begin{aligned} 0 &= -2\sin i\Delta i_0 + \frac{8e}{\eta^2}\cos i\Delta e_0 \\ 0 &= 5\sin 2i\Delta i_0 + \frac{4e}{\eta^2}(1-5\cos^2 i)\Delta e_0 \\ 0 &= 3\eta\sin 2i\Delta i_0 + \frac{6e}{\eta}(1-3\cos^2 i)\Delta e_0 - \frac{3}{2}\frac{n}{a}\frac{1}{K_{J_2}}\Delta a_0 \end{aligned} \tag{6.16}$$

The last equation proves that the effects of the difference of semi-major axis are on the anomaly, and they come from the Keplerian effects. It can be chosen in order to null the other effects on the anomaly.
These equations do not have any solution for arbitrary inclination (the circular case must be treated separately). A possibility to obtain a solution consists in null the sum of the argument of the perigee with the mean anomaly, instead of null them separately.
We obtain following condition for the ascending node:

$$\tan i\Delta i_0 = \frac{4e}{\eta^2}\Delta e_0 \tag{6.17}$$

And the condition for the sum of the argument of the perigee and the anomaly reads:

$$\Delta i_0 \tan i\left[(1+\frac{3}{2}\eta) + \cos^2 i\left(5+\frac{21}{2}\eta\right)\right] = \frac{3}{2}\frac{n}{a}\frac{1}{K_{J_2}}\Delta a_0 \tag{6.18}$$

6.3.2 The circular case

When the reference orbit is circular, we impose no drift conditions using equations (6.11). After some computations, conditions become:

$$\begin{aligned} \Delta\eta_0 &= -\frac{1}{4}\tan i\Delta i_0 \\ 3\frac{n}{a}\Delta a_0 &= K_{J_2}\tan i\left(63\cos^2 i - 5\right)\Delta i_0 \end{aligned} \tag{6.19}$$

Local circular orbits with no drift In chapter 5, we have obtained the following conditions for local circular orbits (5.24):

$$\begin{aligned} \Delta\overrightarrow{ENS}_1 &= (0, \Delta C, -\sqrt{3}\Delta S, \frac{\sqrt{3}\Delta C}{\sin i}, \Delta S, \Delta\lambda)^T \\ \Delta\overrightarrow{ENS}_2 &= (0, \Delta C, \sqrt{3}\Delta S, -\frac{\sqrt{3}\Delta C}{\sin i}, \Delta S, \Delta\lambda)^T \end{aligned} \tag{6.20}$$

When we mix them with no drift conditions we finally obtain:

$$
\begin{aligned}
\Delta C_0 &= \sqrt{-\Delta S_0^2 - \frac{\sqrt{3}}{2}\tan i \Delta S_0} \\
\Delta i_0 &= -\sqrt{3}\Delta S_0 \\
\Delta\Omega_0 &= \frac{\sqrt{3}\Delta C_0}{\sin i} \\
\Delta\lambda_0 &= -\Delta\Omega_0 \cos i \\
\Delta a_0 &= \frac{2}{3}\frac{a}{n} K_{J2}\left((10 - 38\cos^2 i)\Delta\eta_0 + 22\cos i \sin i \Delta i_0\right)
\end{aligned}
\tag{6.21}
$$

The square root demands $-\frac{\sqrt{3}}{2}\tan i < \Delta S_0 < 0$, where ΔS_0 is a free parameter.
If we desire to place more satellites describing a circle around a central point (as it is the case for LISA mission with three satellites), the other satellites cannot have a null drift. We can impose just one condition: $\frac{\partial \Delta\lambda}{\partial t} = 0$.

Numerical simulations In order to prove the interest of precedent conditions, we have tested three different local circular orbits with the same reference orbit. Only the first amongst them accomplishes the non-drift condition for J_2 secular perturbations. Simulations have been done with a simplified analytical model disregarding periodic perturbations.
The parameters of the reference orbit are: $a = 7000\ km, i = 50°, e = 0$, and the length of simulation is 10 days. The differential orbital parameters of the three satellites are given in table 6.1. Only the first satellite respects the relations (6.21), while the two others respect only local circular orbit conditions (6.20).

ΔENS	**SAT 1**	**SAT 2**	**SAT 3**
Δa	$-6,8304.10^{-2}$	$5,9544$	$-5,9729$
ΔC	$1,0159.10^{-3}$	$1,0108.10^{3}$	$1,0108.10^{3}$
Δi	$1,7320.10^{-6}$	$-1,7493.10^{-4}$	$-1,7493.10^{-4}$
$\Delta\Omega$	$2,2970.10^{-3}$	$2,2856.10^{-3}$	$2,2856.10^{-3}$
ΔS	-1.10^{-6}	$1,01.10^{-4}$	$-1,01.10^{-4}$
$\Delta\lambda$	$1,4764.10^{-3}$	$1,4691.10^{-4}$	$1,4691.10^{-4}$

Table 6.1: *Initial differential orbital elements of satellites*

The advantages of the first configuration with respect the two others are clear in figure 6.1. On the left side, there is the relative motion in the local axis RTN. SAT 1 is the only one where there is no significant drift. On the right side, the evolution of the distance to the origin proves that in SAT1 the variations are very small (even if it is not perfectly circular) while in SAT2 and SAT3 there is a linear growth of the size of the variations.
The effects of the perturbation on the osculating local orbital elements are plotted in figure 6.2. SAT2 and SAT3 undergo large variations while the local semi-major axis and local eccentricity of SAT 1 do not change.

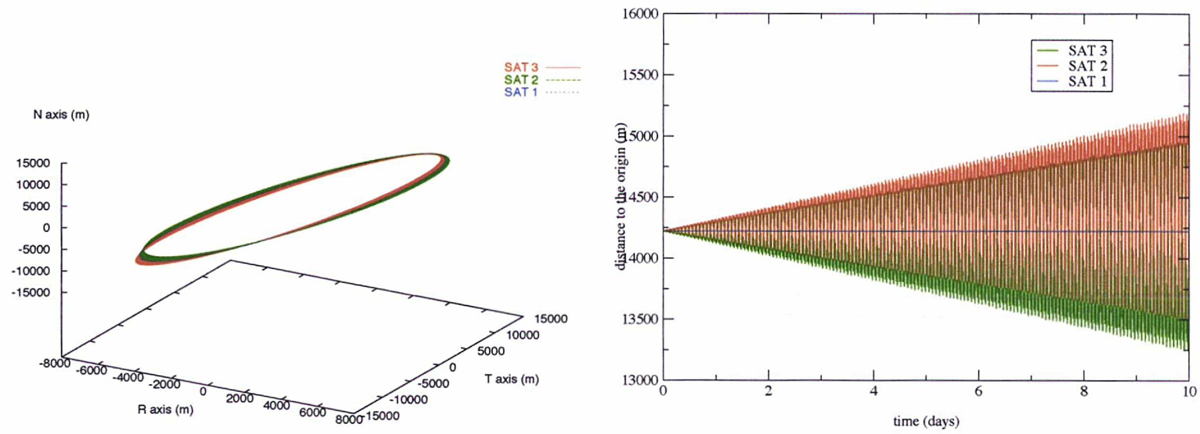

Figure 6.1: *Effects of J_2 on the relative motion.*

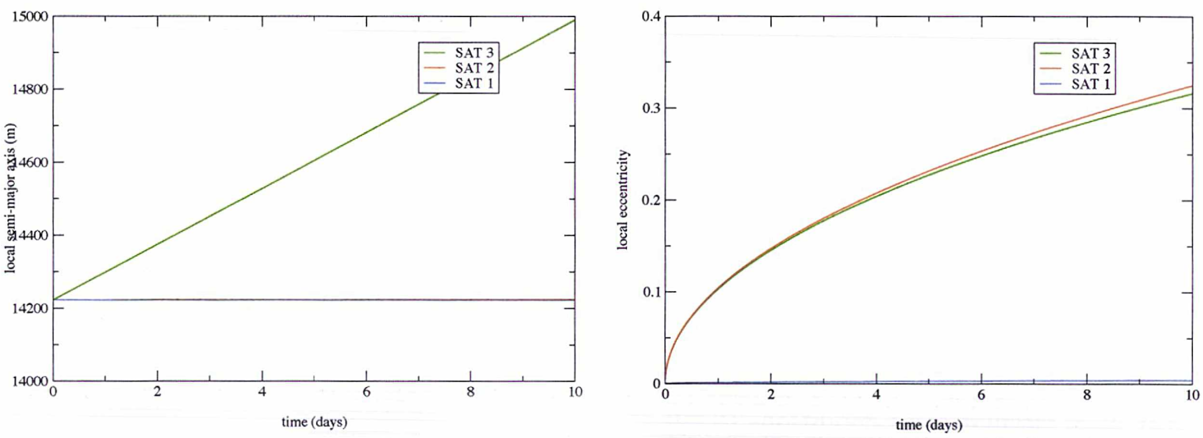

Figure 6.2: *Effects of J_2 on the local orbital elements.*

6.4 Effects on local orbital elements

In chapter 5, we have given the definition of local orbital elements, as function of the differential orbital elements, through equations (5.20). In these equations, we have supposed that the values of $\Delta\overrightarrow{ENS}$ are constant. When we introduce perturbations, they are no more constant, but relations (5.20) keep their meaning in terms of osculating variables. It means that the coordinates are no more constant, but variable in time.

The form of the local orbit is given by its local semi-major axis a_l and its local eccentricity e_l. We focus our study on these two elements. We rewrite the definition of both:

$$\begin{aligned}
&K_1 = a_r^2(\Delta C_0^2 + 4\Delta S_0^2 + \sin^2 i_r \Delta\Omega_0^2) \qquad K_2 = a_r^2(\Delta S_0^2 + 4\Delta C_0^2 + \Delta i_0^2) \\
&K_3 = 2a_r^2(-3\Delta C_0 \Delta S_0 - \sin i_r \Delta\Omega_0 \Delta i_0) \\
&2a_l^2 = K_1 + K_2 + \sqrt{(K_1 - K_2)^2 + K_3^2} \qquad e_l^2 = 2 - \frac{K_1 + K_2}{a_l^2}
\end{aligned} \tag{6.22}$$

We remember that in the circular case (where the local orbital elements are defined), only two local orbital elements undergo J_2 secular effects: $\Delta\Omega$ and $\Delta\lambda$. $\Delta\lambda$ does not take part in the definition of local orbital elements. Only $\Delta\Omega$ plays a role.
The introduction of the analytical expression of temporal perturbations of $\Delta\Omega(t)$ leads to very complicated equations which do not give more insight in the comprehension of the problem. We compute the derivatives of the local orbital elements with respect to the difference of ascending node. These derivatives give the evolution of the variables.

$$\begin{aligned} \frac{dK_1}{d\Omega} &= a_r^2 \left(2\sin^2 i_r \Delta\Omega_0\right) \\ \frac{dK_2}{d\Omega} &= 0 \\ \frac{dK_3}{d\Omega} &= -2a_r^2 \sin i_r \Delta i_0 \end{aligned} \tag{6.23}$$

$$\frac{d(a_l^2)}{d\Omega} = \frac{1}{2}\left[\frac{dK_1}{d\Omega} + \frac{(k_1 - K_2)\frac{dK_1}{d\Omega} + K_3\frac{dK_3}{d\Omega}}{\sqrt{(K_1 - K_2)^2 + K_3^2}}\right] \tag{6.24}$$

$$\frac{d(e_l^2)}{d\Omega} = \frac{1}{a_l^2}\left[\frac{K_1 + K_2}{a_l^2}\frac{d(a_l^2)}{d\Omega} - \frac{dK_1}{d\Omega}\right] \tag{6.25}$$

We can distinguish two temporal horizons on the evolution of the variables:

- *short period*: In the short term, the value of the differences which suffers from the secular effects keep values similar to static ones. The analysis of the effects during this period presents big difficulty, since all the parameters play a role. Anyway, there is a first difference that we can establish in this relative motions. The motions that tend to collapse, and the motions than tend to spread.

- *long period*: In the long term, all the formations spread. There are two different ways of spread due to J_2: (i) It can be through a secular effect on the ascending node, or (ii) through a secular effect on the anomaly. In the first case, the dominant motion is a periodic motion on the N axis. In the second case, the motion is a secular drift on the T axis.

6.5 Conclusions

In this chapter we have analyzed the effects of J_2 on formation flying. We have used two representations: differential orbital elements, and local orbital elements. First representation enables the description of the motion through simple analytical expressions, while second one, gives more comprehension of the resulting motion.
First conclusion is that, after long periods without thrust, J_2 always spreads the formation, except for particular case: the no drift configurations. For short periods, J_2 effects can also group the formation.
No drift configurations exist only when the reference orbit is circular. We have also detected local circular orbits with no drift. When reference orbit is not circular, there is an approximated solution to the no drift configuration, but it goes worst for high reference eccentricities.

Chapter 7

The gravity field

7.1 Introduction

This chapter is devoted to the effects induced on a formation flying by the whole gravity field. In a general point of view, perturbations produced by the gravity field are the main perturbation in low orbit satellites, but most important effects are J_2 effects. Other terms of the gravity field are as relevant as J_2 in a first approach. But, they are necessary when we pretend to analyze geodesy space missions. It is our first motivation when we study these effects.

Effects of the gravity field on the absolute motion of a single satellite have been largely studied in literature. There are several papers obtaining analytical expressions for temporal perturbations. Two of them, among many others, are Kaula theory and Brouwer theory. Brouwer theory is not well adapted because it considers only J_2 effects. Kaula theory has several mismodellisations that diminish the accuracy of the results. An interesting work improving previous work is [73]. In order to obtain a better accuracy, we have developed another solution based on the use of canonical Lie transformations.

The effects of gravity field perturbations on a formation flying mission have also been analyzed. Precedent studies were done in the frame of GRACE mission. In [18] a method based on Hill equations is presented for the integration of gravitational perturbations in a two-satellites coplanar flight formation. Cheng [19] uses Casotto relations to introduce the gravitational effects in RTN reference frame and deduces observable functions. In [70], there is an improvement of Cheng solution. More recently, in [76] there is a numerical approach to the problem. Our approach consists in combining our alternative integration of gravity field effects with the differential orbital methods.

Second section is devoted to the different expressions of the gravity field potential that we find in the literature. In third section, we have analyzed the behavior of Kaula solution. We have detected its main weakness. In the fourth section we propose another solution based on the use of canonical Lie transformations. In fifth section we apply the differential orbital methods to obtain the associated matrix $\mathcal{L}_{GF}$.

7.2 Expression of the gravitational potential

7.2.1 The gravitational potential in spherical coordinates

We use as departure point the generic expression of a potential created by a mass distribution in a point of the space (x, y, z):

$$U = k \iiint \frac{\rho(x,y,z)}{r(x,y,z)} dx\, dy\, dz \tag{7.1}$$

where $\rho(x, y, z)$ is the density at the point (x, y, z) and $r(x, y, z)$ the distance to the satellite. This potential verifies Laplace equation outside the body:

$$\frac{\partial^2 U}{\partial x^2} + \frac{\partial^2 U}{\partial y^2} + \frac{\partial^2 U}{\partial z^2} = 0 \tag{7.2}$$

Classical solution of Laplace equation in terms of spherical coordinates, developed as a series of spherical harmonics is:

$$U = \frac{GM}{R} \sum_{l=1}^{\infty} \left(\frac{R}{r}\right)^{l+1} \sum_{m=0}^{l} \left(\bar{C}_{lm} \cos m\lambda + \bar{S}_{lm} \sin m\lambda\right) \bar{P}_{lm}(\sin\theta) \tag{7.3}$$

where (r, θ, λ) are the spherical coordinates distance, latitude, and longitude. P_{lm} are associated Legendre polynomials. Each spherical harmonic is characterised by its coefficients C_{lm} and S_{lm} which have been normalized to avoid tiny values. Consequently, also Legendre polynomials are normalized. Normalization factor is:

$$N_{lm} = \sqrt{(2 - \delta_{m0})(2l+1)\frac{(l-m)!}{(l+m)!}} \tag{7.4}$$

and:

$$\bar{P}_{lm} = N_{lm} P_{lm} \qquad \bar{C}_{lm} = C_{lm}/N_{lm} \tag{7.5}$$

Working with unnormalized coefficients may lead to serious numerical problems. Since gravity field are usually given in their normalised form, computing their unnormalized form needs to compute coefficients N_{lm}. They can give overflow problems for high degrees. It is seems advisable to work with normalised coefficients.

Complex form

A classical alternative of this representation of gravitational potential is the complex form, as defined for example in [64]:

$$U^c = \frac{GM}{R} \sum_{l=1}^{\infty} \left(\frac{R}{r}\right)^{l+1} \sum_{m=-l}^{l} \bar{K}^c_{lm} \bar{P}^c_{lm}(\sin\theta) e^{jm\lambda} \tag{7.6}$$

where c superscript stands for complex variables. Even if coefficients $\bar{K}^c_{lm}$ are complex numbers, the total imaginary part of the potential is always zero. The advantage of this formulation is its compactness, and its inconvenient is to double the number of coefficients.

The coefficients and the polynomials have been normalized with a different normalization factor:

$$N_{lm}^c = (-1)^m \sqrt{(2l+1)\frac{(l-m)!}{(l+m)!}} \tag{7.7}$$

Relation between complex and real normalization is:

$$N_{lm}^c = \frac{(-1)^m}{\sqrt{(2-\delta_{m0})}} N_{lm} \tag{7.8}$$

Relation between normalized and non-normalized coefficients is rather different:

$$\bar{P}_{lm}^c = \begin{cases} N_{lm}^c P_{lm} & m > 0 \\ (-1)^m \bar{P}_{l-m}^c & m < 0 \end{cases} \tag{7.9}$$

Complex coefficients can also be written as function of normalised real ones:

$$\bar{K}_{lm}^c = \begin{cases} (-1)^m \frac{(\bar{C}_{lm} - j\bar{S}_{lm})}{\sqrt{2}} & m > 0 \\ \bar{C}_{lm} & m = 0 \\ \frac{\bar{C}_{lm} + j\bar{S}_{lm}}{\sqrt{2}} & m < 0 \end{cases} \tag{7.10}$$

7.2.2 Introduction of the orbital elements

The previous expressions of the potential are in terms of spherical coordinates whereas classical orbital elements are better suited for Lagrange equations.
Transformation between the two sets of coordinates systems consists in a rotation of spherical harmonics as described in [64] and [62] for the introduction of the inclination, and a second transformation for the introduction of the eccentricities. An alternative less elegant method can be found in [40]. It is beyond the scope of this thesis to deep on the details of these transformations and we will use just resulting relations.
Once again, real and complex inclination functions are not identical because of different normalizations and the complex component. We study both representations in different paragraphs.

Real formulation

In order to introduce the inclination, we use normalised real inclination functions:

$$\bar{F}_{lmp} = N_{lm} d_{lmk} P_{lk}(0)\ (-1)^{p+E[\frac{l-m+1}{2}]} \tag{7.11}$$

d_{lmk} is issued of the rotation of the spherical harmonics:

$$d_{lmk} = \frac{(l+m)!}{(l+k)!} \sum_{t=t_1}^{t_2} \binom{l+k}{t} \binom{l-k}{l-m-t} (-1)^t \cos^{2l-a} \frac{1}{2}\beta \sin^a \frac{1}{2}\beta \tag{7.12}$$

Details of this formula are given in [62].
The introduction of the eccentricity is done through Hansen functions:

$$\left(\frac{a}{r}\right)^{l+1} e^{j(l-2p)f} = \sum_{q=-\infty}^{\infty} G_{lpq}(e) e^{j(l-2p+q)M} \tag{7.13}$$

and G_{lpq} functions are:

$$G_{lpq}(e) = \mathcal{X}_{l-2p+q}^{-(l+1),l-2p}(e) \tag{7.14}$$

where $\mathcal{X}$ are Hansen functions.

Composing these two transformations, we obtain real potential in terms of orbital elements. Different representations are used. Here, we give just some of them:

$$U = \frac{GM}{R} \sum_{l=1}^{\infty} \left(\frac{R}{a}\right)^{l+1} \sum_{m=0}^{l} \sum_{p=0}^{l} \sum_{q=-\infty}^{\infty} \bar{F}_{lmp} G_{lpq}(e) \left[\alpha_{lm} \cos\phi + \beta_{lm} \sin\phi\right] \tag{7.15}$$

with:

$$[\alpha_{lm}, \beta_{lm}] = \left[\left(\begin{pmatrix} \bar{C}_{lm} \\ -\bar{S}_{lm} \end{pmatrix}\right), \left(\begin{pmatrix} \bar{S}_{lm} \\ \bar{C}_{lm} \end{pmatrix}\right)\right] \begin{pmatrix} l-m & even \\ l-m & odd \end{pmatrix} \tag{7.16}$$

and:

$$\phi = (l-2p)\omega + (l-2p+q)M + m(\Omega - \theta) \tag{7.17}$$

In [75] we find following one:

$$U = \frac{GM}{R} \sum_{l=1}^{\infty} \left(\frac{R}{a}\right)^{l+1} \sum_{m=0}^{l} \sum_{p=0}^{l} \sum_{q=-\infty}^{\infty} \bar{F}_{lmp} G_{lpq}(e) \gamma_{lm} \left[\bar{C}_{lm} \cos(\phi + (l-m)\frac{\pi}{2}) + \bar{S}_{lm} \sin(\phi + (l-m)\frac{\pi}{2})\right] \tag{7.18}$$

with:

$$\gamma_{lm} = (-1)^{E[(l-m+1)/2]} \tag{7.19}$$

Another possible formulation, used in [50] is:

$$U = \frac{GM}{R} \sum_{l=1}^{\infty} \left(\frac{R}{a}\right)^{l+1} \sum_{m=0}^{l} \sum_{p=0}^{l} \sum_{q=-\infty}^{\infty} \bar{F}_{lmp} G_{lpq}(e) \left[\bar{C}_{lm} \cos(\phi + \epsilon_{lm}\frac{\pi}{2}) + \bar{S}_{lm} \sin(\phi + \epsilon_{lm}\frac{\pi}{2})\right] \tag{7.20}$$

Function ϵ_{lm} is defined as follows:

$$\epsilon_{lm} = \begin{cases} 0 & if \quad l-m \quad even \\ 1 & if \quad l-m \quad odd \end{cases} \tag{7.21}$$

And a last that we will use in the following is:

$$U = \frac{GM}{R} \sum_{l=1}^{\infty} \left(\frac{R}{a}\right)^{l+1} \sum_{m=0}^{l} \sum_{p=0}^{l} \sum_{q=-\infty}^{\infty} \bar{F}_{lmp} G_{lpq}(e) \cos\left(\phi - m\lambda_{lm} - \epsilon_{lm}\frac{\pi}{2}\right) J_{lm} \tag{7.22}$$

with:

$$C_{lm} = J_{lm} \cos \lambda_{lm} \qquad S_{lm} = J_{lm} \sin \lambda_{lm} \tag{7.23}$$

In these four cases, inclination functions are defined and normalized in the same way.

Complex formulation

In a parallel way the complex potential is developed:

$$U^c = \frac{GM}{R} \sum_{l=1}^{\infty} \left(\frac{R}{a}\right)^{l+1} \sum_{m=-l}^{l} \sum_{k=-l,2}^{l} \sum_{q=-\infty}^{\infty} \bar{K}^c_{lm} \bar{F}^c_{lmk} G_{lpk} e^{jm\phi} \tag{7.24}$$

with:

$$\phi = k\omega + (k+q)M + m(\Omega - \theta) \tag{7.25}$$

Two comments are relevant in this formulation. First, last summation index has been changed, instead of p, we use k. Relations between both is $p = \frac{1}{2}(l-k)$. Both indexes are equivalent, some authors prefer k because angular argument depends only on two indices when working with k. Second, inclination functions are defined in a different way:

$$\bar{F}^c_{lmk} = j^{k-m} \bar{d}^c_{lmk} \bar{P}^c_{lk}(0) \tag{7.26}$$

with:

$$\bar{d}^c_{lmk} = \left[\frac{(l+k)!(l-k)!}{(l+m)!(l-m)!}\right]^{\frac{1}{2}} \sum_{t=t_1}^{t_2} \binom{l+m}{t} \binom{l-m}{l-k-t} (-1)^t \cos^{2l-a} \frac{1}{2}\beta \sin^a \frac{1}{2}\beta \tag{7.27}$$

In [62], the author does not give the normalization of this function $\bar{d}^c_{lmk}$. To obtain it, we consider the normalization of Legendre polynomials and of the coefficients K_{lm}, and we suppose that the normalization of d function must match with them. We finally obtain:

$$d_{lmk} = N^c_{lmk} \bar{d}^c_{lmk} \tag{7.28}$$

with:

$$N^c_{lmk} = \frac{N^c_{lk}}{N^c_{lm}} = (-1)^{k-m} \sqrt{\frac{(l-k)!(l+m)!}{(l+k)!(l-m)!}} \tag{7.29}$$

7.3 Kaula's integration of the effects of the gravity field

Classical Kaula's integration is detailed in [40]. The author proceeds, first, to the development of the potental of the gravity field in terms of orbital elements (as rewritten in precedent section), and, second, he proposes an analytical integration of resulting Lagrange planetary equations. This solution has been used for many years, inspite of its drawbacks. We give here its solution and we analyze its main drawbacks. They justify the obtention of an improved solution as it is done in the next section.

7.3.1 The method

The effects of a potential force in the orbit of a satellite can be computed using well-known Lagrange equations:

$$\begin{aligned}
\frac{da}{dt} &= \frac{2}{na}\frac{\partial U}{\partial M} \\
\frac{de}{dt} &= -\frac{\sqrt{1-e^2}}{na^2e}\frac{\partial U}{\partial \omega} + \frac{1-e^2}{na^2e}\frac{\partial U}{\partial M} \\
\frac{di}{dt} &= \frac{-1}{na^2\sqrt{1-e^2}\sin i}\frac{\partial U}{\partial \Omega} + \frac{\cos i}{na^2\sqrt{1-e^2}\sin i}\frac{\partial U}{\partial \omega} \\
\frac{d\Omega}{dt} &= \frac{1}{na^2\sqrt{1-e^2}\sin i}\frac{\partial U}{\partial i} \\
\frac{d\omega}{dt} &= \frac{\sqrt{1-e^2}}{na^2e}\frac{\partial U}{\partial e} + \frac{\cos i}{na^2\sqrt{1-e^2}\sin i}\frac{\partial U}{\partial i} \\
\frac{dM}{dt} &= n - \frac{2}{na}\frac{\partial U}{\partial a} - \frac{1-e^2}{na^2e}\frac{\partial U}{\partial e}
\end{aligned} \tag{7.30}$$

Exact analytical integration of resulting equations is not possible. In [40], the author does an approximate integration. It consists in introducing 1) the secular terms, supposing that the variables do not have short period variations, and 2) short and long period variations inserting only secular variations.
This method leads to the following secular effects:

$$\delta\Omega(t)|_{sec} = \frac{n}{\eta\sin i}\sum_l \left(\frac{Re}{a}\right)^l \dot{F}G(-J_l)(t-t_0) \tag{7.31}$$

$$\delta\omega(t)|_{sec} = n\sum_l \left(\frac{Re}{a}\right)^l \left[\frac{\eta}{e}\frac{\dot{G}}{G} - \frac{\cos i}{\eta\sin i}\frac{\dot{F}}{F}\right] FG(-J_l)(t-t_0)$$

$$\delta M|_{sec} = n\sum_l \left(\frac{Re}{a}\right)^l \left[2(l+1) - \frac{\eta^2}{e}\frac{\dot{G}}{G}\right] FG(-J_l)(t-t_0) \tag{7.32}$$

where $J_l = -C_{l,0}$. The periodical variations write:

$$\begin{aligned}
\delta a_{lmpq}|_{per} &= \frac{2\mu}{na^2}\left(\frac{Re}{a}\right)^l (l-2p+q)G_{lpq}F_{lmp}\frac{S_{lmpq}}{\dot{\phi}_{lmpq}} \\
\delta e_{lmpq}|_{per} &= \frac{\mu}{na^2}\left(\frac{Re}{a}\right)^l \left[(l-2p+q)\frac{1-e^2}{e} - (l-2p)\frac{\eta}{e}\right] G_{lpq}F_{lmp}\frac{S_{lmpq}}{\dot{\phi}_{lmpq}} \\
\delta i_{lmpq}|_{per} &= \frac{\mu}{na^2}\left(\frac{Re}{a}\right)^l \frac{(l-2p)\cos i - m}{\eta \sin i} G_{lpq}F_{lmp}\frac{S_{lmpq}}{\dot{\phi}_{lmpq}} \\
\delta \Omega_{lmpq}|_{per} &= -\frac{\mu}{na^2}\left(\frac{Re}{a}\right)^l \frac{1}{\eta \sin i} G_{lpq}\dot{F}_{lmp}\frac{S'_{lmpq}}{\dot{\phi}_{lmpq}} \\
\delta \omega_{lmpq}|_{per} &= \frac{\mu}{na^2}\left(\frac{Re}{a}\right)^l \left[\frac{\cos i}{\eta \sin i} G\dot{F} - \frac{\eta}{e}\dot{G}F_{lmp}\right]\frac{S'_{lmpq}}{\dot{\phi}_{lmpq}} \\
\delta M_{lmpq}|_{per} &= \frac{\mu}{na^3}\left(\frac{Re}{a}\right)^l \left[\frac{1-e^2}{e}\dot{G}_{lpq} - 2(l+1)G_{lpq} + 3\frac{(l-2p+q)n}{\dot{\phi}_{lmpq}}G_{lpq}\right] F_{lmp}\frac{S'_{lmpq}}{\dot{\phi}_{lmpq}}
\end{aligned} \quad (7.33)$$

7.3.2 Main drawbacks of Kaula's integration

In this subsection, we analyze the behavior of the analytical Kaula's solution with respect to a numerical integration of the potential. We aim at to detect the main drawbacks of Kaula's integration. We have used a LEO orbit for numerical applications defined by its orbital elements:

$a_0 = 7.\,10^6\ m$	$e_0 = 0,02$	$i_0 = 40°$
$\Omega_0 = 50°$	$\omega_0 = 60°$	$M_0 = 0$

Initial date is 20th february 1996 at midnight and the model of the gravity field that we use is EGM96_95. By the following, we enumerate some of the main mismodelling.

The role of the inital conditions

Instantaneous value of orbital elements, also known as osculating value ($\overrightarrow{EO}$) can be split artificially in two terms: the mean value ($\bar{\vec{EO}}$), and a periodic oscillation ($\delta\overrightarrow{EO}_{per}$). It is:

$$\overrightarrow{EO} = \bar{\vec{EO}} + \delta\overrightarrow{EO}_{per} \quad (7.34)$$

Mean value evolves with secular perturbations of the gravity field:

$$\bar{\vec{EO}}(t) = \bar{\vec{EO}}(t_0) + \delta\overrightarrow{EO}_{sec} \quad (7.35)$$

while periodic perturbations are given by short and long term perturbations. Secular perturbations are null at initial time (t_0), but it is not the case for periodic effects. So, at t_0, we can write:

$$\overrightarrow{EO}(t_0) = \bar{\vec{EO}}(t_0) + \delta\overrightarrow{EO}_{per}(t_0) \quad (7.36)$$

In Kaula's integration, initial periodic perturbations are disregard:

$$\overrightarrow{EO}(t_0) = E\bar{\vec{O}}(t_0) \tag{7.37}$$

Disregarding this terms has two consequences:

- It produces a constant shift on all the orbital elements. In figure 7.1, we have plotted osculating values of the semi-major axis and the eccentricity all over a day. In both elements, there is a the constant shift.
- Since initial mean orbital elements are not exact, secular terms (7.31) are neither. At the left side of figure 7.2 we have plotted the error (difference between the numerical and Kaula integration) on the osculating value of the ascending node over one hundred years. The main error is the secular term due to the difference of initial conditions.

Second order effects on J_2

All the effects that Kaula considers are linear with respect to the perturbation. Second order effects due to J_2 are the main remaining error. To prove so, we have done the following experience: at the right side of figure 7.2, we have plotted the error considering actual value of Earth J_2 $(1,083.10^{-3})$, and the a fictitious value, the double $(2,166.10^{-3})$. The figure proves that the error is quadratic with J_2 as expected.

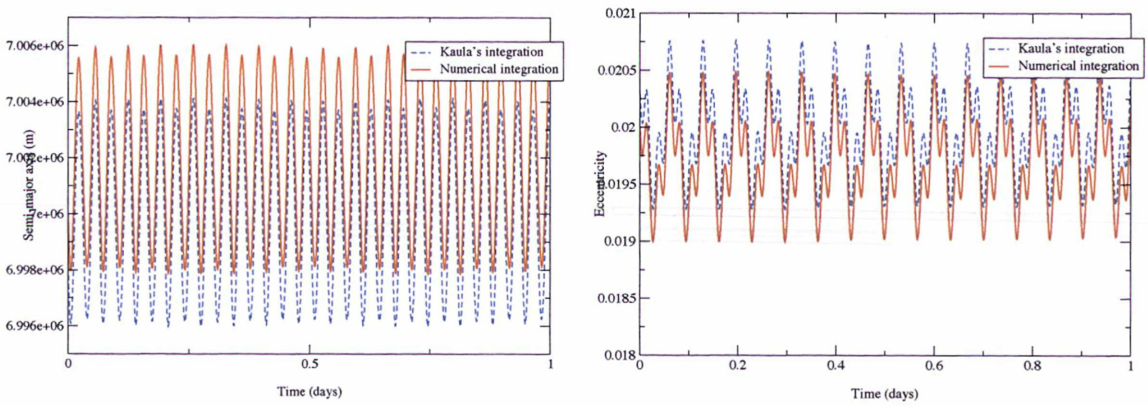

Figure 7.1: *At the left side, order 2 perturbations on semi-major axis. At the right side, perturbations on the eccentricity*

7.4 An alternative integration of the gravity field

7.4.1 The Hamiltonian formulation

In order to solve Kaula's integration drawback's, we have developed a theory based on canonical Lie transformations in order to obtain a better extrapolation of gravity field perturbations. The main advantage of the theory is that it takes into account secular effects proportional to J_2^2 and that also considers initial conditions. Furthermore, the main effects are in closed form, i.e., they are not expanded as power series of the eccentricity. The main limitation is

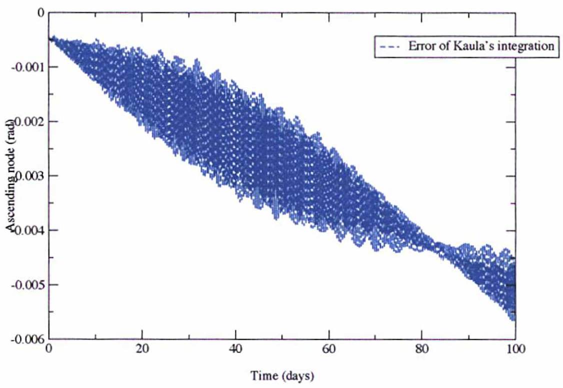

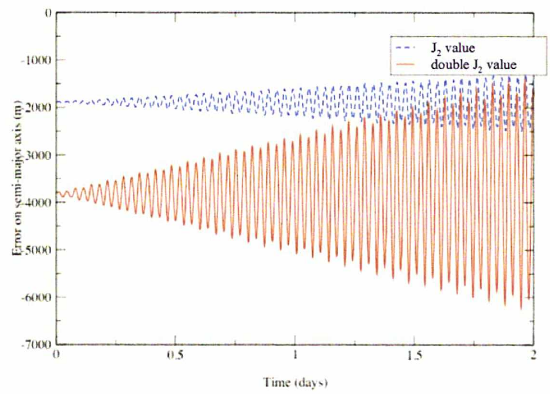

Figure 7.2: *At the left side, order 2 perturbations on ascending node over 100 days. At the right side, errors on semi-major axis considering a fictitious J2*

that the method do not introduce the non-linear effects of J2 in the short periods.

By the following, we use Delaunay variables defined in (2.1) instead of orbital elements because they form a set of canonical variables (necessary to use Hamiltonian formulation). We use the Hamiltonian ($\mathcal{K}$) given by the gravity field potential written as in equation (7.22). Moreover, to take into account that this potential is expressed in the Earth's frame rotating with an angular velocity ω_e (supposed to be constant):

$$\mathcal{K} = U - \omega_e H \tag{7.38}$$

The Hamiltonian is split in three parts, by decreasing magnitude of the perturbations:

$$\begin{aligned}
\mathcal{K} &= \mathcal{K}_0 + \mathcal{K}_1 + \frac{1}{2}\mathcal{K}_2 \\
\mathcal{K}_0 &= \frac{-\mu^2}{2L^2} - \omega_e H \\
\mathcal{K}_1 &= \frac{1}{4} J_2 \frac{\mu R_e^2}{r^3}\left[(1 - 3\cos^2 i) - 3\sin^2 i \cos(2f + 2g)\right] \\
\mathcal{K}_2 &= -2 \sum_{n=2}^{\infty}\sum_{m=0}^{n}\sum_{p=0}^{n}\sum_{q=-\infty}^{\infty} \bar{K}_{lm}^{c} \bar{F}_{lmk}^{c} G_{lpk} e^{im\Phi}
\end{aligned} \tag{7.39}$$

Zero order includes Keplerian effects, the first order includes the J_2 effects, and the second order the rest of the gravity field. This division enables to consider J_2 effects separately from the rest of the gravity field.

7.4.2 Canonical transformations

We use the Deprit-Lie algorithm to obtain canonical transformations. The goal of the method is to obtain a hamiltonian that does not depend on angular variables. In order to do so, we do two transformations. First one transforms the variables:

$$(H, G, L, h, g, l) \rightarrow (H', G', L', h', g', l') \tag{7.40}$$

and the hamiltonian:

$$\mathcal{K} \rightarrow \mathcal{K}' = f(L', G', H', g') \tag{7.41}$$

The first transformation removes the short period terms of the hamiltonian by averaging over the variables l and g. And the second transformation:

$$(H', G', L', h', g', l') \rightarrow (H'', G'', L'', h'', g'', l'') \tag{7.42}$$

$$\mathcal{K}' \rightarrow \mathcal{K}'' = f(L'', G'', H'') \tag{7.43}$$

The second transformation deals with the long periods. It is important to mention that when we construct the transformations, we respect only the lower order terms, but we may do some changes in higher terms.

Once this last hamiltonian obtained, its integration is really simple. Using classical hamiltonian theory we know that:

$$\frac{dP_i}{dt} = -\frac{\partial \mathcal{K}}{\partial Q_i} \qquad \frac{dQ_i}{dt} = \frac{\partial \mathcal{K}}{\partial P_i} \tag{7.44}$$

where P, Q are a couple of action-angle variables. Application of precedent equations leads to:

$$\frac{dH''}{dt} = 0 \qquad \frac{dG''}{dt} = 0 \qquad \frac{dL''}{dt} = 0 \tag{7.45}$$

$$\frac{dh''}{dt} = \delta h_{sec} \qquad \frac{dg''}{dt} = \delta g_{sec} \qquad \frac{dl''}{dt} = \delta l_{sec} \tag{7.46}$$

This method uses an exact integration of the equations but the errors come from the canonical transformations which neglect high order terms.

Use of the method For simplicity sake, we transform our Delaunay variables in orbital elements for its use. We use three sets of orbital elements $\overrightarrow{EO}$, $\overrightarrow{EO}'$, $\overrightarrow{EO}''$ corresponding to the three sets of Delaunay variables. The method is composed by three steps:

- Transformation of initial conditions:

$$\overrightarrow{EO}'(t_0) = \overrightarrow{EO}(t_0) + \delta\overrightarrow{EO}|_{sp}(t_0) \tag{7.47}$$

$$\overrightarrow{EO}''(t_0) = \overrightarrow{EO}'(t_0) + \delta\overrightarrow{EO}'|_{lp}(t_0) \tag{7.48}$$

- Extrapolation of the motion including secular terms:

$$\overrightarrow{EO}''(t) = \overrightarrow{EO}''(t_0) + \delta\overrightarrow{EO}''|_{sec}.(t - t_0) \tag{7.49}$$

- Recuperation of initial variables:

$$\overrightarrow{EO}'(t) = \overrightarrow{EO}''(t) - \delta\overrightarrow{EO}''|_{lp}(t) \tag{7.50}$$
$$\overrightarrow{EO}(t) = \overrightarrow{EO}'(t) - \delta\overrightarrow{EO}'|_{sp}(t) \tag{7.51}$$

The exact expressions of perturbations are detailed in annex A.

7.4.3 Numerical simulations

Numerical simualtions confirm that our new solutions works better than Kaula solution, and it also points the non-considered terms. In order to improve our theory, these terms should be included.

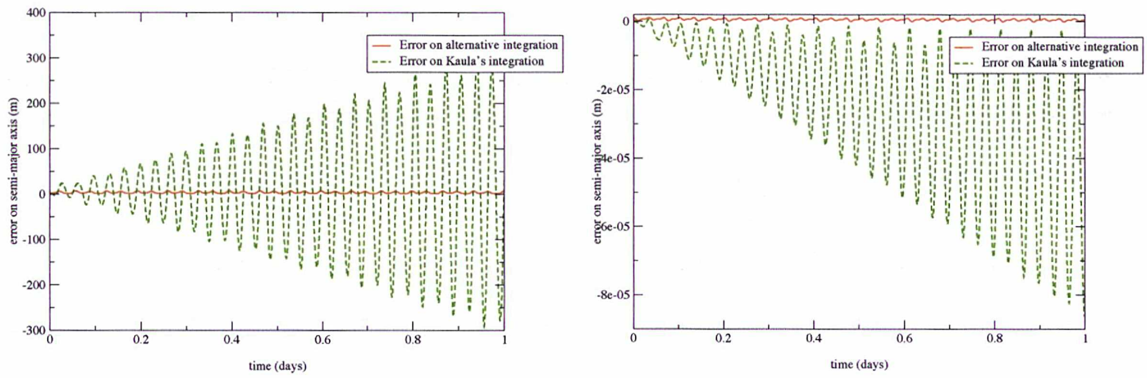

Figure 7.3: *Comparison of J2 errors between two analytical integrations*

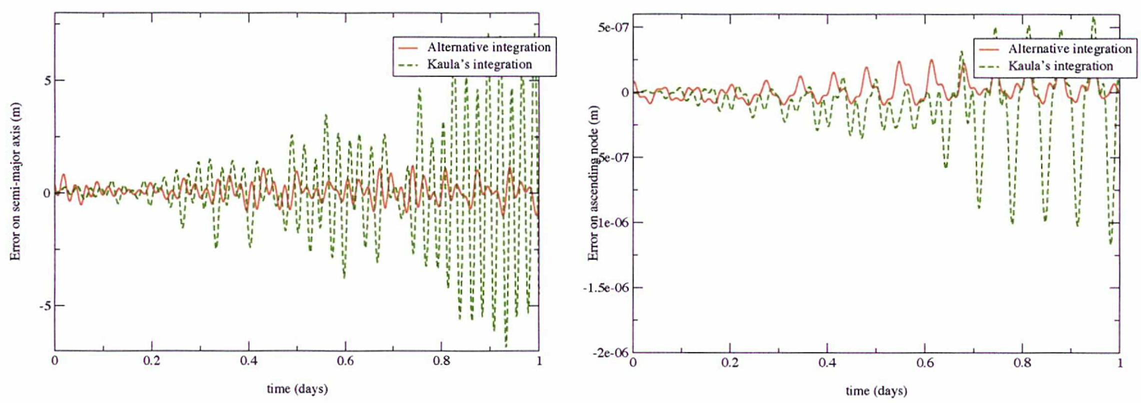

Figure 7.4: *Comparison of order 3 errors between two analytical integrations*

In figure 7.3, I have plotted the errors on semi-major axis and ascending node considering only J_2 effects for both analytical theories. I have disregard constant shift in Kaula's integration for clarity's sake. The figure proves the improvement of our method. In figure 7.4, I have plotted the same errors, for the same orbital elements, considering the effects of the third degree of the gravity field. Once again, the results are improved. Similar results are found for higher orders of the gravity field.

7.5 Differential effects

In this section, we explain how to obtain the matrix $\mathcal{L}_{GF}$ used in differential orbital elements method in order to integrate gravity field effects on formation flying. We write extrapolation process on orbital elements as follows (where we neglect vector sign in order to simplifiy expressions):

$$EO'(t_0) = f(EO(t_0)) \quad \rightarrow \quad \Delta EO'(t_0) = \left[\frac{df}{dEO}|_{EO(t_0)}\right] \Delta EO(t_0) \tag{7.52}$$

$$EO''(t_0) = g(EO'(t_0)) \quad \rightarrow \quad \Delta EO''(t_0) = \left[\frac{dg}{dEO'}|_{EO'(t_0)}\right] \Delta EO'(t_0)$$

$$EO''(t) = h(EO''(t_0)) \quad \rightarrow \quad \Delta EO''(t) = \left[\frac{dh}{dEO''}|_{EO''(t_0)}\right] \Delta EO''(t_0)$$

$$EO'(t) = g^{-1}(EO''(t)) \quad \rightarrow \quad \Delta EO'(t) = \left[\frac{dg^{-1}}{dEO''}|_{EO''(t)}\right] \Delta EO''(t) \tag{7.53}$$

$$EO(t) = f^{-1}(EO'(t)) \quad \rightarrow \quad \Delta EO(t) = \left[\frac{df^{-1}}{dEO'}|_{EO'(t)}\right] \Delta EO'(t)$$

Matrix $\mathcal{L}_{GF}$ is given by the compilation of all the derivatives:

$$\mathcal{L}_{GF} = \left[\frac{df^{-1}}{dEO'}|_{EO'(t)}\right]\left[\frac{dg^{-1}}{dEO''}|_{EO''(t)}\right]\left[\frac{dh}{dEO''}|_{EO''(t_0)}\right]\left[\frac{dg}{dEO'}|_{EO'(t_0)}\right]\left[\frac{df}{dEO}|_{EO(t_0)}\right] \tag{7.54}$$

7.6 Conclusions

First part of the chapter is devoted to clarify the different representations of the gravity field potential. We have proved that they are equivalent but normalization and inclination functions are different. Once the potential settled, we present two methods to compute its effects on the gravity field.

First method is Kaula's integration. It is a very useful method but its precision is not very high. That's why we have developed an alternative method. The alternative method uses Lie canonical transformation to obtain a new hamiltonian that can be integrated in a trivial way. Precision of this method is improved with respect to Kaula's method.

At last we use the differential orbital elements in order to obtain the perturbative effects of the gravity field in the relative motion.

Chapter 8

The solar radiation pressure

8.1 Introduction

For high orbits, the effects of the Earth's gravity field are much reduced and the main perturbations are solar radiation pressure and lunisolar effects. As I will prove, solar radiation pressure may be predominant in formation flying when satellites do not have the same area to mass ratio ($\frac{S}{m}$). That's the reason why we dedicate a chapter to obtain analytical expressions for the effects of solar radiation pressure on orbital elements.
First section is devoted to the modellization of the solar radiation pressure. Different models are used in literature. We use the simplest one.
Under some simplifications, solar radiation pressure is a conservative force and derives from a potential. The effects of the potential on orbital elements and the integration of resulting equations is done in second section. A similar procedure is followed in [45], [5], and [12], but we use mean anomaly instead of true anomaly as independent variable.
Last section is devoted to the differential effects. We prove that the effects induced by difference of $\frac{S}{m}$ are usually much bigger than the effects induced by the difference of position.

8.2 Solar radiation pressure

Solar radiation pressure is the force exerted by solar radiation on objects within its reach. The force can be expressed as:

$$\vec{a} = -\left(1+\beta\right) P_s \frac{S}{m} \left(\frac{a_s}{r_s}\right)^2 \vec{u}_{sat} \tag{8.1}$$

where:

- β : index of reflection of the satellite. Its value is usually around 0.3
- P_s : it is a pressure, with a value: $P_S = 4,6510^{-6}$ Pa
- $\frac{S}{m}$: area to mass ratio of the satellite
- $\frac{a_s}{r_s}$: ratio distance to the Sun from satellite and from Earth
- $\vec{u}_{sat}$: unit vector of the position of the satellite in the used reference frame

In order to take into account perturbations induced by this force, two ways are possible. (1) using the Gauss equations directly with the force, (2) computing the potential associated to the force, and use Lagrange planetary equations. Both methods are equivalent.
The main difficulty for both of them is the modellization of shadow regions, the regions where due to the cone of shadow projected by the Earth over the satellite, there is no solar radiation pressure. In low orbits, shadow regions are computed numerically and considered apart. But, since we are interested in very high eccentric orbits, with high semi-major axis, shadow regions are negligible (for Simbol-X mission shadow regions are never bigger than a 4 % of total orbit).
By the following, we evaluate the perturbations of the SRP on the orbital elements using its associated potential.

8.2.1 Integration of the potential

If we neglect the shadow regions, precedent force is conservative, and its associated potential is:

$$U_{SRP} = -\sigma \frac{S}{m} r_{sat} \vec{u}_{sun} \cdot \vec{u}_{sat} \tag{8.2}$$

with:

$$\sigma = (1 + \beta)\, P_s \left(\frac{a_s}{r_s} \right)^2 \tag{8.3}$$

and $\vec{u}_{sun}$ is the unit vector of the the position of the Sun with respect to the used reference frame. We work in a Earth-centered inertial equatorial frame. In this reference frame, the unit vector of the satellite is:

$$\vec{u}_{sat} = (\cos\Omega \cos u - \sin\Omega \sin u \cos i, \sin\Omega \cos u + \cos\Omega \sin u \cos i, \sin u \sin i)^T \tag{8.4}$$

To compute the unit vector of the Sun, we use the following simplified model:
In an Earth-centered ecliptic frame, the unit vector of the Sun is:

$$\vec{u}_{sun}|_{ecliptic} = (\cos\alpha, \sin\alpha, 0)^T \tag{8.5}$$

with the angle:

$$\alpha = 2\pi \frac{\text{day number}}{365} - 0,4452\pi \tag{8.6}$$

where day number is the number of the day of the year. Transformation into Earth-centered inertial equatorial frame can be easily done using matrix:

$$\mathcal{P} = \begin{pmatrix} 1 & 0 & 0 \\ 0 & \cos\epsilon & -\sin\epsilon \\ 0 & \sin\epsilon & \sin\epsilon \end{pmatrix} \tag{8.7}$$

where the obliquity $\epsilon = 23,4364°$ is the angle between the equatorial and the ecliptic planes of the Earth. We get:

$$\overrightarrow{u}_{sun}|_{equatorial} = [\mathcal{P}] \,.\, \overrightarrow{u}_{sun}|_{ecliptic} = (A_s, B_s, C_s)^T \tag{8.8}$$

Introducing previous expressions for Sun and satellite position, we get following expression for the potential:

$$\begin{aligned} U = -\sigma \frac{S}{m} \frac{a(1-e^2)}{1+e\cos f} \Big[& A_s \left(\cos\Omega \cos u - \sin\Omega \sin u \cos i\right) \\ & + B_S \left(\sin\Omega \cos u + \cos\Omega \sin u \cos i\right) + C_S \sin u \sin i \Big] \end{aligned} \tag{8.9}$$

We rewrite the potential introducing auxiliary functions:

$$\begin{aligned} \mathcal{F} &= A_s \left(\cos\Omega \cos\omega - \sin\Omega \sin\omega \cos i\right) + B_S \left(\sin\Omega \cos\omega + \cos\Omega \sin\omega \cos i\right) + C_S \sin\omega \sin i \\ \mathcal{G} &= -A_s \left(\cos\Omega \sin\omega + \sin\Omega \cos\omega \cos i\right) + B_S \left(-\sin\Omega \sin\omega + \cos\Omega \cos\omega \cos i\right) + C_S \cos\omega \sin i \end{aligned}$$

to get:

$$U = -\sigma \frac{S}{m} \frac{a(1-e^2)}{1+e\cos f} \left(\cos f \mathcal{F}(i,\Omega,\omega) + \sin f \mathcal{G}(i,\Omega,\omega)\right) \tag{8.10}$$

We will also need the derivatives of $\mathcal{F}$ and $\mathcal{G}$ with respect to the angles:

$$\begin{aligned} \mathcal{F}_i &= A_S \left(\sin\Omega \sin i \sin\omega\right) - B_S \left(\cos\Omega \sin i \sin\omega\right) + C_S \cos i \sin\omega \\ \mathcal{F}_\Omega &= A_S \left(-\sin\Omega \cos\omega - \cos\Omega \cos i \sin\omega\right) + B_S \left(\cos\Omega \cos\omega - \sin\Omega \cos i \sin\omega\right) \\ \mathcal{F}_\omega &= A_S \left(-\cos\Omega \sin\omega - \sin\Omega \cos i \cos\omega\right) + B_S \left(-\sin\Omega \sin\omega + \cos\Omega \cos i \cos\omega\right) + C_S \sin i \cos\omega \end{aligned} \tag{8.11}$$

$$\begin{aligned} \mathcal{G}_i &= A_S \left(\sin\Omega \sin i \cos\omega\right) - B_S \left(\cos\Omega \sin i \cos\omega\right) + C_S \cos i \cos\omega \\ \mathcal{G}_\Omega &= A_S \left(\sin\Omega \sin\omega - \cos\Omega \cos i \cos\omega\right) - B_S \left(\cos\Omega \sin\omega + \sin\Omega \cos i \cos\omega\right) \\ \mathcal{G}_\omega &= -A_S \left(\cos\Omega \cos\omega - \sin\Omega \cos i \sin\omega\right) - B_S \left(\sin\Omega \cos\omega + \cos\Omega \cos i \sin\omega\right) - C_S \sin i \sin\omega \end{aligned} \tag{8.12}$$

The last step consists in substituting the mean anomaly to the true anomaly in eq. (8.10) in order to use Lagrange planetary equations. We use the well-known classical development with Bessel functions, as can be found, for example, in [16]:

$$\begin{aligned} r\cos f &= a \left(-\frac{3}{2}e + \sum_1^\infty \frac{2}{s} J_s'(se) \cos sM \right) \\ r\sin f &= \frac{2a\eta}{e} \sum_1^\infty \frac{1}{s} J_s(se) \sin sM \end{aligned} \tag{8.13}$$

where $J_s(se)$ is the Bessel function of order s and argument se, and $J_s'(se)$ are the derivatives of Bessel functions with respect to the argument. We also compute the derivatives of equations (8.13) with respect to the argument, se, because it is required thereafter:

$$\begin{aligned}
\frac{d}{de}(r\cos f) &= a\left(-\frac{3}{2}+\sum_{1}^{\infty}2J_s''(se)\cos sM\right) \\
\frac{d}{de}(r\sin f) &= 2a\sum_{1}^{\infty}\left(\frac{\eta}{e}J_s'(se)-\frac{1}{\eta e^2}\frac{1}{s}J_s(se)\right)\sin sM
\end{aligned} \tag{8.14}$$

Once the mean anomaly introduced, the potential has the right form to use Lagrange equations:

$$\begin{aligned}
\frac{da}{dt} &= -\frac{2\sigma}{n}\frac{S}{m}\sum_{s=1}^{\infty}\left(-2J_s'(se)\sin sM\mathcal{F}+\frac{2\eta}{e}J_s(se)\cos sM\mathcal{G}\right) \\
\frac{de}{dt} &= -\frac{\eta\sigma}{nae}\frac{S}{m}\Big[-\frac{3}{2}e\mathcal{F}_\omega+\sum_{s=1}^{\infty}\Big(-\sin sM\left(2\eta J_s'(se)\mathcal{F}+\frac{2\eta}{es}J_s(se)\mathcal{G}_\omega\right)+ \\
&\quad \cos sM\left(\frac{2\eta^2}{e}J_s(se)\mathcal{G}-\frac{2}{s}J_s'(se)\mathcal{F}_\omega\right)\Big)\Big] \\
\frac{di}{dt} &= -\frac{\sigma}{na\eta\sin i}\frac{S}{m}\Big[-\frac{3}{2}e\left(\cos i\mathcal{F}_\omega-\mathcal{F}_\Omega\right)+\sum_{s=1}^{\infty}\Big(\frac{2}{s}J_s'(se)\cos sM\left(\cos i\mathcal{F}_\omega-\mathcal{F}_\Omega\right)+ \\
&\quad \frac{2\eta}{es}J_s(se)\sin sM\left(\cos i\mathcal{G}_\omega-\mathcal{G}_\Omega\right)\Big)\Big] \\
\frac{d\Omega}{dt} &= -\frac{\sigma}{na\eta\sin i}\frac{S}{m}\left[-\frac{3}{2}e\mathcal{F}_i+\sum_{s=1}^{\infty}\left(\frac{2}{s}J_s'(se)\cos sM\mathcal{F}_i+\frac{2a\eta}{es}J_s(se)\sin sM\mathcal{G}_i\right)\right] \\
\frac{d\omega}{dt} &= -\frac{\sigma}{na}\frac{S}{m}\Big[-\frac{3}{2}\left(\frac{\eta}{e}\mathcal{F}-\frac{e\cot i}{\eta}\mathcal{F}_i\right)+\sum_{s=1}^{\infty}\Big(2\cos sM\left(\frac{\eta}{e}J_s''(se)\mathcal{F}-\frac{\cot i}{\eta}\frac{1}{s}J_s'(se)\mathcal{F}_i\right)+ \\
&\quad 2\sin sM\left(\frac{\eta}{e}\left(\frac{\eta}{e}J_s'(se)-\frac{1}{\eta e^2}\frac{1}{s}J_s(se)\right)\mathcal{G}-\frac{\cot i}{\eta}\frac{\eta}{es}J_s(se)\mathcal{G}_i\right)\Big)\Big] \\
\frac{dM}{dt} &= \frac{\sigma}{na}\frac{S}{m}\Big[-\frac{3}{2}\mathcal{F}\left(2e+\frac{\eta^2}{e}\right)+\sum_{s=1}^{\infty}\Big(2\cos sM\mathcal{F}\left(\frac{2}{s}J_s'(se)+\frac{\eta^2}{e}J_s''(se)\right)+ \\
&\quad 2\sin sM\mathcal{G}\left(\frac{2\eta}{es}J_s(se)+\frac{\eta^3}{e^2}J_s'(se)-\frac{\eta}{e^3 s}J_s(se)\right)\Big)\Big]
\end{aligned}$$

Exact integration of these equations is not possible, but a first approach, considering just secular keplerian evolution of orbital elements is done. This approach is similar to Kaula's approach for integration of the gravity field.

In order to improve the precision, we should consider secular effects when computing short periods. It may also be possible to consider coupling between J_2 effects and SRP introducing J_2 effects as secular ones on the integration. But, the obtained precision (relative error lower than 10%) using the Keplerian model for secular terms seems reasonable for our purposes. We finally obtain:

$$
\begin{aligned}
\delta a(t) &= -\frac{2\sigma}{n^2}\frac{S}{m}\sum_{s=1}^{\infty}\left(\frac{2}{s}J_s'(se)\cos sM\mathcal{F} + \frac{2\eta}{es}J_s(se)\sin sM\mathcal{G}\right) \\
\delta e(t) &= -\frac{\eta\sigma}{nae}\frac{S}{m}\Big[\frac{3}{2}e\mathcal{F}_\omega(t-t_0) + \sum_{s=1}^{\infty}\Big(\frac{\cos sM}{sn}\left(2\eta J_s'(se)\mathcal{F} + \frac{2\eta}{es}J_s(se)\mathcal{G}_\omega\right) + \\
&\quad \frac{\sin sM}{sn}\left(\frac{2\eta^2}{e}J_s(se)\mathcal{G} - \frac{2}{s}J_s'(se)\mathcal{F}_\omega\right)\Big)\Big] \\
\delta i(t) &= -\frac{\sigma}{na\eta\sin i}\frac{S}{m}\Big[-\frac{3}{2}e\left(\cos i\mathcal{F}_\omega - \mathcal{F}_\Omega\right)(t-t_0) + \sum_{s=1}^{\infty}\Big(\frac{2}{s}J_s'(se)\frac{\sin sM}{sn}\left(\cos i\mathcal{F}_\omega - \mathcal{F}_\Omega\right) - \\
&\quad \frac{2\eta}{es}J_s(se)\frac{\cos sM}{sn}\left(\cos i\mathcal{G}_\omega - \mathcal{G}_\Omega\right)\Big)\Big] \\
\delta\Omega(t) &= -\frac{\sigma}{na\eta\sin i}\frac{S}{m}\left[-\frac{3}{2}e\mathcal{F}_i(t-t_0) + \sum_{s=1}^{\infty}\left(\frac{2}{ns^2}J_s'(se)\sin sM\mathcal{F}_i - \frac{2a\eta}{ens^2}J_s(se)\cos sM\mathcal{G}_i\right)\right] \\
\delta\omega(t) &= -\frac{\sigma}{na}\frac{S}{m}\Big[-\frac{3}{2}\left(\frac{\eta}{e}\mathcal{F} - \frac{e\cot i}{\eta}\mathcal{F}_i\right)(t-t_0) + \sum_{s=1}^{\infty}\left(2\frac{\sin sM}{sn}\left(\frac{\eta}{e}J_s''(se)\mathcal{F} - \frac{\cot i}{\eta}\frac{1}{s}J_s'(se)\mathcal{F}_i\right) - \right. \\
&\quad 2\frac{\cos sM}{sn}\left(\frac{\eta}{e}\left(\frac{\eta}{e}J_s'(se) - \frac{1}{\eta e^2}\frac{1}{s}J_s(se)\right)\mathcal{G} - \frac{\cot i}{\eta}\frac{\eta}{es}J_s(se)\mathcal{G}_i\right)\Big)\Big] \\
\delta M(t) &= \frac{\sigma}{na}\frac{S}{m}\Big[-\frac{3}{2}\mathcal{F}\left(2e + \frac{\eta^2}{e}\right)(t-t_0) + \sum_{s=1}^{\infty}\Big(2\frac{\sin sM}{sn}\mathcal{F}\left(\frac{2}{s}J_s'(se) + \frac{\eta^2}{e}J_s''(se)\right) - \\
&\quad 2\frac{\cos sM}{sn}\mathcal{G}\left(\frac{2\eta}{es}J_s(se) + \frac{\eta^3}{e^2}J_s'(se) - \frac{\eta}{e^3 s}J_s(se)\right)\Big)\Big]
\end{aligned}
$$

Our method has the same inconvenient that Kaula's method. It is, there is a difference between the osculating ($\overrightarrow{EO}$) and the mean ($\vec{\bar{EO}}$) variables. This difference can be mitigated by taking into account the initial phase of the perturbation. It is:

$$\vec{\bar{EO}}(t_0) = \overrightarrow{EO}(t_0) - \delta\overrightarrow{EO}(t_0) \tag{8.15}$$

When considering mean elements, we must include a second term on the evolution of the mean anomaly:

$$\delta M^{(2)}(t) = -\frac{3}{2}\frac{n}{a}\Delta a(t_0)\,(t-t_0) \tag{8.16}$$

And temporal evolution of osculating orbital elements is given by keplerian terms plus SRP perturbations:

$$\overrightarrow{EO}(t) = \overrightarrow{EO}(t)|_{kep} + \delta\overrightarrow{EO}(t) - \delta\overrightarrow{EO}(t_0) \tag{8.17}$$

8.2.2 Numerical tests

In order to verify precedent equations, we have tested them using as bench mark numerical integration of the forces. We use as test orbit a typical HEO orbit, for which the SRP effects are the most important in comparaison to other perturbations. Parameters of the orbit are:

$a_0 = 1.\ 10^8\ m$	$e_0 = 0,7$	$i_0 = 10°$
$\Omega_0 = 10°$	$\omega_0 = 10°$	$M_0 = 0$

Initial date is 20th february 1996, the duration of the simulation is 4 days and $\Delta\frac{S}{m}$ is $3.\ 10^{-3}\ m^2/kg$. Figure (8.1) shows obtained results using the analytical extrapolation and numerical integration.

Some conclusions can be drawn from these simulations. First, we detect residual secular variations in the inclination and the ascending node. In fact, longer simulations show that in numerical integrations we find not only secular effects, but also long periods which are not modeled in our analytical expressions. We have verified that these long periods are not linked with changing position of Sun with respect to the Earth.
In spite of these mismodellizations, results are accurate enough to provide necessary information for mission analysis.

8.2.3 Differential effects

Differential effects have two origins (i) a difference on the ratio $\frac{S}{m}$, and (ii) a difference of position. Figures 8.2 show the importance of each of them. Figures prove that, even for very large configurations, the effects due to the difference of $\frac{S}{m}$ are dominant over the others. That's the reason why in this section we have considered the effects providing from a difference of $\frac{S}{m}$ and we disregard the effects providing from a difference of position.

Terms providing from a $\frac{S}{m}$ are not linear with the orbital elements, but with $\Delta\frac{S}{m}$. In order to keep the matricial formulation we introduce following enlarged vectors:

$$\Delta\overrightarrow{EO}^{+} = (\Delta\overrightarrow{EO}, \Delta\frac{S}{m})^T \tag{8.18}$$

$$\Delta\overrightarrow{x}^{+} = (\Delta\overrightarrow{x}, \Delta\frac{S}{m})^T \tag{8.19}$$

Matrices will also be enlarged in following way:

$$(\mathcal{M}^{-1})^{+} = \left(\begin{array}{c|c} \mathcal{M}^{-1} & 0 \\ \hline 0 & 1 \end{array}\right) \qquad \mathcal{M}^{+} = \left(\begin{array}{c|c} \mathcal{M} & 0 \\ \hline 0 & 1 \end{array}\right) \qquad \mathcal{L}^{+} = \left(\begin{array}{c|c} \mathcal{L} & 0 \\ \hline 0 & 1 \end{array}\right) \tag{8.20}$$

$\mathcal{L}_{SRP}$ matrix for solar radiation pressure reads:

$$\mathcal{L}^{+}_{SRP} = \begin{pmatrix} 0 & 0 & 0 & 0 & 0 & 0 & \frac{\delta a(t)}{S/m} \\ 0 & 0 & 0 & 0 & 0 & 0 & \frac{\delta e(t)}{S/m} \\ 0 & 0 & 0 & 0 & 0 & 0 & \frac{\delta i(t)}{S/m} \\ 0 & 0 & 0 & 0 & 0 & 0 & \frac{\delta \Omega(t)}{S/m} \\ 0 & 0 & 0 & 0 & 0 & 0 & \frac{\delta \omega(t)}{S/m} \\ 0 & 0 & 0 & 0 & 0 & 0 & \frac{\delta M(t)}{S/m} \\ 0 & 0 & 0 & 0 & 0 & 0 & 1 \end{pmatrix} \tag{8.21}$$

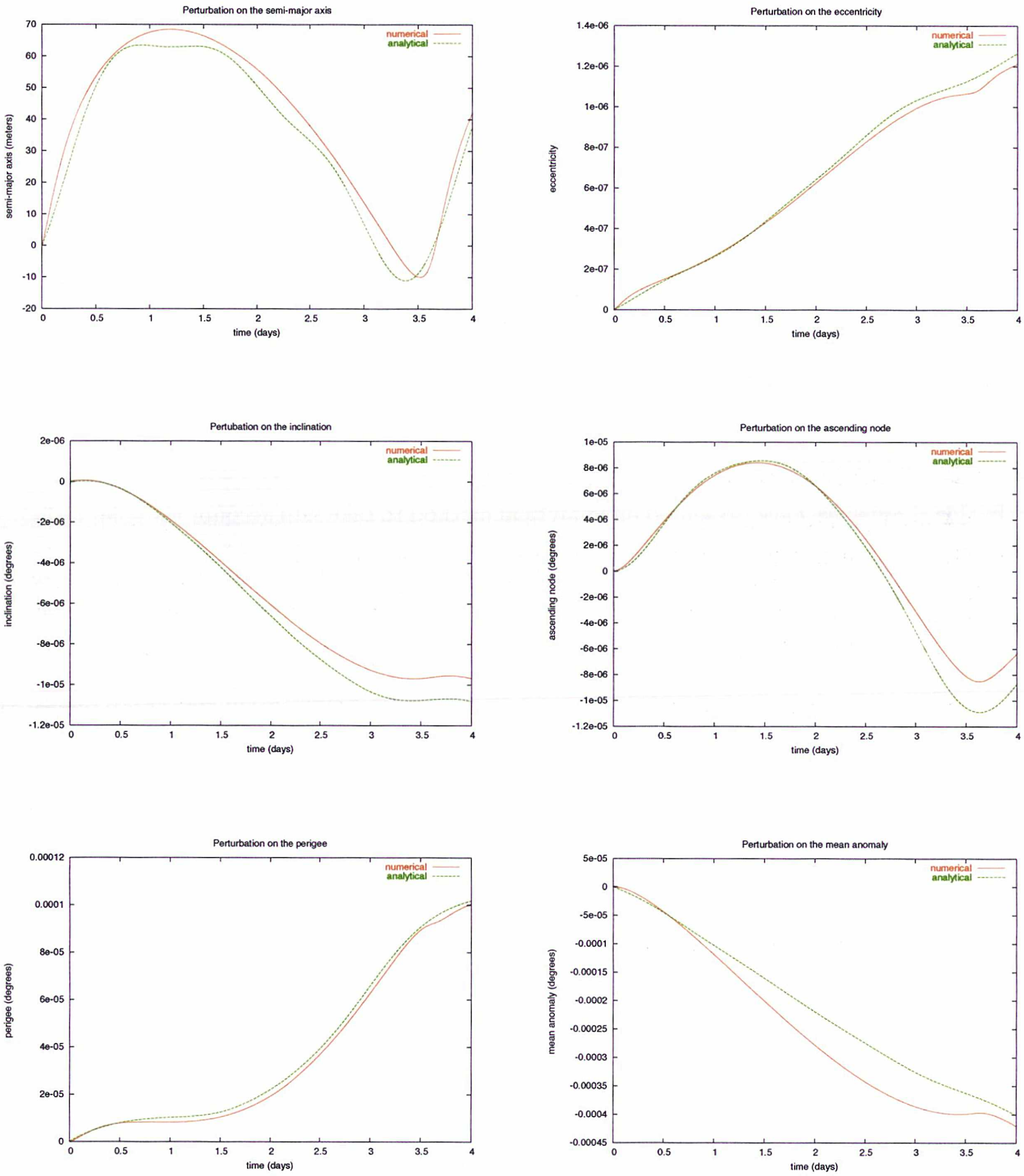

Figure 8.1: *Numerical tests for solar radiation pressure effects*

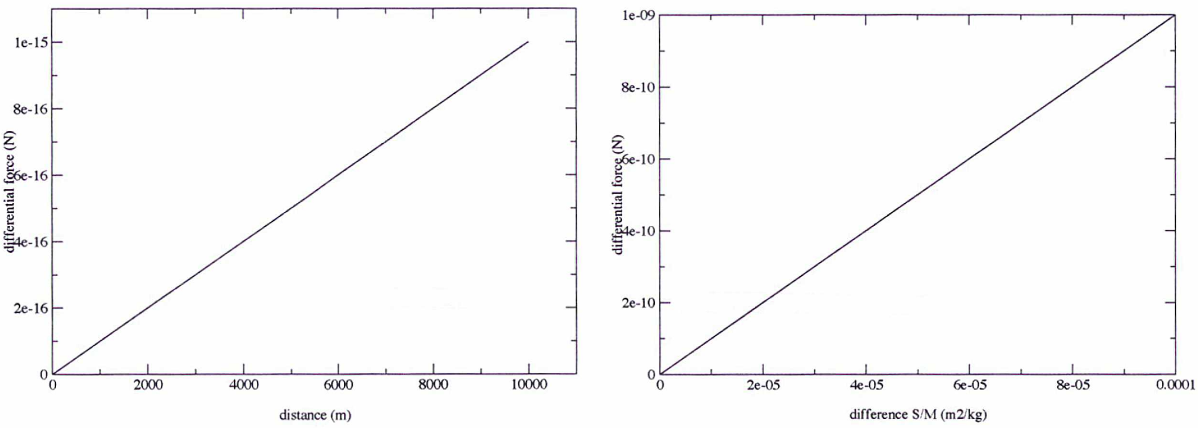

Figure 8.2: *Differential force for different configurations*

8.3 Conclusions

In this chapter we have presented an analytical method to take into account the solar radiation pressure. Even if the accuracy of the method is not very high, it is well suited for our purposes of mission analysis. Simplifications are done in two ways: (i) in the modellization of the solar radiation pressure, and (ii) in the integration of the potential. The model that we use neglects perpendicular forces, and shadow regions. The integration is done considering Keplerian secular effect as the only variation.

In last section we present differential effects on formation flying. Main effects are due to the difference of $\frac{S}{m}$. For big values of these variable, we join solar sails concept. It might be an interesting alternative to formation flying control.

Part III

Future missions for Earth and Universe observation

Chapter 9

Space missions to measure the gravity field

9.1 Introduction

One of the first scientific formation flying missions was GRACE. This mission is devoted to the study of the Earth gravity field. As it was described in chapter 1, the formation is composed of two satellites with the same orbit and separated by a difference of anomaly.
Data from GRACE missions have been analysed during the last six years producing new models of gravity field [67], [68]. Future gradiometry mission GOCE [2] will help to improve the accuracy of the gravity field. Data from these two missions will improve our knowledge of the gravity field, but some authors claim that the precision should be still improved. [53], [24], [1], [65].
We have explored the possibilities of two different technologies for future space geodesy missions: (i) formation flying missions, and (ii) tethered systems. In order to do so, I have analyzed the possibilities of the systems through the study of its covariance matrix as explained in [43] and [64].
The interest of formation flying for space geodesy has been studied before in [66], [49]. We can find several studies in the literature about the sensitivity of the configuration to the gravity field [18], [41], [63], [6]. The originality of our method is the use of a completely analytical model of the perturbations of the gravity field. Tethers for gravity field determination have been studied in [32], but we do not have found any papers analyzing the covariance matrix.
In the first part of the chapter, we introduce the covariance matrix. In the second section, we analyze the future needs for gravity field determination as well as the different available technologies. Section three and four deal with tethered systems and formation flying respectively. In the last section, we present the sensitivity analysis.

9.1.1 The covariance matrix

The principle of the determination of the gravity field is as follows. Gravity field perturbs the trajectories of the satellites around the central body. Hence, measuring the perturbations of the trajectories, we can go back to the coefficients characterizing the gravity field. The measurement linked to effects of the gravity field can be performed directly on the absolute trajectory, or on the relative trajectory. The gradiometric technics is slightly different because

it is not based on the deformation of the trajectory but, in any case, the procedure to obtain the coefficients of the gravity field from the observations, is the following.
First, a model of the observable is done. The model includes the parameters characterising the gravity field and many others, as the initial position of the satellite, the Earth atmosphere, or other perturbations that can affect the motion of the satellite. In a general way, we write the model as:

$$\overrightarrow{obs} = \overrightarrow{f}\,(\overrightarrow{coef}) \tag{9.1}$$

We assign a priori values to all the unknown coefficients of the model $(\overrightarrow{coef_0})$. With these values we compute the a priori values of the observation $(\overrightarrow{obs_0})$, which are certainly different of the real observed values $(\overrightarrow{obs_c})$. Supposing that a priori values of the unknown coefficients are close enough to the real ones, we linearize the observables in order to obtain following matricial system:

$$\overrightarrow{obs_c} - \overrightarrow{obs_0} = \frac{d\overrightarrow{f}}{d\overrightarrow{coef}}|_{\overrightarrow{coef_0}}(\overrightarrow{coef_c} - \overrightarrow{coef_0}) \tag{9.2}$$

The derivatives are computed with a priori values of the coefficients. The determination of the coefficients can be obtained through the inversion of the matrix $\frac{d\overrightarrow{f}}{d\overrightarrow{coef}}|_{\overrightarrow{coef_0}}$. The system can iterate until the convergence. If the matrix is overdetermined, one seeks those unknowns $\overrightarrow{coef}$ that minimize the weighted discrepancies in quadratic sense. Even if the principle of the resolution of a least squares method is simple, its practical application is a highly complicated technique on itself where several parameters play an important role (length of the arcs, combination of observations, considerer perturbations,...) and we do not deep on it. By the following, we summarize its main aspects.

Least squares method We write precedent matricial form as follows:

$$y = Ax \tag{9.3}$$

Since measurements contain noise by nature, the vector of observations is a stochastic variable, with an expectation:

$$E\{y\} = Ax \tag{9.4}$$

and a dispersion:

$$D\{y\} = Q_y \tag{9.5}$$

where Q_y is the covariance matrix of the vector of observations. Least squares estimator gives the dispersion of the unknowns vector, also known as the posterior covariance matrix:

$$D\{x\} = \left(A^T P_y A\right)^{-1} = N^{-1} = Q_x \tag{9.6}$$

where $P_y = Q_y^{-1}$. The posterior covariance matrix is the inverse of the normal matrix. Analysis of the covariance matrix gives a lot of information about the observation system. In particular, it gives the error spectrum of the coefficients:

- *Two-Dimensional Error Spectrum*: Inverting thet total normal matrix N yields the covariance matrix $Q_{\bar{x}}$ of estimated parameters. This is the basic output of least square method error simulation. In particular the square root of the diagonal represents the standard deviations σ_{lm} of single coefficients. The full set of σ_{lm} represents the error spectrum of the coefficients (in our case, $\bar{K}_{lm}$).

$$\mathrm{diag}(Q_{\bar{x}}) \rightarrow \mathrm{var}(\bar{K}_{lm}) = \sigma^2_{lm} \tag{9.7}$$

- *One-Dimensional Error Spectrum*: For representation reasons we might be more interested in obtaining a one-dimensional parameter which is defined as follows:

$$\sigma^2 = \sum_{m=-l}^{l} \sigma_{lm} \tag{9.8}$$

$$RMS_l = \sqrt{\frac{1}{2l+1}\sigma^2_l} \tag{9.9}$$

9.2 New challenges

With the data received from GRACE mission, and expected data from GOCE mission, the knowledge of the Earth gravity field will be significantly improved. In [53], following table is given for the remaining uncertainties:

Geoid (mm)	Gravity (mGal)	Spatial Scale (km)
1	0.03	200
10	0.2	100
45	2.0	65

Table 9.1: *Static field: geoid and gravity uncertainties after GRACE and GOCE missions*

In the same paper, the author points out three areas which would benefit from an improvement of the knowledge of the global gravity field:

- *Geoid and Gravity anomalies*: They reflect primarily mass anomalies of the inner configuration of the Earth, in particular, the lithosphere and the upper mantle. The precision of 1 cm for the geoid with a spatial resolution of 100 km expected with GOCE should be increased to a lower space resolution, 50-60 km.

- *Dynamic Ocean Topography*: Dynamic ocean topography is given by the difference between actual ocean surface (measured by satellite altimetry) and the geoid. An improvement of the geoid has direct repercussions on the dynamic ocean topography. In this area, an ultimate goal could be the determination of the geoid with a precision of 1 cm with a spatial resolution shorter than 50 km.

- *Temporal Variations of the Gravitational Field*: This item is the most complex because of the temporal dimension of the problem. A new variable appears: the time scale. Mass re-distribution of our planet can give information about global change phenomena as climate changing. GRACE is the first space mission specifically designed to monitor the temporal dimension of the gravity field, but its information is not sufficient. Future missions should focus on: monitoring, appropriate sampling in space and time, complementarity of data sets.

Until present, space geodesy has used absolute satellite trajectories tracking and inter-satellite distance ranging (GRACE). GOCE mission will introduce gradiometry. Different possibilities are considered for next generation of gravity field missions [65]. Different improvements (temporal scale, space scale, accuracy) should require different technologies.
By the following, we present two of them. We do not claim to be exhaustive in our research, but we focus only on the sensitivity of the observables to the gravity field.

9.3 Tethered systems

In collaboration with Ph. D. candidate Manuel Sanjurjo from 'Universidad Politécnica de Madrid' , we have worked in order to analyze the interest of using a tethered system for the study of the gravity field.

9.3.1 Introduction

Tethers have been studied since 1960's. It consists in a thin cable connecting two satellites. This concept can have different uses: orbiting antennas, shuttle-borne tethered satellites, electrodynamic-powered tethers, space station tether systems, or formation flying tethers. Several missions has been launched (TSS-1, TiPS, MAST,...) in order to test the feasibility of the technology and detect its main technological difficulties. In this subsection, we focus on the interest of tethers for space geodesy.
They can be advantageous in two ways: (i) tethers can be used as a propulsion system in order to null drag effects and enable lower (so more sensitive) orbits. This direction is not explored in this report, even if there are previous work in this direction [32], [48]; and (ii) tethers can be seen as very large base gradiometers [37], [17], [33].
We suppose a satellite composed by two masses, m_1 and m_2, joined by a thin cable, the *tether* with a length L and a negligible mass. Each mass undergoes the force of the gravity field, so they act as a gradiometer, but the distance between proof masses can be larger than in a one-satellite gradiometers. Since the differential effects are almost linear with the distance, the further are accelerometers from each other, the stronger are the effects that we look for. The tether is the paradigm of the gradiometer, for which the distance between detectors can reach several kilometers. But this method presents also several drawbacks: from a dynamical point of view, tether is highly perturbed, and these effects must be perfectly modellized. From a technological point of view, tethers are not still operational, and technological missions should be scheduled before scientific applications.

9.3.2 Dynamical model

First, we will use an Earth-fixed coordinate system. The tethered system will be represented by a simple model with the aim of clarity. Furthermore, we consider a massless dumbbell

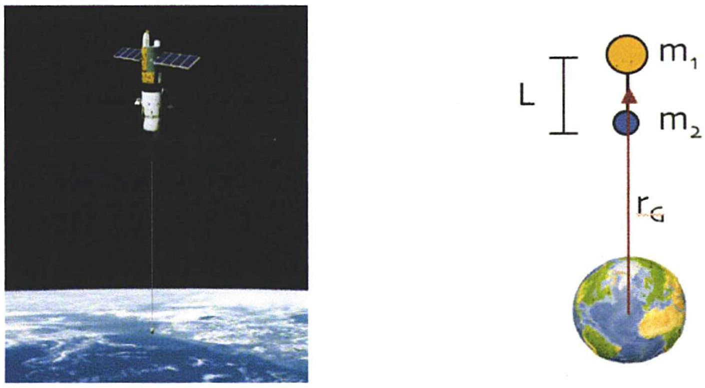

Figure 9.1: *At the left side, an artistic view of a tether. At the right side, its modellization*

model, i.e., a rigid massless cable attaching two point masses. Tethers present a unique equilibrium position: when the tether points to the radial direction. We suppose that the tether has the equilibrium configuration. In this particular case, equilibrium equations for each mass write:

$$\vec{F}_G(\vec{r}_1) \cdot (-\vec{u}_r) - T = m_1 \, \Omega_0^2 \, r_1 \tag{9.10}$$

$$\vec{F}_G(\vec{r}_2) \cdot (-\vec{u}_r) + T = m_2 \, \Omega_0^2 \, r_2 \tag{9.11}$$

where $\vec{F}_G$ is the gravitational force, T is the tension on the tether, Ω_0 is the angular velocity of the system and $\vec{r}_1$, $\vec{r}_2$ the positions of the masses. Gravitational force, in spherical coordinates can be computed as:

$$\vec{F}_G = -m \left[\frac{\partial U(r,\theta,\lambda)}{\partial r} \vec{u}_r + \frac{1}{r \, \cos(\lambda)} \frac{\partial U(r,\theta,\lambda)}{\partial \theta} \vec{u}_\theta + \frac{1}{r} \frac{\partial U(r,\theta,\lambda)}{\partial \lambda} \vec{u}_\lambda \right] \tag{9.12}$$

For the sake of compactness, the full gravitational model will be considered in its representation on a sphere by means of spherical harmonics with complex-valued factors 7.6:

$$U(r,\theta,\lambda) = \frac{GM}{R} \sum_{l=0}^{\infty} \sum_{m=-l}^{l} \left(\frac{R}{r} \right)^{l+1} \bar{K}_{lm} \bar{Y}_{lm}(\theta,\lambda) \tag{9.13}$$

in this expression, $\bar{Y}_{lm}(\theta,\lambda)$ is the normalized spherical harmonic of degree l and order m: $\bar{Y}_{lm} = \bar{P}_{lm} e^{jm\lambda}$.

Introducing expressions (9.12) and (9.13) in the equilibrium equations, we obtain the angular velocity of the whole system:

$$\Omega_0^2 = \frac{\mu}{r_G^3} \sum_{l=0}^{\infty} \sum_{m=-l}^{l} \frac{\cos^2(\xi)}{(1 - \epsilon \, \sin^2(\xi))^{l+2}} + \frac{\sin^2(\xi)}{(1 + \epsilon \, \cos^2(\xi))^{l+2}} (l+1) \left(\frac{R_e}{r_G} \right)^l \bar{K}_{lm} \bar{Y}_{lm}(\theta,\lambda) \tag{9.14}$$

where two parameters have been introduced: the total mass of the system m, and the distance of the center of mass r_G:

$$m = m_1 + m_2 \qquad m\, r_G = m_1\, r_1 + m_2\, r_2 \tag{9.15}$$

In order to describe the mass distribution of the tether we introduce the massic angle, ξ, which is defined as follows:

$$\cos^2(\xi) = \frac{m_1}{m} \qquad \sin^2(\xi) = \frac{m_2}{m} \tag{9.16}$$

Setting $\epsilon = \frac{L}{r_G}$, these relations lead to:

$$r_1 = \left(1 - \epsilon \sin^2 \xi\right) \qquad r_1 = \left(1 + \epsilon \cos^2 \xi\right) \tag{9.17}$$

Using the expressions (9.10)-(9.11) and (9.14), and after some computations we can obtain the tension T as a function of the spherical coordinates of the center of mass, and the system parameters:

$$T(r_G, \theta, \lambda; \varepsilon, \xi) = \frac{m\mu}{r_G^2} \chi(\varepsilon, \xi) \sum_{l=0}^{\infty} \sum_{m=-l}^{l} g_l(\varepsilon, \xi)(l+1) \left(\frac{R_e}{r_G}\right)^l \bar{K}_{lm} \bar{Y}_{lm}(\theta, \lambda) \tag{9.18}$$

where the following auxiliary dimensionless functions are introduced:

$$\chi(\varepsilon, \xi) = \frac{\cos^2(\xi)\sin^2(\xi)}{(1 - \epsilon\, \sin^2(\xi))^2 (1 + \epsilon\, \cos^2(\xi))^2} \tag{9.19}$$

$$g_l(\varepsilon, \xi) = (1 + \epsilon\, \cos^2(\xi))^{l+3} - (1 - \epsilon\, \sin^2(\xi))^{l+3} \tag{9.20}$$

$$f_l(\varepsilon, \xi) = \frac{\cos^2 \xi}{\left(1 - \varepsilon \sin^2 \xi^{l+2}\right)} + \frac{\sin^2 \xi}{\left(1 + \varepsilon \cos^2 \xi^{l+2}\right)} \tag{9.21}$$

These auxiliary functions depend only on the mass configuration of the tethered system, therefore they are fixed once the tether parameters are established.
We will perform the spectral analysis of this observable T in terms of the orbital elements, so we introduce these elements on the former relationship (9.18). In order to achieve that, we perform a rotation of the spherical harmonics. After some computations the expression for the tension takes the form:

$$T(a, e, I, \Omega, \omega, M; \varepsilon, \xi) = \frac{m\mu}{a^2} \frac{\chi(\epsilon, \xi)}{f_0^{2/3}(\varepsilon, \xi)} \sum_{l=0}^{\infty} (l+1) \frac{g_l(\varepsilon, \xi)}{f_0^{l/3}(\varepsilon, \xi)} \left(\frac{R_e}{a}\right)^l \sum_{m=-l}^{l} \sum_{k=-l}^{l} \bar{K}_{lm} \bar{\mathcal{F}}_{lmp}(I) \exp j(k\, u + m\, \Lambda) \tag{9.22}$$

The argument of latitude is $u = \omega + M$ and $\Lambda = \Omega - \theta_G$ is the longitude of the ascending node in an Earth-fixed system (θ_G, Greenwich sideral time).

9.4 Formation flying missions

9.4.1 Introduction

Dynamical model of formation flying has been described in detail in the two first parts of the thesis. In order to introduce the effects of the gravity field, we use the differential orbital elements approach described in chapter 4. Initial conditions can be expressed in terms of differential orbital elements, and the linear approach reads:

$$\Delta\overrightarrow{X}(t) = [\mathcal{M}][\mathcal{L}]\Delta\overrightarrow{EO}(t_0) \tag{9.23}$$

The introduction of the gravity field is detailed in chapter 7 where we obtained perturbative matrix $\mathcal{L}_{GF}$. We obtained final expressions of relative motion:

$$\Delta\overrightarrow{X} = f(\overrightarrow{EO}_{ref}, \Delta\overrightarrow{EO}(t_0), C_{lm}, S_{lm}, t) \tag{9.24}$$

This model is not well adapted for least square method because relations are not linear with coefficients. Linearized relations can be obtained by linearizing precedent equations or obtaining a simplified perturbative matrix $\mathcal{L}_{GF}$. We have used the second method. Finally, we obtain the following matricial form:

$$\Delta\overrightarrow{X} = \mathcal{Q}[C_{lm}, S_{lm}] \tag{9.25}$$

where:

$$\mathcal{Q} = f(\overrightarrow{EO}_{ref}, \Delta\overrightarrow{EO}(t_0), t) \tag{9.26}$$

In these equations we see that the sensitivity of the observable depends on the reference orbit as well as on the formation. The influence of the reference orbit in space geodesy is well-known: usually, very low, near circular, and near polar orbits are used. But the influence of the formation has not been yet explored. Technological reasons encourage the leader-follower configuration, but, other configurations could be more sensitive to gravity field perturbations. That is why we obtain an analytical expression for a general configuration, and we test it numerically.
First, we obtain a linear model of the effect of gravity field on the differential orbital elements, and second, we transform it in terms of relative position.

9.4.2 Simplified perturbations model

Our departure point is the expression of the gravity field potential, in terms of orbital elements, where we keep the first term of the development in eccentricity (we suppose low eccentricity of the orbit). It reads:

$$U = \sum_{l=1}^{\infty}\sum_{m=-l}^{l}\sum_{k=-l}^{l}\frac{GM}{R}\left(\frac{R}{a}\right)^{l+1}\bar{K}_{lm}\bar{F}_{l,m,p}G_{l,m,0}e^{j\phi} = \sum_{lmk}U_{lmk} \tag{9.27}$$

$$\phi = k(\omega + M) + m(\Omega - \theta_G) \tag{9.28}$$

Application of planetary Lagrange equations, and a posteriori simplified integration leads to:

$$\begin{aligned}
\delta a(t) &= \sum_{lmk} \frac{2}{na} k \frac{U_{lmk}}{\dot{\phi}} \\
\delta e(t) &= \sum_{lmk} \frac{-\eta}{na^2 e} \frac{U_{lmk}}{\dot{\phi}} k(1-\eta) \\
\delta i(t) &= \sum_{lmk} \frac{-m + k\cos i}{na^2 \eta \sin i} \frac{U_{lmk}}{\dot{\phi}} \\
\delta\Omega(t) &= \sum_{lmk} \frac{-j}{na^2 \eta \sin i} \frac{\dot{F}}{F} \frac{U_{lmk}}{\dot{\phi}} \\
\delta\omega(t) &= \sum_{lmk} \frac{jU_{lmk}}{na^2\dot{\phi}} \left(\frac{\cos i}{\eta \sin i} \frac{\dot{F}}{F} - \frac{\eta}{e} \frac{\dot{G}}{G} \right) \\
\delta M(t) &= n(t-t_0) + \sum_{lmk} \frac{jU_{lmk}}{\dot{\phi} na^2} \left(\frac{\eta^2}{e} \frac{\dot{G}}{G} - 2(l+1) \right)
\end{aligned}$$

$\dot{\phi}$ can be computed considering secular J_2 effects.
In these equations, we disregard secular effects on differential orbital elements because they tend to destroy the formation and they are periodically removed using maneuvers. Observations deal basically with the periodic perturbations. Moreover, the frequencial method that we use cannot stand for secular terms.

$\mathcal{L}_{GF}$ is obtained by the derivation of precedent equations:

$$\mathcal{L}_{GF} = \begin{bmatrix} \frac{\partial(\delta a(t))}{\partial a} & \frac{\partial(\delta a(t))}{\partial e} & \ldots\ldots & \frac{\partial(\delta a(t))}{\partial M} \\ \frac{\partial(\delta a(t))}{\partial a} & & \ldots\ldots & \frac{\partial(\delta e(t))}{\partial M} \\ \ldots\ldots\ldots\ldots & & & \\ \frac{\partial(\delta M(t))}{\partial a} & & & \frac{\partial(\delta M(t))}{\partial M} \end{bmatrix} \tag{9.29}$$

The exact expressions of the terms are given in annex. Introducing the potential, we can write this matrix as:

$$\mathcal{L}_{GF} = \sum_l \sum_m \sum_k H_{l,m,k}^{EO,EO} \bar{K}_{lm} e^{j\phi} \tag{9.30}$$

Taking into account initial conditions we obtain final perturbations on the orbital elements:

$$\Delta\overrightarrow{EO}(t) = \sum_l \sum_m \sum_k \vec{H}_{l,m,k}^{\Delta EO} \bar{K}_{lm} e^{j\phi} \tag{9.31}$$

where:

$$\vec{H}_{l,m,k}^{\Delta EO} = H_{l,m,k}^{EO,EO} \cdot \Delta\overrightarrow{EO}(t_0) \tag{9.32}$$

These expressions are valid for any initial configuration, with the exception of secular drifts that are not taken into account. Since main secular drifts are given by keplerian motion when there is a difference of semi-major axis, we suppose $\Delta a(t_0) = 0$. We do not consider the secular effects produced by J_2 described in chapter 6.

9.4.3 Conversion to relative positions and velocities

Conversion to relative position and velocity can be done using matrix $\mathcal{M}$, but the introduction of new frequencies makes it more difficult if we want to keep precedent formulation. That is why we explain in detail the procedure that we use.
First, we write the matrix $\mathcal{M}$ simplified for small eccentricities:

$$\begin{aligned}
\Delta R(t) &= -a\cos M\Delta e + ae\sin M\Delta M \\
\Delta T(t) &= -\frac{ae}{2}\sin 2M\Delta e + a(1-e\cos M)\cos i\Delta\Omega + a(1-e\cos M)\Delta\omega + a(1+e\cos M)\Delta M \\
\Delta N(t) &= a(1-e\cos M)\sin u\Delta i - a(1+e\cos M)\sin i\cos u\Delta\Omega
\end{aligned} \tag{9.33}$$

We introduce in these equations, equations (9.31) in order to obtain expressions:

$$\Delta X(t) = \sum_l \sum_m \sum_k H^{\Delta X}_{l,m,k}\bar{K}_{lm}e^{j\phi} \tag{9.34}$$

We now derive the coefficients $H^{\Delta X}_{l,m,k}$; to do this, we must decompose all the frequencies that appear in the relative motion in order to obtain exclusively terms $e^{j\phi}$. In order to do so, we use following trigonometric relations:

$$\begin{aligned}
\cos(u-\omega) &= \cos u\cos\omega + \sin u\sin\omega \\
\sin(u-\omega) &= \sin u\cos\omega - \cos u\sin\omega \\
\cos u &= \frac{e^{ju}+e^{-ju}}{2} \\
\sin u &= \frac{e^{ju}-e^{-ju}}{2j}
\end{aligned} \tag{9.35}$$

With these relations and a little bit of algebra, we obtain following expressions final expressions for three axis.

R axis

$$\begin{aligned}
\Delta R(t) = \sum_{lmk} \Bigg(& \frac{\bar{K}_{lm}}{2}e^{j\phi^+}\left[H^{\Delta e}_{lmk}(-a\cos\omega + ja\sin\omega) + H^{\Delta M}_{lmk}(-ae\sin\omega - jae\cos\omega)\right] + \\
& + \frac{\bar{K}_{lm}}{2}e^{j\phi^-}\left[H^{\Delta e}_{lmk}(-a\cos\omega - ja\sin\omega) + H^{\Delta M}_{lmk}(-ae\sin\omega + jae\cos\omega)\right]\Bigg)
\end{aligned} \tag{9.36}$$

with:

$$e^{j\phi^+} = e^{j\phi}e^{ju} \qquad e^{j\phi^-} = e^{j\phi}e^{-ju}$$

We introduce intermediary variables:

$$\begin{aligned}
A^{R(+)}_{l,m,k} &= \frac{1}{2}\left[H^{\Delta e}_{lmk}(-a\cos\omega + ja\sin\omega) + H^{\Delta M}_{lmk}(-ae\sin\omega - jae\cos\omega)\right] \\
A^{R(-)}_{l,m,k} &= \frac{1}{2}\left[H^{\Delta e}_{lmk}(-a\cos\omega - ja\sin\omega) + H^{\Delta M}_{lmk}(-ae\sin\omega + jae\cos\omega)\right]
\end{aligned} \tag{9.37}$$

Rearranging summatories we obtain the expression of final coefficients:

$$H^{\Delta R}_{l,m,k} = A^{R(+)}_{l,m,k-1} + A^{R(-)}_{l,m,k+1} \tag{9.38}$$

T axis

$$\begin{aligned}
\Delta T = & \frac{ae}{4}\left[e^{j2u}\left(j\cos\omega + \sin 2\omega\right) + e^{-j2u}\left(-j\cos\omega - \sin 2\omega\right)\right]\Delta e \\
& + a\left(\cos i\Delta\Omega + \Delta\omega + \Delta M\right) \\
& - \frac{ae}{2}\left[e^{ju}\left(\cos\omega - j\sin\omega\right) + e^{-ju}\left(\cos\omega + j\sin\omega\right)\right]\left(\cos i\Delta\Omega + \Delta\omega - \Delta M\right)
\end{aligned} \tag{9.39}$$

and the coefficients are:

$$\begin{aligned}
A^{T(+,+)}_{lmk} &= \frac{ae}{4}\left(j\cos 2\omega + \sin 2\omega\right)H^{e}_{lmk} \\
A^{T(+)}_{lmk} &= -\frac{ae}{2}\left(\cos\omega - j\sin\omega\right)\left(\cos iH^{\Omega}_{lmk} + H^{\omega}_{lmk} - H^{M}_{lmk}\right) \\
A^{T}_{lmk} &= a\left(\cos iH^{\Omega}_{lmk} + H^{\omega}_{lmk} + H^{M}_{lmk}\right) \\
A^{T(-)}_{lmk} &= -\frac{ae}{2}\left(\cos\omega + j\sin\omega\right)\left(\cos iH^{\Omega}_{lmk} + H^{\omega}_{lmk} - H^{M}_{lmk}\right) \\
A^{T(-,-)}_{lmk} &= \frac{ae}{4}\left(-j\cos 2\omega - \sin 2\omega\right)H^{e}_{lmk}
\end{aligned} \tag{9.40}$$

and:

$$H^{\Delta T}_{l,m,k} = A^{T(+,+)}_{l,m,k-2} + A^{T(+)}_{l,m,k-1} + A^{T}_{l,m,k} + A^{T(-)}_{l,m,k+1} + A^{T(-,-)}_{l,m,k-2} + \tag{9.41}$$

N axis

$$\begin{aligned}
\Delta N = & \frac{ae}{2}\sin\omega\Delta i - \frac{ae}{2}\sin i\cos\omega\Delta\Omega \\
& + e^{j2u}\frac{ae}{4}\left(\Delta i\sin\omega - \sin i\cos\omega\Delta\Omega\right) + e^{-j2u}\frac{ae}{4}\left(\Delta i\sin\omega - \sin i\cos\omega\Delta\Omega\right) \\
& + e^{ju}\left[\frac{-ja}{2}\Delta i - \frac{1}{2}a\sin i\Delta\Omega + \frac{aej}{4}\left(\Delta i\cos\omega + \sin i\Delta\Omega\sin\omega\right)\right] \\
& + e^{-ju}\left[\frac{ja}{2}\Delta i - \frac{1}{2}a\sin i\Delta\Omega - \frac{aej}{4}\left(\Delta i\cos\omega + \sin i\Delta\Omega\sin\omega\right)\right]
\end{aligned} \tag{9.42}$$

The coefficients are:

$$\begin{aligned}
A^{N(+,+)}_{lmk} &= \frac{ae}{4}\left[j\left(H^{i}_{lmk}\cos\omega + \sin iH^{\Omega}_{lmk}\sin\omega\right) + \left(H^{i}_{lmk}\sin\omega - \sin i\cos\omega H^{\Omega}_{lmk}\right)\right] \\
A^{N(+)}_{lmk} &= -\frac{a}{2}\left(jH^{i}_{lmk} + \sin iH^{\Omega}_{lmk}\right) \\
A^{N}_{lmk} &= -\frac{ae}{2}\sin\omega H^{i}_{lmk} + \frac{ae}{2}\sin i\cos\omega H^{\Omega}_{lmk} \\
A^{N(-)}_{lmk} &= \frac{a}{2}\left(jH^{i}_{lmk} - \sin iH^{\Omega}_{lmk}\right) \\
A^{N(-,-)}_{lmk} &= -\frac{ae}{4}\left[j\left(H^{i}_{lmk}\cos\omega + \sin iH^{\Omega}_{lmk}\sin\omega\right) - \left(H^{i}_{lmk}\sin\omega - \sin i\cos\omega H^{\Omega}_{lmk}\right)\right]
\end{aligned} \tag{9.43}$$

9.5 Analysis of sensitivity

9.5.1 The lumped coefficients approach

In [64] we have an original method to obtain the covariance matrix for different observables. By the following we summarize the method and we apply it in following sections to formation flying and tethered systems.
The method is developed specially for circular orbits which are the most used for geodesy purposes. For eccentric orbits, the method could be adapted.
At the sight of the complex form of the gravity field:

$$U^c = \frac{GM}{R_e} \sum_{l=0}^{\infty} \left(\frac{R}{r}\right)^{l+1} \sum_{m=-l}^{l} \sum_{k=-l}^{l} \bar{K}_{lm} \bar{F}_{lmk} e^{j(ku+m\lambda)} \tag{9.44}$$

The author develops the different observables in order to obtain the following form:

$$f = \sum_{m=-l}^{l} \sum_{k=-l}^{l} A_{mk} e^{j(ku+m\lambda)} \tag{9.45}$$

with:

$$A_{mk} = \sum_{l=1}^{\infty} H_{lmk} K_{lm} \tag{9.46}$$

The determination of A_{mk} can be done using the Fourier transformation of the temporal series of observables. Moreover, this method enables to separate the different coefficient of each degree m in different matricial systems, enabling a very easy inversion of the system.
By the following, we use this methodology.

9.5.2 Normal matrices of tethered systems and formation flying

In this section we compare the results obtained for precedent missions, with the results of tethered systems and formation flying. In order to do so, we must do some hypothesis. The most difficult part is the estimation of the errors of the instruments. That is why our results are strongly dependent on the technologies.

Tethered systems Then, the lumped coefficients could be written as:

$$A^T_{mk} = \sum_{l=\max(|m|,|k|)}^{\infty} H^T_{lmk} \bar{K}_{lm} \tag{9.47}$$

with

$$H^T_{lmk} = \frac{m\mu}{a^2} \frac{\chi(\varepsilon,\phi)\, g_l(\varepsilon,\phi)}{f_0^{(l+2)/3}(\varepsilon,\phi)} (l+1) \left(\frac{R_e}{a}\right)^l \bar{\mathcal{F}}_{lmk}(I) \tag{9.48}$$

With this expressions, the tension expression reduces to:

$$\begin{aligned} T(u,\Lambda;\varepsilon,\phi) &= \sum_{m=-\infty}^{m=\infty}\sum_{k=-\infty}^{k=\infty} A^T_{mk}e^{j\psi_{mk}} \\ \psi_{mk} &= ku + m\Lambda \end{aligned} \tag{9.49}$$

Formation Flying Matrices for formation flying are given in equations (9.36), (9.39), and (9.42).

9.5.3 Numerical results

We will test different configurations to compare:

- *classical gradiometry*: It is used as a benchmark and also for comparison purposes with tethered systems.
- *tethered system*: in a low Earth orbit.
- *Leader-follower configuration*: the same configuration as GRACE mission.
- *Normal axis difference*: It is complementary with previous one.
- *LISA configuration*: where all the satellites keep initial configuration.

9.6 Conclusions

In this chapter we have applied the 'lumped coefficients' approach to the analysis of new technologies for the gravity field. Tethered systems have been studied for a particular configuration: with the tether aligned with the radial direction because the other directions are unstable. We have obtained analytical results doing a certain number of hypothesis. The results show that this observable may be very interesting, but there is a number of technological difficulties that have not been solved.
Analytical model for formation flying is more simplified than model developed in chapter 7. In particular, we have neglected secular terms because they tend to destroy the formation.

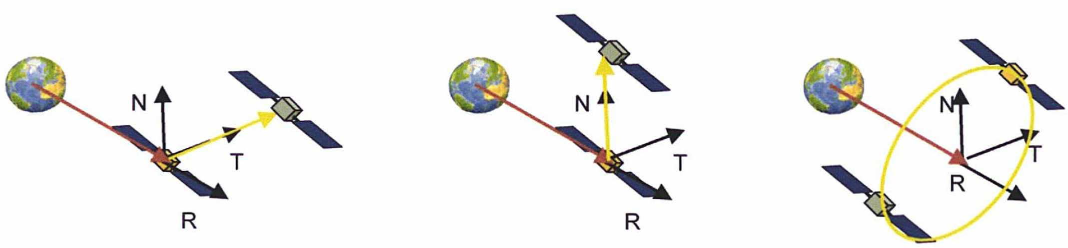

Figure 9.2: *Different tested configurations for formation flying. On the left, leader-follower configuration, at center a difference on N axis, and on the right, the LISA configuration*

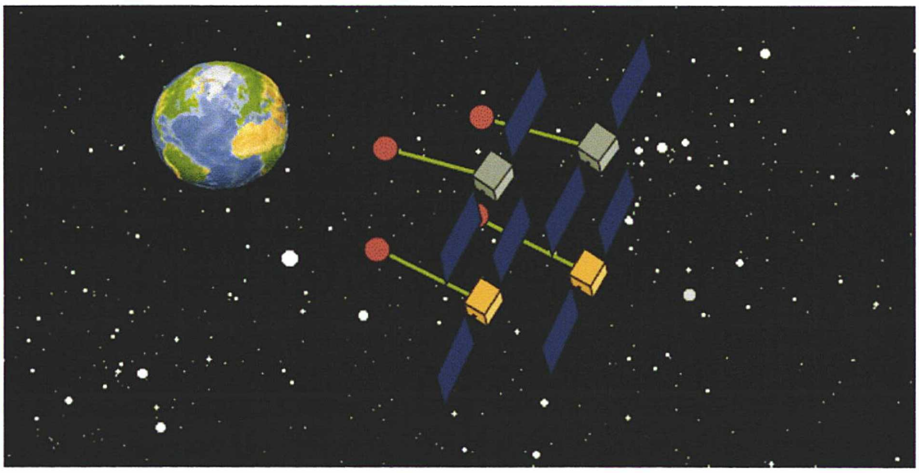

Figure 9.3: *Proposition of space mission for detection of gravity field combining tethered systems and formation flying*

We have analyzed the different configurations except the difference on semi-major axis. Numerical simulations will prove the interest of these new technologies. We propose a combination of both of them: formation flying in T-N plane, and tethered systems in R axis as it is plot in figure (9.3).

Chapter 10

HEO for Universe observation

10.1 Introduction

Formation flying presents some advantages also for space observation missions. Multiple satellites systems enable large base interferometry and telescopes with high focal length. As these systems need a very high precision on control orbit and determination, Lagrange point orbits are very well-suited because they are weakly perturbed. A real alternative to Lagrange points are high eccentric orbits (HEO) around the Earth with very large semi-major axis. This kind of orbits has a short very perturbed passage around the perigee, which is not well-adapted for observations, and a very long weakly perturbed passage around the apogee, where the conditions for observation are particulary good. Observations are possible since the formation is above Van Allen radiation belt. In some cases, more than 85% of the orbit can be used for observation. The dynamics of formations on HEO is quite particular. First, because of the so high eccentricity (larger than 0.7), and second because main perturbations are not the same as in low Earth orbits (LEO). While in LEO orbits drag and J_2 perturbations have important effects, in HEO orbits main perturbations are solar radiation pressure (SRP) and lunisolar effects. Lunisolar differential perturbation on the formation remains small because of the small distance between satellites. Differential SRP remains the main perturbation when the satellites do not have the same area to mass ratio ($\frac{S}{m}$) as can be seen in table 10.1. This is the case in many formations. In this chapter, we study the effects of SRP perturbations in formations on HEO orbits. We focus on three recurrent problems concerning formation flying: satellite formation keeping, risk collision and collision avoidance maneuvers (CAM).

The control system computes and applies continuously the necessary accelerations to force satellites to keep the desired relative trajectory for observations. As control method, I have

Kepler	$6.10^{-9}\ m/s^2$
J_2	$7.10^{-14}\ m/s^2$
Lunisolar	$2.10^{-12}\ m/s^2$
SRP (due to the relative distance)	$4.10^{-18}\ m/s^2$
SRP(due to the $\Delta\frac{S}{m}$)	$2.10^{-8}\ m/s^2$

Table 10.1: *Differential effects on HEO orbits for Simbol-X mission*

used an open loop without errors. I have analyzed the influence of different factors on the maneuvers. In order to do so, it is necessary i) to model natural and desired accelerations, and ii) to do numerical simulations.
Modeling relative motion has been done through classical cartesian coordinates, with Lawden equations (3.8).
For numerical simulations, we use the parameters of the Italian-French formation flying Simbol-X. These simulations characterize the influence of the solar radiation pressure.

The second problem deals with the collision risk. It appears in case of failure of the propulsion system. In case of failure, relative trajectory is no more the necessary trajectory for observation, but natural non-propelled trajectory. The natural trajectory can lead to a collision between satellites. It is necessary to evaluate the risk associated to each observation depending on its direction and the epoch. This allows to classify observations and to avoid the most dangerous ones. Thus, for each of these numerous configurations, we have to extrapolate resulting natural motions since failure occurrence.
In order to do very fast extrapolations of natural motions, we have used the analytical model of the relative motion developed in chapter 4 based on the differential orbital elements.

Collision avoidance maneuvers are the last studied problem. In case of failure of propulsion system, satellites must be placed in a safe and stable orbit called parking orbit. In parking orbit, natural relative motion between satellites do not drift away and respects a safety distance. We have worked on the definition of the parking orbit as well as in the computation of the maneuvers to reach it.

This chapter is structured as follows. Second section is devoted to the presentation of Universe observation mission. The third section is dedicated to the satellite formation keeping. Section four deals with collision risk, and last section describes collision avoidance maneuvers.

10.2 Universe observation missions

In this section we present the relative trajectories for a Universe observation mission, placed in a HEO orbit, using a single telescope with a large focal length. The mirrors of the telescope would be distributed on two satellites. One satellite would be in free flight while the position of the second satellite would be forced to relative distance and observation direction. The orbit of the first satellite will be used as reference orbit, and we will compute necessary maneuvers on the second satellite. For our simulations, we use the orbital parameters of the Italian-French mission Simbol-X [26]. It is:

$$\begin{array}{lll} a_{ref} = 106247\ km & e_{ref} = 0,752 & i_{ref} = 6^\circ \\ \Omega_{ref} = 90^\circ & \omega_{ref} = 0^\circ & \end{array}$$

Observations are done while the satellite is above the Van Allen radiation belt, and different sources should be observed during a single orbit. When satellites are not observing, i.e. when they are below the Van Allen belt, observation relative trajectory has not to be kept, but for operability reasons it seems easier to keep it all along the orbit.
The most determining variable of the formation is the distance between satellites d, which

must be fixed during observations. Observation relative trajectory is defined by this distance, and by the position of the observed source on the sky, which is given through its longitude (α) and latitude (β) with respect to an inertial equatorial Earth-centered reference frame. In this inertial reference frame, observation relative position ($\overrightarrow{x}|_{obs}$) reads:

$$\overrightarrow{x}|_{IJK} = d(\cos\alpha\cos\beta, \sin\alpha\cos\beta, \sin\beta)^T \tag{10.1}$$

Transforming this motion in the local orbital frame, we get:

$$\begin{aligned}\overrightarrow{x}|_{RTN} =& \big(K_1\cos u_{ref} + K_2\sin u_{ref},\\ & K_3\cos u_{ref} + K_4\sin u_{ref}, K_5\big)^T\end{aligned} \tag{10.2}$$

with the coefficients:

$$\begin{aligned}
K_1 &= d\big(\cos\Omega_{ref}\cos\alpha\cos\beta + \sin\Omega_{ref}\sin\alpha\cos\beta\big)\\
K_2 &= d\big(-\sin\Omega_{ref}\cos i_{ref}\cos\alpha\cos\beta\\
&\quad+\cos\Omega_{ref}\cos i_{ref}\sin\alpha\cos\beta + \sin i_{ref}\sin\beta\big)\\
K_3 &= d\big(-\sin\Omega_{ref}\cos i_{ref}\cos\alpha\cos\beta\\
&\quad+\cos\Omega_{ref}\cos i_{ref}\sin\alpha\cos\beta + \sin i_{ref}\sin\beta\big)\\
K_4 &= d\big(-\cos\Omega_{ref}\cos\alpha\cos\beta - \sin\Omega_{ref}\sin\alpha\cos\beta\big)\\
K_5 &= d\big(\sin\Omega_{ref}\sin i_{ref}\cos\alpha\cos\beta\\
&\quad-\cos\Omega_{ref}\sin i_{ref}\sin\alpha\cos\beta + \cos i_{ref}\sin\beta\big)
\end{aligned}$$

10.3 Satellite Formation keeping

10.3.1 Differential acceleration

As we did in chapter 3, we can get the natural acceleration relative to a rotating reference frame linked to an eccentric orbit which corresponds to the orbit of the free satellite. We rewrite equations (3.8) including the SRP differential force.

$$\begin{aligned}\overrightarrow{a}_{nat} = \ddot{\overrightarrow{\rho}} =& -\mu\frac{\overrightarrow{\rho}}{r^3} + \frac{3\mu}{r^3}(\rho_R, 0, 0)^T + \dot{\omega}(\rho_T, -\rho_R, 0)^T\\ & -\omega^2(\rho_R, \rho_T, 0)^T + 2\omega(-\dot{\rho}_R, \dot{\rho}_T, 0)^T + \Delta\overrightarrow{f}_{SRP}|_{RTN}\end{aligned} \tag{10.3}$$

SRP differential perturbation We use the same model that we used in chapter 8 for the solar radiation pressure:

$$\overrightarrow{f}_{SRP} = -\sigma\frac{S}{m}\overrightarrow{u}_{Sun} \tag{10.4}$$

Since the Earth-satellite distance is very small with respect to the Sun-Earth distance, we neglect it, so $\frac{a_s}{r_s} = 1$ and $\sigma = cte$. For our simulations we use $\sigma = 7.10^{-6}$. SRP force does not act when Earth shadows the Sun. As we work in eccentric orbits with very high semi-major axis, shadow regions are not considered. Indeed, for Simbol-X mission, the passage through shadow region never lasts more than 4% of the orbital period (This maximum is reached when the direction of the Sun is in the orbital plane and shadow region in the apogee).

$\Delta\overrightarrow{f}_{SRP|RTN}$ is only induced by a difference of $\frac{S}{m}$ $(\Delta\frac{S}{m})$:

$$\Delta\overrightarrow{f}_{SRP|RTN} = -\sigma\Delta\frac{S}{m}\overrightarrow{u}_{Sun} \tag{10.5}$$

10.3.2 Computing keeping thrust

Positions corresponding to observation trajectories (10.2) do not correspond in any case to the natural relative motion of the satellite $\overrightarrow{x}_{nat}$ which is determined by equations (10.3). They are forced through a certain number of maneuvers. The frequency of the maneuvers depends on the necessary precision of the observation trajectory. In order to simplify, we suppose continuous thrust (Δa), which is not far from the reality. The thrust can be estimated as the difference between the natural acceleration and observation acceleration:

$$\Delta a = |\overrightarrow{a}_{nat} - \overrightarrow{a}_{obs}| \tag{10.6}$$

Natural acceleration is computed using equations (10.3) and observation acceleration is obtained by double derivation of equation (10.2).
The magnitude of impulsions depends on a certain number of variables: position of observed source, epoch of observation, position along the orbit, and the difference of $\frac{S}{m}$. Thereafter we analyze them.

Thrust along the orbit For all simulations, we use the expected values of Simbol-X mission:

$$d = 20\ m \qquad \Delta\frac{S}{m} = 3,522.10^{-3} m^2/kg$$

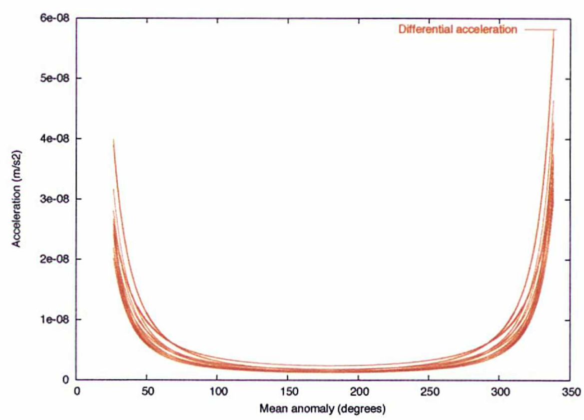

Figure 10.1: *Thrust along orbit for Keplerian motion*

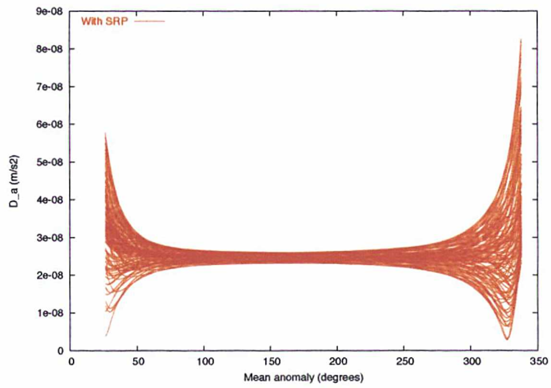

Figure 10.2: *Thrust along orbit for SRP perturbed motion*

Figures (10.1) and (10.2) show the variation of the thrust along the orbit. Different curves correspond to different observation directions. Simulations have been done with initial time 20th february 2012 at midnight. Figure (10.1) corresponds to Δa for keplerian motion, while figure (10.2) corresponds to motion perturbed with SRP. Both figures show that main thrust is concentrated around the perigee, while around the apogee thrust remains small and nearly constant. In both cases, observation direction does not play a major role. The mean value of thrust in unperturbed motion is $3.10^{-9} m/s^2$, while it is $2,5.10^{-8} m/s^2$ in case of SRP perturbed motion. As we will see later, this difference is function of the parameter $\Delta\frac{S}{m}$.

Influence of the epoch of the year Figures (10.3) and (10.4) show the mean thrust along an orbit for the different directions of observations on the sky, and for two different dates: in summer (21st june) and winter (21st december).

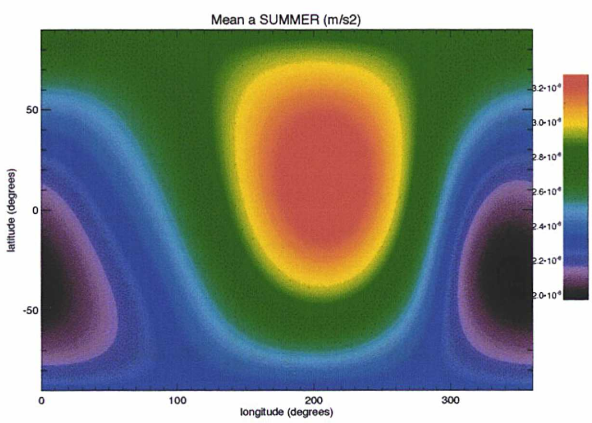

Figure 10.3: *Thrust as function of observation position in summer*

Figures (10.3) and (10.4) show how there are privileged regions where observations are less

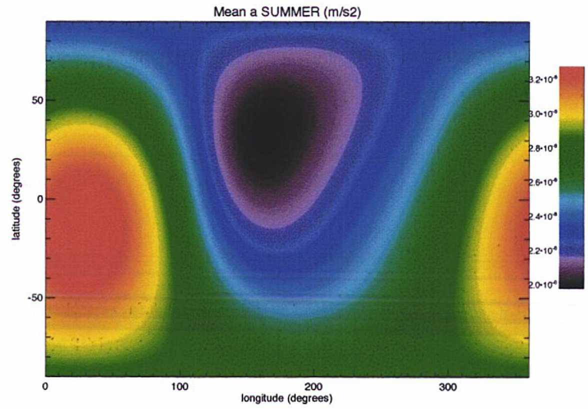

Figure 10.4: *Thrust as function of observation position in winter*

fuel consumers than others. These regions change along the year. Constraints on observations (observation direction must be perpendicular to the direction of the Sun) prevents to take advantage of these privileged regions. In both dates, mean thrust varies between $2.10^{-8}N$ and $3.10^{-8}N$, which correspond with the mean value of figure 10.2.

Influence of the difference of SRP Figure (10.5), shows the effect of changing the value of $\Delta\frac{S}{m}$ on the mean thrust Δa. Mean value of thrust has been computed along the orbit and for the different observation directions. Different curves correspond to different epochs of observation.

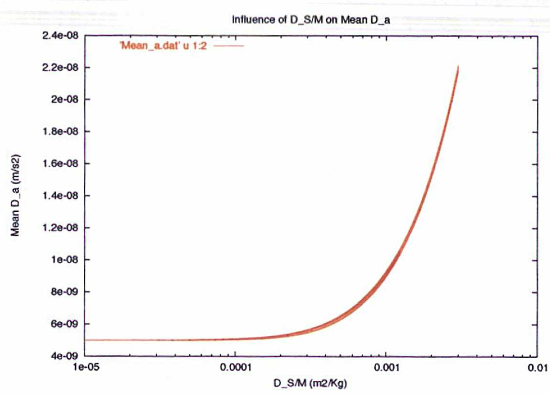

Figure 10.5: *Influence of* $\Delta\frac{S}{m}$ *on the thrust*

The figure presents three regions: i) keplerian zone ($\Delta\frac{S}{m} < 10^{-4}m^2/kg$), ii) transition zone ($10^{-4}m^2/kg < \Delta\frac{S}{m} < 2.10^{-3}m^2/kg$), iii) SRP zone ($\Delta\frac{S}{m} > 2.10^{-3}m^2/kg$). In the first zone SRP effects are negligible with respect to the keplerian effects: changes in the value of $\Delta\frac{S}{m}$ have little impact on the total thrust which remains almost constant. In the third zone, SRP effects dominate keplerian ones. Since the perturbation is linear with $\Delta\frac{S}{m}$, so it is the thrust. The second zone is the transition between the two regimes. It may be interesting to design spacecraft in order to operate in first zone.

10.4 Collision risk

10.4.1 Extrapolation of relative motion

The extrapolation of the relative motion is done using the differential orbital elements (chapter 4) including solar radiation pressure perturbations (chapter 8). The equations of the extrapolation in a matricial form reads:

$$\Delta\vec{x}(t) = [\mathcal{M}] \cdot [\mathcal{L}_{KEP} + \mathcal{L}_{SRP}] \cdot [\mathcal{M}]^{-1}\Delta\vec{x}(t_0) \tag{10.7}$$

where matrices $[\mathcal{M}]$ and $[\mathcal{M}]^{-1}$ are given in (4.14) and (4.23), matrix $\mathcal{L}_{KEP}$ in (4.28), and matrix $\mathcal{L}_{SRP}$ in (8.21).

10.4.2 Numerical simulations and results

Collision risk appears in case of propulsion system failure. Supposing that the failure may be recoverable after a while, it is necessary to verify that during this time satellites do not collide. In order to do so, we have analyzed different observation trajectories and the influence of the parameter $\Delta\frac{S}{m}$.
We have used differential orbital elements including differential SRP effects for orbit extrapolation. It enables very fast computation and computation time is shorter than numerical integration of the relative acceleration.
For each observation trajectory we have defined two parameters:

- *minimum distance:* for different instants distributed along an observation orbit associated to an observation direction, we suppose a failure of the system and we propagate resulting non-propulsed motion during a security time. We determine the smallest distance between satellites during this security time corresponding to the different instants of failure. Minimum distance is defined as the minimum of all the smallest distances. If minimum distance is larger than a safety radius, observation direction is safe. If not, the direction presents a risk. The second parameter evaluates this risk.

- *percentage of orbit with collision risk:* in the case where observation direction is not safe, this parameter is used to evaluate how risky it is. It measures the percentage of the observation trajectory associated to the observation direction for which a failure of the system leads to a no-propulsed trajectory violating the safety radius.

Safety radius (R_S) and security time (T_S) must be specified in mission requirements. In our simulations we use: $R_S = 5\ m$, $T_S = 1$ orbit (4 days).

Figures (10.6), (10.7) have been obtained for Simbol-X mission, on 21th June 2012. Figure (10.6) shows the minimum distance as function of the direction of observation. A large part of observations presents no risk, while risky regions are concentrated around the poles. Figure (10.7) represents the percentage of orbit with collision risk in the same precedent case. We remark that the observation regions for which the minimum distance computed in figure (10.6) approaches zero, the collision risk is not restricted to a small part of the observation orbit, but exists all along the orbit. (i. e. percentage of orbit with collision risk 100 %).

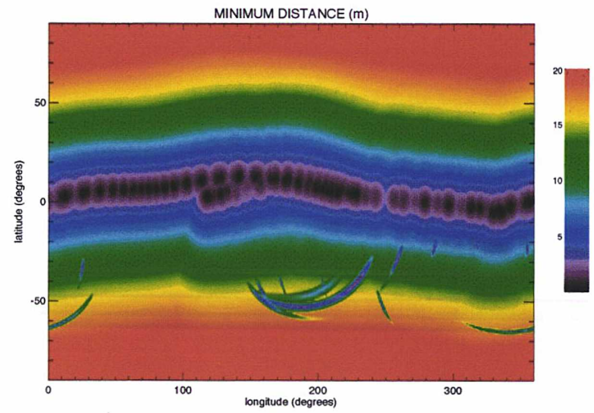

Figure 10.6: *Minimum distance in case of propulsion failure*

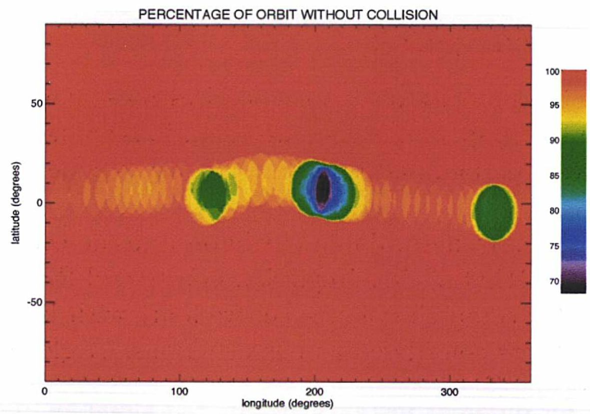

Figure 10.7: *Percentage of orbit without collision risk*

Role of $\Delta\frac{S}{m}$ The last figure (10.8) shows the influence of the parameter on the collision risk. We have computed the mean percentage of orbit with collision risk over all the observation directions as function of the $\Delta\frac{S}{m}$. Figure (10.8) shows that larger values of $\Delta\frac{S}{m}$ are less risky than smaller ones. This was expected since the difference of SRP tends to separate the satellites. At the sight of the figure, parameter $\Delta\frac{S}{m}$ should be, at least, 4.10^{-4}. We have obtained the same curve for different epochs proving that the epoch has minor influence on the result.

10.5 Collision avoidance maneuvers

In case of failure of propulsion system, it is necessary to place satellites in a stable relative orbit called parking orbit. Satellite keeps on the parking orbit while trying to recover the failure. In parking orbit no maneuvers are allowed. The problem can be split in two parts (i) the choice of the parking orbit , and (ii) the computation of optimal transfer between observation orbit and parking orbit. Both aspects of the problem are studied in this section.

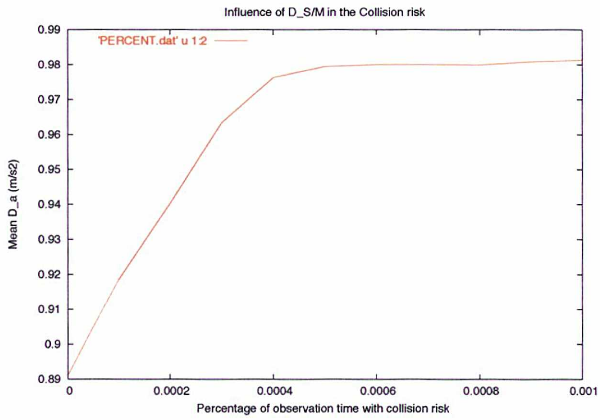

Figure 10.8: *Influence of* $\Delta\frac{S}{m}$ *in the collision risk*

10.5.1 Definition of parking orbit

Parking orbit must respect two constraints: (i) satellites must have a small drift, and (ii) satellite must not violate a safety sphere. These two conditions are necessary to avoid collision risk during the no-maneuvers period, and to ensure an easy recuperation of the observation configuration.
In this section we analyze different natural motions in order to detect the most suitable ones. As we show in table 10.1, in HEO orbits, Keplerian effects and SRP effects have the same order of magnitude. But, for comprehension sake, we start with keplerian effects and in a second time we add SRP effects considered as perturbations. A global strategy is proposed after the analysis of these two effects.

Keplerian motion

Relative non-perturbed natural motion is given by equations (5.1). We rewrite them:

$$\begin{aligned}
\Delta R(t) &= \frac{r_r}{a_r}\Delta a_0 - a_r\cos f_r \Delta e_0 + \frac{a_r e_r}{\eta_r}\sin f_r \Delta M_0 - \frac{3}{2}\frac{n_r e_r}{\eta_r}\sin f_r (t-t_0)\Delta a_0 \\
\Delta T(t) &= a_r\left(1+\frac{1}{\eta_r^2}\frac{r_r}{a_r}\right)\sin f_r \Delta e_0 + r_r\cos i_r \Delta\Omega_0 + r_r\Delta\omega_0 + \frac{a_r^2\eta_r}{r_r}\Delta M_0 \\
&\quad - \frac{3}{2}\frac{a_r n_r \eta_r}{r_r}(t-t_0)\Delta a_0 \\
\Delta N(t) &= r_r \sin u_r \Delta i_0 - r_r \sin i_r \cos u_r \Delta\Omega_0
\end{aligned} \tag{10.8}$$

These equations show the relative motion induced by each difference of orbital element. We plot different relative motions in figure 10.5.1. At the sight of the figure we analyze the most interesting ones.
A difference on the semi-major axis produces a secular drift on the R and T axis. It should be introduced only to null the other secular effects produced by SRP perturbations.
In order to obtain a safe orbit, most interesting initial conditions are: $\Delta M_0, \Delta\Omega_0; \Delta\omega_0$, because they introduce a constant term on T axis that guarantees no collision with the reference orbit.

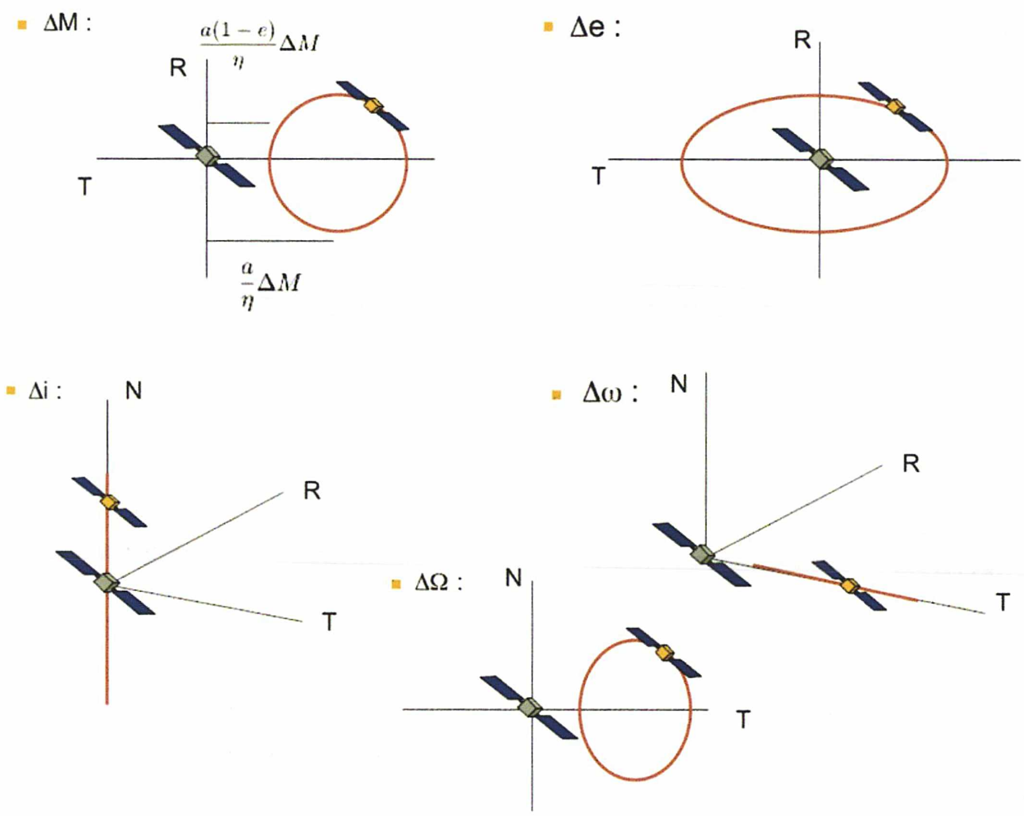

Figure 10.9: *Possible relative motions*

SRP effects

Differential effects of SRP perturbation are given by matrix (8.21). In table (10.2) we give an estimation of the secular terms and of the amplitude of the periodic terms. Secular terms play an important role on the stability of the orbit while periodic terms are involved on the security of the trajectory. Exact value of the terms depends on the reference orbit and on the epoch of the year, but is independent of the relative position and velocity.

Strategy for the definition of the parking orbit Relative motion in parking orbit is determined by the addition of Keplerian motion and SRP effects. We analyze this motion in order to find safe and stable orbits.

Completely stable orbits do not exist because of the SRP secular drift. The drift on the T axis can be controlled changing the difference of semi-major axis, but the other axis cannot be controlled.

Different strategies can be used to define the parking orbit. We propose the following one: (i) ensure the security of the satellites through a minimal distance on the T axis (ii) neglect the motion on the other two axis, (iii) secular effects on the T axis should tend to move away the two satellites.

The orbit can be computed by the following steps:

orbital element	secular term	periodic term
Δa	0	150m
Δe	$9.10^{-12}(t-t_0)$	$4,5.10^{-7}$
Δi	$3,5.10^{-10}(t-t_0)$	2.10^{-5}
$\Delta\Omega$	$3,5.10^{-10}(t-t_0)$	2.10^{-5}
$\Delta\omega$	$2.10^{-11}(t-t_0)$	10^{-6}
ΔM	$2.10^{-11}(t-t_0)$	10^{-6}

Table 10.2: *SRP effects on Simbol-X mission*

- *Computation of SRP secular effects*: Particularization of the SRP effects for the epoch of the year and the reference orbit. Compute the secular effects on the T axis using equations (10.8) and (8.21).

- *Choice of the region where settle the satellite*: Region must be chosen in order to anticipate natural drift of the formation and avoid null distance along the T axis. It is, if natural drift is positive, satellite should be placed in the positive side of T axis, and vice-versa.

- *Computation of SRP periodic effects*: Particularization of the SRP effects for the epoch of the year and the reference orbit. Compute the periodic effects on the T axis using equations 10.8 and 8.21.

- *Choice of* Δa: In order to minimize the effects over the T axis.

- *Choice of the initial values of the other* $\Delta\overrightarrow{EO}$: Initial values of $\Delta\overrightarrow{EO}$ must keep a minimal distance on the T axis (including SRP periodic effects). The values of the variables concerning the other two axis are irrelevant.

- *Verification of the orbit*: A numerical simulation in order to verify that all constraints are respected.

10.5.2 Transfer orbit

Transition between observation orbit and parking orbit uses an intermediary orbit called 'transfer orbit'. The transfer orbit is computed in order to minimize transition maneuvers. The optimization of the maneuvers can be done in a global way; it is, considering that the number of maneuvers and their instants of applications are not defined. The resolution of an optimal control problem is very complex and far beyond the scoop of this thesis.
Here, we present two different strategies: a 1 ΔV strategy, and a 2 ΔV strategy. Even if these strategies are not optimal in a global way, they can also be optimized.

$1\Delta V$ strategy

A $1\Delta V$ strategy may be interesting to minimize the number of maneuvers. The main inconvenient of the strategy is that only a limited number of parking orbits is reachable.
In this strategy, there is no transfer orbit and the observation orbit becomes the parking orbit

just with one maneuver. In order to compute this maneuver we use the equations that link the changes on the differential orbital elements with the ΔV:

$$\begin{pmatrix} \delta a \\ \delta e \\ \delta i \\ \delta\Omega \\ \delta\omega \\ \delta M \end{pmatrix} = \begin{pmatrix} 2\left(\frac{a}{r}\right)^2 & 0 & 0 \\ \frac{\eta^2}{re}\left(\frac{a}{r}-1\right) & \frac{\sin f}{a} & 0 \\ 0 & 0 & \frac{\sin u + e\sin\omega}{\eta^2}\frac{1}{a} \\ 0 & 0 & -\frac{\cos u + e\cos\omega}{\eta^2 a\sin i} \\ \frac{\sin f}{re} & -\frac{e+\cos f}{\eta^2 ae} & \frac{\cos u + e\cos\omega}{\eta^2 a\tan i} \\ -\frac{\sin f}{\eta}\left(\frac{\eta^2}{re}+\frac{e}{a}\right) & \frac{1}{\eta}\left(\frac{e+\cos f}{ea}-\frac{\eta^2}{r}\right) & 0 \end{pmatrix} \begin{pmatrix} \Delta V_R \\ \Delta V_T \\ \Delta V_N \end{pmatrix} \tag{10.9}$$

At the sight of these equations, we can conclude that only three elements of the vector $\Delta\overrightarrow{EO}$ can be chosen. The variations of the remaining three are fixed. We propose the three following constraints:

1. Choose the value of Δa (null or very small in order to null secular SRP effects on the T axis).

2. choose $\Delta e = 0$.

3. Choose the value of $\Delta\omega$ in order to guarantee the safety of the formation.

$2\Delta V$ strategy

The main advantage of a 2 ΔV strategy is that all parking orbits are achievable with a minimum number of maneuvers. Moreover, previous experience shows that in other optimal transfer problems, the $2\Delta V$ optimum is not far from the global optimum.

Statement of the problem We suppose a formation flying composed by two satellites. First spacecraft is following a reference orbit which corresponds to its natural motion. At initial time t_0 the second spacecraft is placed in a collision trajectory with a known relative position $\Delta\overrightarrow{r}_0$ and a relative velocity $\Delta\overrightarrow{v}_0$. The natural trajectory of the second spacecraft which will be changed through two maneuvers $\Delta\overrightarrow{V}_i$, and $\Delta\overrightarrow{V}_f$ performed at instants t_i and t_f. The aim of the problem is to compute $\Delta\overrightarrow{V}_i$ and $\Delta\overrightarrow{V}_f$ in order to reach a final state $\Delta\overrightarrow{EO}_f(t_f)$ at final instant t_f.

Solution of the problem Initial relative motion at instant t_0 is known through its relative position and velocity: $\Delta\overrightarrow{r}_0, \Delta\overrightarrow{v}_0$. Natural extrapolation of the motion can be easily done using equations 4.10 in order to obtain conditions at instant i before the maneuver: $\Delta\overrightarrow{r}_i^-, \Delta\overrightarrow{v}_i^-$. So, collision trajectory is perfectly known.
Parking orbit is also perfectly defined through its differential orbital elements. At the instant f, $\Delta\overrightarrow{EO}_f(t_f)$ can be transformed in $\Delta\overrightarrow{r}_f, \Delta\overrightarrow{v}_f$ using equations 10.8.
As maneuvers change only the velocity but not the position, the position at the beginning and at the end of the transfer trajectory are also known:

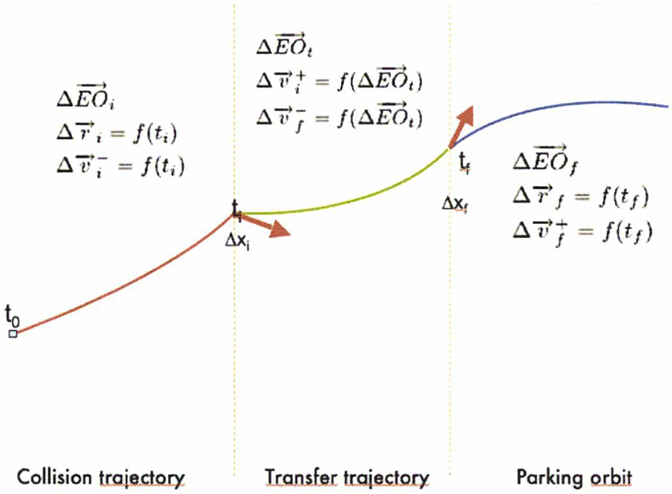

Figure 10.10: *Statement of the problem*

$$\begin{aligned} \Delta\overrightarrow{r}_i^+ &= \Delta\overrightarrow{r}_i^- \\ \Delta\overrightarrow{r}_f^- &= \Delta\overrightarrow{r}_f^+ \end{aligned} \tag{10.10}$$

The problem consists in finding the maneuvers necessary to get a natural motion that passes through points $\Delta\overrightarrow{r}_i$ at instant t_i and $\Delta\overrightarrow{r}_f$ at instant t_f. In order to do so, first, we compute the differential orbital elements of the transfer orbit at instant t_i ($\Delta\overrightarrow{EO}_t$), and, second, we transform them in differences of velocities at instants t_i and t_f.

Since we know the position at instant i $\Delta\overrightarrow{r}_i^+$, we have three equations relating this position and $\Delta\overrightarrow{EO}_t(t_i)$:

$$\Delta\overrightarrow{EO}_t(t_i) = [\mathcal{M}]\Delta\overrightarrow{r}_i \tag{10.11}$$

Another equivalent set of three equations can be obtained for instant t_f:

$$\Delta\overrightarrow{EO}_t(t_f) = [\mathcal{M}]\Delta\overrightarrow{r}_f \tag{10.12}$$

Relations between $\Delta\overrightarrow{EO}_t(t_i)$ and $\Delta\overrightarrow{EO}_t(t_f)$ can be easily obtained thanks to the matrix $\mathcal{L}$.

Finally we obtained a matricial system that writes:

$$\begin{pmatrix} \Delta R_i \\ \Delta T_i \\ \Delta N_i \\ \Delta R_f - \Delta R_{SRP} \\ \Delta T_f - \Delta T_{SRP} \\ \Delta N_f - -\Delta N_{SRP} \end{pmatrix} = \begin{pmatrix} \frac{r_i}{a} & -a\cos f_i & 0 & 0 & 0 & \frac{ae}{\eta}\sin f_i \\ 0 & a\left(1+\frac{1}{\eta^2}\frac{r_i}{a}\right)\sin f_i & 0 & r_i\cos i & r_i & \frac{a^2\eta}{r_i} \\ 0 & 0 & r\sin u_i & -r_i\sin i\cos u_i & 0 & 0 \\ \frac{r_f}{a} - \frac{3}{2}\frac{ne}{\eta}\sin f_f(t_f - t_i) & -a\cos f_f & 0 & 0 & 0 & \frac{ae}{\eta}\sin f_f \\ -\frac{3}{2}\frac{n\eta}{r_t}(t_f - t_i) & a\left(1+\frac{1}{\eta^2}\frac{r_f}{a}\right)\sin f_f & 0 & r_f\cos i & r_f & \frac{a^2\eta}{r_f} \\ 0 & 0 & r\sin u_f & -r_f\sin i\cos u_f & 0 & 0 \end{pmatrix} \begin{pmatrix} \Delta a_t \\ \Delta e_t \\ \Delta i_t \\ \Delta\Omega_t \\ \Delta\omega_t \\ \Delta M_t \end{pmatrix} \tag{10.13}$$

The effects of SRP on the relative position are linked to the SRP effects on differential orbital elements by the equations:

$$\begin{pmatrix} \Delta R_{SRP} \\ \Delta T_{SRP} \\ \Delta N_{SRP} \end{pmatrix} = \begin{pmatrix} \frac{r_f}{a} - \frac{3}{2}\frac{ne}{\eta}\sin f_f (t_f - t_i) & -a\cos f_f & 0 & 0 & 0 & \frac{ae}{\eta}\sin f_f \\ -\frac{3}{2}\frac{n\eta}{r_t}(t_f - t_i) & a\left(1 + \frac{1}{\eta^2}\frac{r_f}{a}\right)\sin f_f & 0 & r_f \cos i & r_f & \frac{a^2\eta}{r_f} \\ 0 & 0 & r\sin u_f & -r_f \sin i \cos u_f & 0 & 0 \end{pmatrix} \begin{pmatrix} \delta a_{SRP} \\ \delta e_{SRP} \\ \delta i_{SRP} \\ \delta\Omega_{SRP} \\ \delta\omega_{SRP} \\ \delta M_{SRP} \end{pmatrix}$$

The effects of the SRP on the differential orbital elements are given by matrix $\mathcal{L}_{SRP}$.
If transfer time is short enough, equations (10.13) can be simplified to keplerian motion:

$$\begin{pmatrix} \Delta R_i \\ \Delta T_i \\ \Delta N_i \\ \Delta R_f \\ \Delta T_f \\ \Delta N_f \end{pmatrix} = \begin{pmatrix} \frac{r_i}{a} & -a\cos f_i & 0 & 0 & 0 & \frac{ae}{\eta}\sin f_i \\ 0 & a\left(1 + \frac{1}{\eta^2}\frac{r_i}{a}\right)\sin f_i & 0 & r_i \cos i & r_i & \frac{a^2\eta}{r_i} \\ 0 & 0 & r\sin u_i & -r_i \sin i \cos u_i & 0 & 0 \\ \frac{r_f}{a} - \frac{3}{2}\frac{ne}{\eta}\sin f_f (t_f - t_i) & -a\cos f_f & 0 & 0 & 0 & \frac{ae}{\eta}\sin f_f \\ -\frac{3}{2}\frac{n\eta}{r_t}(t_f - t_i) & a\left(1 + \frac{1}{\eta^2}\frac{r_f}{a}\right)\sin f_f & 0 & r_f \cos i & r_f & \frac{a^2\eta}{r_f} \\ 0 & 0 & r\sin u_f & -r_f \sin i \cos u_f & 0 & 0 \end{pmatrix} \begin{pmatrix} \Delta a_t \\ \Delta e_t \\ \Delta i_t \\ \Delta\Omega_t \\ \Delta\omega_t \\ \Delta M_t \end{pmatrix} \tag{10.14}$$

Numerical algorithm In order to optimize final ΔV, we can scan the values of t_i and t_f.

Hereafter, we present an algorithm to implement optimization process.

1. Detection of the collision trajectory at t_0
2. Double loop to scan initial and final maneuvers instant of realization.

$$\begin{aligned} t_i &= t_0 + \Delta t_i \\ t_f &= t_i + \Delta t_f \end{aligned} \tag{10.15}$$

3. Compute initial and final transfer positions:

$$\begin{aligned} \Delta\overrightarrow{x}(t_i) &= \left[\mathcal{M}(t_i)\,\mathcal{L}(t_i)\,\mathcal{M}^{-1}(t_0)\right]\Delta\overrightarrow{x}(t_0) \\ \Delta\overrightarrow{x}(t_f) &= \left[\mathcal{M}(t_f)\right]\Delta\overrightarrow{EO}(t_f) \end{aligned}$$

4. Compute transfer differential orbital elements at instant t_i ($\Delta\overrightarrow{EO}_t(t_i)$) with keplerian equations (10.14) or including SRP effects (10.13)
5. Compute initial and final transfer differential velocities:

$$\begin{aligned} \Delta\overrightarrow{v}_i^+ &= \mathcal{M}(t_i)\Delta\overrightarrow{EO}_t(t_i) \\ \Delta\overrightarrow{v}_f^- &= \mathcal{M}(t_f)\Delta\overrightarrow{EO}_t(t_i) \end{aligned}$$

6. Compute total maneuvers ΔV:

$$\delta V = \delta V_1 + \delta V_2 = \|\Delta\overrightarrow{v}_i^+ - \Delta\overrightarrow{v}_i^-\| + \|\Delta\overrightarrow{v}_f^+ - \Delta\overrightarrow{v}_f^-\| \tag{10.16}$$

This algorithm has been implemented and tested using FORTRAN language.

10.5.3 Example

In order to prove the interest of our algorithm we have tested it on the following example for Simbol-X mission.

Collision orbit We have chosen the following observation orbit to test our algorithm:

- date: 21 June
- $\alpha = 2.792\,\text{rad}$
- $\beta = -0.87266\,\text{rad}$
- $M_{ref} = 6.09468\,\text{rad}$

In these conditions, natural motion leads to a collision after $1,54.10^5$ s $(1,79$ days) when the distance between satellites would be 2.5 m. In this situation, a collision avoidance maneuver should be trigged off.

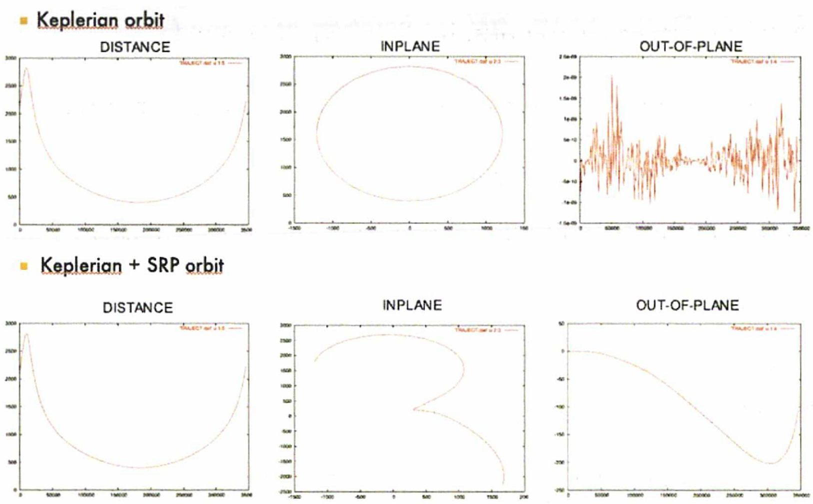

Figure 10.11: *Parking orbit*

Parking orbit We have chosen a very simple parking orbit: $\Delta\overrightarrow{EO}_f(t_f) = 0$ except $\Delta M_f(t_f) = 10^{-5}$ rad. In figure (10.11) we have plotted parking orbit for a period of 4 days considering only Keplerian effects (up), and including SRP effects (bottom). Figure proves that the solution is safe and that the drift over four days is acceptable.

Transfer orbit We have computed transfer orbit using keplerian equations (10.14). The choice of possible values of t_i and t_f corresponds to a certain number of technical criteria. In this example, we do not pretend to take into account these criteria. We have chosen a small region just in order to show the good behavior of the developed method. Results are summarized in figure (10.11). In this figure we show the influence of t_i and t_f on the total amount of propellant necessary for the maneuvers.

At the sight of these results, we propose following maneuvers as preliminary solution:

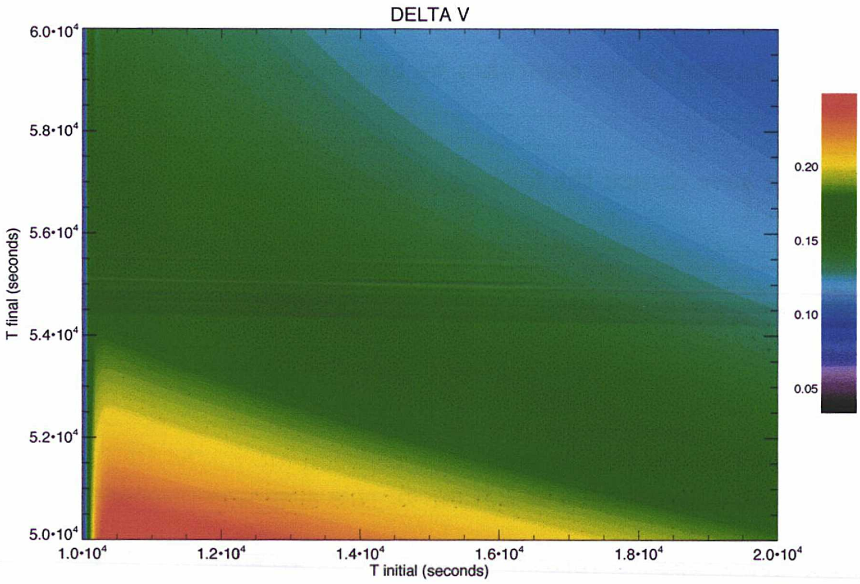

Figure 10.12: ΔV *as function of* t_i *and* t_f

- $\Delta V_i = 2,079.10^{-2}m/s$, $T_i = 10000s$.
- $\Delta V_f = 1,288.10^{-2}m/s$, $T_f = 50000s$.

10.6 Conclusions

This chapter presents the advantage of using cartesian coordinates or differential orbital elements to study different problems. Cartesian coordinates are well-adapted for control problems, but, they do not enable easy analytical integration. On the other hand, for fast extrapolation of orbits, differential orbital elements are better suited.

We have studied the effects of the SRP perturbation on HEO orbits for Universe observation. We have focused on the role of the parameter $\Delta\frac{S}{m}$. We have showed how it plays an important role on the size of the maneuvers and how it can also be used to minimize the collision risk. For Simbol-X, figures (10.5) and (10.8) suggest an optimal value of $\Delta\frac{S}{m}$ near 5.10^{-4}. Bigger values ($> 6.10^{-4}$) lead to more fuel consumer configurations, while smaller values ($< 4.10^{-4}$) increase collision risk.

We also have presented a method to compute collision avoidance maneuvers. The method is based on the analytical model of the relative motion that we have developed taking into account solar radiation pressure perturbations. The method has the advantage to have a very simple formulation and to produce interesting results.

Chapter 11

Conclusions

11.1 Actual knowledge of formation flying

Formation flying is one of the most promising technologies for future space missions. It reduces risks, costs, and enables better performances. But this technology is difficult to master. Each mission has its own particularities. Quite often, the reader has the impression that each mission requires particular solutions.
Fortunately, all of them have a common point: satellites are not far from each other. This characteristic enables to treat them in a similar way. Different theories are used in formation flying papers. Only Hill equations (also known as Clohessy-Wilthsire) and Lawden equations (also known as Yamanaka-Ankersen) are used recurrently. But, when these equations are not well-adapted, several techniques appear. There is not a homogeneous basis about the relative motion. A first part of my work consisted in compiling and classifying precedent work.
The goal of these studies would be to settle a certain number of common basis about the dynamical aspects of the relative motion that could be used in future applications. In several aspects, where I considered that precedent work was not sufficient, I go deeply in to the problem. In particular, I have worked on differential orbital elements, in the topology of the relative motion, and in the search of invariant configurations.
I hope my work completes precedent research on dynamical aspects of formation flying, even if there are still several topics to investigate. It gives a basis for posterior applications larger than classical Lawden's or Hill's equations. For completeness sake, my work should be completed with an equivalent research about control techniques on formation flying.
Analytical models present several advantages with respect to numerical simulations. First, they enable a better comprehension of the problem. Second, they enable fast computations. Low computational time is interesting for onboard applications (anti-collision maneuvers for Simbol-X). Third, they give direct relations between certain parameters and the observables, which is necessary, for example, for analysis of space geodesy missions. I've proved it analysing two future missions.

11.2 Relative motions

The equations of non-perturbed motion can be obtained using classical developments (Hill and Lawden equations) or using differential orbital elements. In circular reference case, obtained results are similar. In eccentric reference case, the advantage of using differential orbital is

double: (i) we avoid the integrals that appear in Lawden's solution, and (ii) we obtain the relations between the parameters of the motion and the initial conditions.
At the sight of the resulting equations, we can get some conclusions. First, a difference of semi-major axis splits the formation, as well as any kind of secular effect. When we consider a Keplerian motion, all the satellites of the formation must have the same semi-major axis.
When there is no difference of semi-major axis and the reference orbit is circular, the relative trajectory is an ellipse. This ellipse can be centered or not on the origin of the reference frame. We propose a new representation to describe this ellipse: the local orbital elements. The local orbital elements enable to find relations between the parameters of the ellipse and the initial conditions. Among all the possible ellipses, there are particularly interesting configurations. The local circular motions are one of them. They exist in two particular plans: the invariant plans, where all the initial configurations are constants on time.
When the reference orbit is not circular, relative motions are more complicated. We have done an effort to minimize the number of parameters describing the relative trajectories and we have reduced it to four. We also have explored the possibility to obtain local circular motions, unluckily, they do no exist.
We can conclude that when we consider non-perturbed linearized motion with circular reference orbit, we can find natural motions well-adapted for space missions. But, when we introduce eccentricity, second order effects, or perturbations, formations must be always controlled. Relative motions describe trajectory that present secular effects and collision risk. That's the reason why, when possible, formation flying uses a very simple leader-follower configuration where the satellites are separated only by a difference of semi-major axis.

11.3 Perturbations on formation flying

Even if some methods have been proposed to introduce perturbations in Hill or Lawden equations, the best representation to introduce them are the differential orbital elements. The method has shown its interest for the introduction of the perturbations, in spite of the complexity of resulting analytical expressions.
When we consider perturbations, there are other secular effects in addition to the Keplerian secular effect produced by a difference of semi-major axis. All secular effects must be treated as a whole in order to null them and avoid the splitting of the formation. Existing studies shows that natural stable relative motions do not exist (with the exception of trivial cases).
Our experience proves that formations inherit the characteristics of absolute motions. It means that main perturbations on absolute motion are also main perturbations on relative motion. The exceptions are the perturbations which depend on the physical characteristics of the satellites instead of the relative distance; i. e., the atmospheric drag and the solar radiation pressure.
When considering perturbations, we must treat separately low and high orbits. Low orbits are dominated by the gravity field perturbations, mainly J_2 effects. Secular effects of J_2 should always be considered, because they can be very important. Trying to null them is not simple. It is possible for circular reference orbit, but not in the eccentric reference orbit. Instead to focus on the secular effect, it seems more reasonable to find a compromise between different criteria (global fuel consumption, collision risk, injection trajectory,...). In this sense, numerical simulations are necessary. Things are different for HEO orbits. First, high eccentricity leads to uncomfortable relative motions. Second, the effects of solar

radiation pressure can be very important when the two satellites do not have the same ratio surface/mass. Our experience on HEO orbits shows the interest to use the difference of $\frac{S}{m}$ as a kind of solar sail to do corrections of relative trajectories. The difference of pressure tends to spread the formation. It may be interesting in order to avoid collisions, but it can be expensive in terms of fuel because the formation is completely unstable. A second problem is the non-existence of stable orbits as we have proved using analytical developments.

11.4 Mission analysis

The last part of the thesis is dedicated to the application of precedent developments to mission analysis.
We have used classical analysis techniques to compare the theoretical performances of different configurations. Once again, the use of analytical developments enable to obtain the spectra of the gravity field perturbation as function of the configuration.
Moreover, we have introduced another technique which is very similar to formation flying: the space tether. A tether can be seen as a formation flying with an additional constraint on the relative distance. For geodesy purposes, tethers are complementary with formation flying because they do not suffer from differential drift due in particular to the difference of semi-major axis.

The second analysed mission is Simbol-X. The use of differential orbital elements combined with cartesian coordiantes has shown its interest. We have obtained a completely analytical model of natural motion including solar radiation pressure perturbation. This model has been very useful to do the extrapolation of the orbit, compute the collision risk, the effects of the coefficient $\Delta\frac{S}{m}$, and propose a method to compute collision avoidance manoeuvres.
We have proved that actual configuration is not optimal from a dynamical point of view: the $\Delta\frac{S}{m}$ is too high and the formation is highly unstable. Main problem is not fuel consumption but the instability of the formation. The reduction of the difference of the coefficient $\frac{S}{m}$ would be the solution to this problem. We have also obtained an analytical method to compute transfer maneuvers. The advantage of the method is its low computational effort and the possibility of onboard the algorithm. The drawback of the method is that it does not optimize the consumption in a global way because it is limited to two maneuvers.

11.5 Perspectives

There are still several dynamical problems with open questions:

- *Second order effects*: Introduction of second order effects in differential orbital elements, and in local orbital elements. This would be very interesting for missions with a large inter-satellite distance. For example, in LISA mission, second order effects introduce a sort of 'breathing' that must be canceled through control maneuvers.

- *Drag perturbation*: This perturbation may be especially complicated because it is not a conservative force. The method of differential orbital elements is not useful since there is no satisfactory model of effects of drag perturbation on orbital elements.

- *Lagrange points*: This problem represents a different challenge because the dynamics near these points is different from the dynamics around the Earth studied in this thesis. In spite of this difficulty, this remains a very interesting study because of all the future missions planed to flight near Lagrange points.

A good knowledge of the dynamics is also very interesting to treat other problems:

- *Navigation problems*: The inclusion of relative measurements in the navigation filters might improve precision but this could also generate instabilities.

- *Control of the formation*: In this category we can include the development of control laws but also optimal control problems. In both cases it is necessary to have a set of differential equations describing the system. Our studies plays a second role because the classical Hill and Lawden equations are the best suited for this problem. But, the comprehension of the dynamics enables the interpretation of the results.

Appendix A

Perturbations of the gravity field

Secular variations For the keplerian and first order contributions we get the classical variations

$$\left\{\begin{aligned} \frac{dl''_{K,J_2}}{dt} =& \omega''_0\left[1+6\gamma''_2\eta''(1-3c''^2)\right] \\ \frac{dg''_{K,J_2}}{dt} =& 6\gamma''_2\omega''_o(1-5c''^2)=\omega''_g \\ \frac{dh''_{K,J_2}}{dt} =& -\omega_e+12\gamma''_2\omega''_o c'' \end{aligned}\right. \tag{A.1}$$

Secular variations proportional to J_2^2 are

$$\left\{\begin{aligned} \frac{dl''_{J_2^2}}{dt} =& \frac{3}{2}\gamma_2''^2\omega''_o\eta''\Big[15e^2\left(8-16s''^2+7s''^4\right)+16\eta''\left(4-12s''^2+9s''^4\right) \\ &\qquad +10\eta''^2\left(8-20s''^2+13s''^4\right)\Big] \\ \frac{dg''_{J_2^2}}{dt} =& \frac{3}{2}\gamma_2''^2\omega''_o\Big[5e''^2\left(88-172s''^2+77s''^4\right)+24\eta''\left(8-22s''^2+15s''^4\right) \\ &\qquad +2\eta''^2\left(192-412s''^2+215s''^4\right)\Big] \\ \frac{dh''_{J_2^2}}{dt} =& -2\gamma_2''^2\omega''_o c''\Big[15e''^2\left(8-7s''^2\right)+36\eta''\left(2-3s''^2\right) \\ &\qquad +12\eta''^2\left(9-10s''^2\right)\Big] \end{aligned}\right. \tag{A.2}$$

The remaining secular variations are due the other even zonal harmonics:

$$\left\{\begin{aligned} \frac{dl''_{zon}}{dt} =& \sum_{p>1}\omega''_o\left[2(2p+1)\mathcal{G}_{2p,p,0}(e'')-\frac{\eta''^2}{e''}\dot{\mathcal{G}}_{2p,p,0}(e'')\right]\left(\frac{R_e}{a''}\right)^{2p}\mathcal{F}_{2p,0,p}(I'')C_{2p,0} \\ \frac{dg''_{zon}}{dt} =& \sum_{p>1}\frac{\omega''_o}{\eta''}\left[\frac{\eta''^2}{e''}\dot{\mathcal{G}}_{2p,p,0}(e'')\mathcal{F}_{2p,0,p}(I'')-\frac{c''}{s''}G_{2p,p,0}(e'')\dot{\mathcal{F}}_{2p,0,p}(I'')\right]\left(\frac{R_e}{a''}\right)^{2p}C_{2p,0} \\ \frac{dh''_{zon}}{dt} =& \sum_{p>1}\frac{\omega''_o}{\eta''s''}\left(\frac{R_e}{a''}\right)^{2p}\mathcal{G}_{2p,p,0}(e'')\dot{\mathcal{F}}_{2p,0,p}(I'')C_{2p,0} \end{aligned}\right. \tag{A.3}$$

where $\dot{\mathcal{F}}(I)$ stands for the derivative of $\mathcal{F}(I)$ with respect to I and $\dot{\mathcal{G}}(e)$ stands for the derivative of $\mathcal{G}(e)$ with respect to e.

Short periods short period variations proportional to J_2 are

$$
\begin{aligned}
\Delta a_{SP,J_2} &= 4a'\gamma_2'\eta'\Big[\eta'^3\left(\frac{a'}{r'}\right)^3(-2+3s'^2-3s'^2\cos(2f'+2g'))+2-3s'^2\Big]\\
\Delta e_{SP,J_2} &= 2\gamma_2'\eta'^2\Big[\frac{\eta'}{e'}\left(\eta'^3\left(\frac{a'}{r'}\right)^3(-2+3s'^2-3s'^2\cos(2f'+2g'))+2-3s'^2\right)\\
&\quad+s'^2\Big(\frac{3}{e'}\cos(2f'+2g')+3\cos(f'+2g')+\cos(3f'+2g')\Big)\Big]\\
\Delta I_{SP,J_2} &= -2\gamma_2'c's'\Big[3\cos(2f'+2g')+3e'\cos(f'+2g')+e'\cos(3f'+2g')\Big]\\
\Delta h_{SP,J_2} &= 2\gamma_2'c'\Big[6(f'-l'+e'\sin f')-3\sin(2f'+2g')-3e'\sin(f'+2g')-e'\sin(3f'+2g')\Big]\\
\Delta g_{SP,J_2} &= \gamma_2'\Big[6(5s'^2-4)(f'-l'+e'\sin f')-\frac{4-6s'^2}{e'}[B'(1+e'\cos f')+\eta'^2\sin f']\\
&\quad+(2-5s'^2)[3\sin(2f'+2g')+3e'\sin(f'+2g')+e'\sin(3f'+2g')]\\
&\quad-s'^2\,[6\frac{B'}{e'}\cos(2f'+2g')+3\frac{\eta'^2}{e'}\sin(f'+2g')+3B'\cos(f'+2g')\\
&\quad+\frac{\eta'^2}{e'}\sin(3f'+2g')+3B'\cos(3f'+2g')]\Big]\\
\Delta l_{SP,J_2} &= \gamma_2'\eta'\Big[\frac{4-6s'^2}{e'}[B'(1+e'\cos f')+\eta'^2\sin f']\\
&\quad+s'^2\,[6\frac{B'}{e'}\cos(2f'+2g')+3\frac{\eta'^2}{e'}\sin(f'+2g')+3B'\cos(f'+2g')\\
&\quad+\frac{\eta'^2}{e'}\sin(3f'+2g')+3B'\cos(3f'+2g')]\Big]
\end{aligned}
\tag{A.4}
$$

Short period variations due to the remaining part of the potential are

$$
\begin{aligned}
\Delta a_{SP,pot} &= 2a'\sum_{\tilde{n}\tilde{m}\tilde{p}\tilde{q}}\frac{\omega_o'}{(\tilde{n}-2\tilde{p}+\tilde{q})\omega_o'-\tilde{m}\omega_e}\left(\frac{R_e}{a'}\right)^{\tilde{n}}J_{\tilde{n}\tilde{m}}(\tilde{n}-2\tilde{p}+\tilde{q})\mathcal{G}_{\tilde{n}\tilde{p}\tilde{q}}(e')\mathcal{F}_{\tilde{n}\tilde{m}\tilde{p}}(I')\cos\psi_{\tilde{n}\tilde{m}\tilde{p}\tilde{q}}\\
\Delta e_{SP,pot} &= \sum_{\tilde{n}\tilde{m}\tilde{p}\tilde{q}}\frac{\omega_o'}{(\tilde{n}-2\tilde{p}+\tilde{q})\omega_o'-\tilde{m}\omega_e}\left(\frac{R_e}{a'}\right)^{\tilde{n}}\times\\
&\quad\left[(\tilde{n}-2\tilde{p}+\tilde{q})\frac{\eta'^2}{e'}-(\tilde{n}-2\tilde{p})\frac{\eta'}{e'}\right]J_{\tilde{n}\tilde{m}}\mathcal{G}_{\tilde{n}\tilde{p}\tilde{q}}(e')\mathcal{F}_{\tilde{n}\tilde{m}\tilde{p}}(I')\cos\psi_{\tilde{n}\tilde{m}\tilde{p}\tilde{q}}\\
\Delta I_{SP,pot} &= \sum_{\tilde{n}\tilde{m}\tilde{p}\tilde{q}}\frac{\omega_o'}{(\tilde{n}-2\tilde{p}+\tilde{q})\omega_o'-\tilde{m}\omega_e}\left(\frac{R_e}{a'}\right)^{\tilde{n}}\frac{(\tilde{n}-2\tilde{p})c'-\tilde{m}}{\eta's'}J_{\tilde{n}\tilde{m}}\mathcal{G}_{\tilde{n}\tilde{p}\tilde{q}}(e')\mathcal{F}_{\tilde{n}\tilde{m}\tilde{p}}(I')\cos\psi_{\tilde{n}\tilde{m}\tilde{p}\tilde{q}}
\end{aligned}
\tag{A.5}
$$

$$\Delta h_{SP,pot} = \sum_{\tilde{n}\tilde{m}\tilde{p}\tilde{q}} \frac{\omega'_o}{(\tilde{n}-2\tilde{p}+\tilde{q})\omega'_o - \tilde{m}\omega_e} \left(\frac{R_e}{a'}\right)^{\tilde{n}} \frac{1}{\eta' s'} J_{\tilde{n}\tilde{m}} \mathcal{G}_{\tilde{n}\tilde{p}\tilde{q}}(e') \dot{\mathcal{F}}_{\tilde{n}\tilde{m}\tilde{p}}(I') \sin\psi_{\tilde{n}\tilde{m}\tilde{p}\tilde{q}}$$

$$\Delta g_{SP,pot} = \sum_{\tilde{n}\tilde{m}\tilde{p}\tilde{q}} \frac{\omega'_o}{(\tilde{n}-2\tilde{p}+\tilde{q})\omega'_o - \tilde{m}\omega_e} \left(\frac{R_e}{a'}\right)^{\tilde{n}} \times$$
$$J_{\tilde{n}\tilde{m}} \left[\frac{\eta'}{e'} \dot{\mathcal{G}}_{\tilde{n}\tilde{p}\tilde{q}}(e') \mathcal{F}_{\tilde{n}\tilde{m}\tilde{p}}(I') - \frac{c'}{\eta' s'} \mathcal{G}_{\tilde{n}\tilde{p}\tilde{q}}(e') \dot{\mathcal{F}}_{\tilde{n}\tilde{m}\tilde{p}}(I')\right] \sin\psi_{\tilde{n}\tilde{m}\tilde{p}\tilde{q}}$$

$$\Delta l_{SP,pot} = \sum_{\tilde{n}\tilde{m}\tilde{p}\tilde{q}} \frac{\omega'_o}{(\tilde{n}-2\tilde{p}+\tilde{q})\omega'_o - \tilde{m}\omega_e} \left(\frac{R_e}{a'}\right)^{\tilde{n}} J_{\tilde{n}\tilde{m}} \mathcal{F}_{\tilde{n}\tilde{m}\tilde{p}}(I') \times$$
$$\left[2(\tilde{n}+1)\mathcal{G}_{\tilde{n}\tilde{p}\tilde{q}} - \frac{\eta'^2}{e'} \dot{\mathcal{G}}_{\tilde{n}\tilde{p}\tilde{q}}(e') - 3(\tilde{n}-2\tilde{p}+\tilde{q}) \frac{\omega'_o}{(\tilde{n}-2\tilde{p}+\tilde{q})\omega'_o - \tilde{m}\omega_e} \mathcal{G}_{\tilde{n}\tilde{p}\tilde{q}}(e')\right] \sin\psi_{\tilde{n}\tilde{m}\tilde{p}\tilde{q}} \tag{A.6}$$

Long periods We get for long period variation proportional to J_2:

$$\begin{aligned}
\Delta a_{LP,J_2} &= 0 \\
\Delta e_{LP,J_2} &= -\frac{1}{2}\gamma_2 \eta''^2 e'' s''^2 \alpha'' \cos(2g'') \\
\Delta I_{LP,J_2} &= \frac{1}{2}\gamma_2 e''^2 s'' c'' \alpha'' \cos(2g'') \\
\Delta h_{LP,J_2} &= \frac{1}{2}\gamma_2 e''^2 c'' \beta'' \sin(2g'') \\
\Delta g_{LP,J_2} &= \frac{1}{4}\gamma_2 \left[(2+e''^2)s''^2\alpha'' - 2e''^2 c''^2 \beta''\right] \sin(2g'') \\
\Delta l_{LP,J_2} &= -\frac{1}{2}\gamma_2 \eta''^3 s''^2 \alpha'' \sin(2g'').
\end{aligned} \tag{A.7}$$

Long period variations due to the remaining part of the potential are

$$\begin{aligned}
\Delta a_{LP,pot} &= 0 \\
\Delta e_{LP,pot} &= -\frac{\omega''_o}{\omega''_g}\frac{\eta''}{e''} \sum_{n=3}^{+\infty} \sum_{\substack{p=1 \\ 2p\neq n}}^{n-1} C_{n0} \left(\frac{R_e}{a''}\right)^n \mathcal{F}_{n,0,p}(I'')\mathcal{G}_{n,p,2p-n}(e'') \cos\left((n-2p)g'' - \epsilon_{n,0}\frac{\pi}{2}\right) \\
\Delta I_{LP,pot} &= \frac{\omega''_o}{\omega''_g}\frac{1}{\eta''}\frac{c''}{s''} \sum_{n=3}^{+\infty} \sum_{\substack{p=1 \\ 2p\neq n}}^{n-1} C_{n0} \left(\frac{R_e}{a''}\right)^n \mathcal{F}_{n,0,p}(I'')\mathcal{G}_{n,p,2p-n}(e'') \cos\left((n-2p)g'' - \epsilon_{n,0}\frac{\pi}{2}\right)
\end{aligned} \tag{A.8}$$

$$\Delta h_{LP,pot} = \frac{\omega''_o}{\omega''_g}\frac{1}{\eta''}\sum_{n=3}^{+\infty}\sum_{\substack{p=1\\2p\neq n}}^{n-1}\frac{1}{(n-2p)}C_{n0}\left(\frac{R_e}{a''}\right)^n \sin\left((n-2p)g'' - \epsilon_{n,0}\frac{\pi}{2}\right)$$
$$\left[\frac{\dot{\mathcal{F}}_{n,0,p}(I'')}{s''} - 10\frac{c''}{1-5c''^2}\mathcal{F}_{n,0,p}(I'')\right]\mathcal{G}_{n,p,2p-n}(e'')$$
$$\Delta g_{LP,pot} = \frac{\omega''_o}{\omega''_g}\sum_{n=3}^{+\infty}\sum_{\substack{p=1\\2p\neq n}}^{n-1}\frac{1}{(n-2p)}C_{n0}\left(\frac{R_e}{a''}\right)^n \sin\left((n-2p)g'' - \epsilon_{n,0}\frac{\pi}{2}\right)$$
$$\left[\frac{\eta''}{e''}\mathcal{F}_{n,0,p}(I'')\dot{\mathcal{G}}_{n,p,2p-n}(e'') - \frac{2}{\eta''}\frac{2-15c''^2}{1-5c''^2}\mathcal{F}_{n,0,p}(I'')\mathcal{G}_{n,p,2p-n}(e''))\right. \tag{A.9}$$
$$\left. - \frac{c''}{\eta'' s''}\dot{\mathcal{F}}_{n,0,p}(I'')\mathcal{G}_{n,p,2p-n}(e'')\right]$$
$$\Delta l_{LP,pot} = \frac{\omega''_o}{\omega''_g}\sum_{n=3}^{+\infty}\sum_{\substack{p=1\\2p\neq n}}^{n-1}\frac{1}{(n-2p)}C_{n0}\left(\frac{R_e}{a''}\right)^n \sin\left((n-2p)g'' - \epsilon_{n,0}\frac{\pi}{2}\right)$$
$$\left[(2n-1)\mathcal{G}_{n,p,2p-n}(e'') - \frac{\eta''^2}{e''}\dot{\mathcal{G}}_{n,p,2p-n}(e'')\right]\mathcal{F}_{n,0,p}(I'')$$

In these formula, we have used following auxiliary expressions:

$$c' = \cos i \qquad s' = \sin i \tag{A.10}$$

$$\begin{aligned}
\gamma_2 &= -\frac{J_2}{8}\frac{\mu^2 R^2}{G^4}\\
\omega'_g &= -\frac{3}{4}J_2\omega'_0\left(\frac{R}{a'}\right)^2\frac{1-5^{\prime 2}}{\eta^4}\\
\alpha' &= \frac{1-15c'^2}{1-5c'^2}\\
\omega''_{J_2} &= \omega''_0\frac{J_2}{\eta''^4}\left(\frac{R}{a'}\right)^2\\
\beta &= \frac{11-30c^2+75c^4}{1-5c^2}
\end{aligned} \tag{A.11}$$

Appendix B

Perturbations matrix used for sensitivity analysis

Here the coefficients of the obtained perturbation matrix $\mathcal{L}_{GF}$.

$$\mathcal{L}_{GF} = \sum_{lmk} [L_{ij}]\, U_{lmk} \tag{B.1}$$

And the elements are:

$$\begin{aligned}
L_{16} &= \frac{2}{na}k^2\frac{1}{\dot{\phi}} & L_{26} &= \frac{-\eta}{na^2e}\frac{1}{\dot{\phi}}k^2(1-\eta) \\
L_{36} &= \frac{-m+\cos ik}{na^2\eta\sin i}\frac{1}{\dot{\phi}}k & L_{46} &= \frac{-ik}{na^2\eta\sin i}\frac{\dot{F}}{F}\frac{1}{\dot{\phi}} \\
L_{56} &= \frac{ik}{na^2\dot{\phi}}\left(\frac{\cos i}{\eta\sin i}\frac{\dot{F}}{F} - \frac{\eta}{e}\frac{\dot{G}}{G}\right) & L_{66} &= \frac{ik}{\dot{\phi}na^2}\left(\frac{\eta^2}{e}\frac{\dot{G}}{G} - 2(l+1)\right)
\end{aligned} \tag{B.2}$$

$$\begin{aligned}
L_{15} &= \frac{2}{na}k^2\frac{1}{\dot{\phi}} & L_{25} &= \frac{-\eta}{na^2e}\frac{1}{\dot{\phi}}k^2(1-\eta) \\
L_{35} &= \frac{-m+\cos ik}{na^2\eta\sin i}\frac{1}{\dot{\phi}}k & L_{45} &= \frac{-ik}{na^2\eta\sin i}\frac{\dot{F}}{F}\frac{1}{\dot{\phi}} \\
L_{55} &= \frac{ik}{na^2\dot{\phi}}\left(\frac{\cos i}{\eta\sin i}\frac{\dot{F}}{F} - \frac{\eta}{e}\frac{\dot{G}}{G}\right) & L_{65} &= \frac{ik}{\dot{\phi}na^2}\left(\frac{\eta^2}{e}\frac{\dot{G}}{G} - 2(l+1)\right)
\end{aligned} \tag{B.3}$$

$$\begin{aligned}
L_{14} &= \frac{2}{na}km\frac{1}{\dot{\phi}} & L_{24} &= \frac{-\eta}{na^2e}\frac{1}{\dot{\phi}}km(1-\eta) \\
L_{34} &= \frac{-m+\cos ik}{na^2\eta\sin i}\frac{1}{\dot{\phi}}m & L_{44} &= \frac{-im}{na^2\eta\sin i}\frac{\dot{F}}{F}\frac{1}{\dot{\phi}} \\
L_{54} &= \frac{im}{na^2\dot{\phi}}\left(\frac{\cos i}{\eta\sin i}\frac{\dot{F}}{F} - \frac{\eta}{e}\frac{\dot{G}}{G}\right) & L_{64} &= \frac{im}{\dot{\phi}na^2}\left(\frac{\eta^2}{e}\frac{\dot{G}}{G} - 2(l+1)\right)
\end{aligned} \tag{B.4}$$

$$L_{11} = (2l-1)\sqrt{\frac{\mu}{a}}k\frac{1}{\dot{phi}} \qquad L_{21} = \frac{1}{\dot{phi}}k(1-\eta)\frac{\eta}{e}\left(\frac{1}{2}n + \frac{l+1}{na^3}\right) \tag{B.5}$$

$$L_{31} = \frac{1}{\dot{phi}}k\frac{-m+\cos i}{\eta\sin i}\left(-\frac{1}{2}n - \frac{l+1}{na^3}\right) \qquad L_{41} = \frac{1}{\dot{phi}}\frac{\dot{F}}{F}\frac{i}{\eta\sin i}\left(\frac{1}{2}n + \frac{l+1}{na^3}\right)$$

$$L_{51} = -\frac{i}{\dot{phi}}\left(\frac{\cos i}{\eta\sin i}\frac{\dot{F}}{F} - \frac{\eta}{e}\frac{\dot{G}}{G}\right)\left(\frac{1}{2}n + \frac{l+1}{na^3}\right) \quad L_{61} = -\frac{i}{\dot{phi}}\left(\frac{\eta^2}{e}\frac{\dot{G}}{G} - 2(l+1)\right)\left(\frac{1}{2}n + \frac{l+1}{na^3}\right)$$

$$\begin{aligned}
L_{12} &= \frac{2}{na}k\frac{\dot{G}}{G}\frac{1}{\dot{phi}} \\
L_{22} &= \frac{1}{\dot{phi}}k\frac{1}{na^2}\left[\frac{\dot{G}}{G}\frac{\eta(1-\eta)}{e} + \frac{\eta(1+e^2)-1}{\eta e^2}\right] \\
L_{32} &= \frac{1}{\dot{phi}}\frac{-m+\cos ik}{na^2\eta\sin i}\left(\frac{\dot{G}}{G} + \frac{e}{\eta^2}\right) \\
L_{42} &= \frac{1}{\dot{phi}}\frac{\dot{F}}{F}\frac{-i}{na^2\eta\sin i}\left(\frac{\dot{G}}{G} + \frac{e}{\eta^2}\right) \\
L_{52} &= \frac{i}{na^2}\frac{1}{\dot{phi}}\frac{\dot{G}}{G}\left[\frac{\cos i}{\sin i}\frac{\dot{F}}{F}\left(1 + \frac{e}{\eta^3}\right) - \frac{\eta}{e}\frac{\ddot{G}G - (\dot{G})^2}{G^2} + \frac{\dot{G}}{G}\frac{1}{\eta^2}\right] \\
L_{62} &= \frac{i}{na^2}\frac{1}{\dot{phi}}\left[\frac{\dot{G}}{G}\left(\frac{\eta^2}{e}\frac{\dot{G}}{G} - 2(l+1) - \frac{1+e^2}{e^2}\right) + \frac{\eta^2}{e}\frac{\ddot{G}G - (\dot{G})^2}{G^2}\right]
\end{aligned} \tag{B.6}$$

$$\begin{aligned}
L_{13} &= \frac{2}{na}k\frac{\dot{F}}{F}\frac{1}{\dot{phi}} \\
L_{23} &= \frac{-\eta}{na^2e}\frac{1}{\dot{phi}}\frac{\dot{F}}{F}k(1-\eta) \\
L_{33} &= \frac{1}{\dot{phi}}k\frac{1}{n\eta a^2}\frac{\dot{F}}{F}\left(\frac{-m+\cos ik}{\sin i} - \frac{k+m\cos i}{\sin^2 i}\right) \\
L_{43} &= -\frac{i}{na^2\eta}\frac{1}{\sin i}\frac{1}{\dot{\phi}}\left[\left(\frac{\dot{F}}{F}\right)^2 - \frac{\cos i}{\sin i}\frac{\dot{F}}{F} + \left(\frac{\ddot{F}F - \dot{F}^2}{F^2}\right)\right] \\
L_{53} &= \frac{1}{\dot{phi}}k\frac{i}{n\eta a^2}\left[\frac{\dot{F}}{F}\left(\frac{\dot{F}}{F}\frac{\cos i}{\eta\sin i} - \frac{1}{\eta\sin^2 i} - \frac{\eta}{e}\frac{\dot{G}}{G}\right) + \frac{\cos i}{\eta\sin i}\frac{\ddot{F}F - (\dot{F})^2}{F^2}\right] \\
L_{63} &= \frac{i}{na^2\dot{\phi}}\left(\frac{\eta^2}{e}\frac{\dot{G}}{G} - 2(l+1)\right)\frac{\dot{F}}{F}
\end{aligned} \tag{B.7}$$

Appendix C

Papers and others

C.1 Papers from the thesis

J. Fontdecaba, G. Métris & P. Exertier, *An alternative representation of relative motion : the local orbital elements*, submitted in Advances in Space Research

J. Fontdecaba, M. Sanjurjo, G. Métris, J. Peláez, P. Exertier, *Future geodesy missions: Tethered systems and formation flying*, Advances in Space Research, Proceedings of the 2008 Cospar Assembly, July 2008, Montreal, in preparation

G. Métris, J. Fontdecaba, F. Deleflie, P. Exertier, *Analytical theory of the motion of a point mass in the gravity field of a central body: the role of the initial conditions*, in preparation

C.2 Proceedings

J. Fontdecaba, G. Métris, P. Exertier, F. Deleflie, *Perturbations of the gravity field on a flight formation for an eccentric reference frame.* Proceedings of the AAS/AIAA 2007 summer meeting, Mackinack Island, August 2007

J. Fontdecaba, G. Métris, P. Exertier, *Topology of the relative motion : circular and eccentric reference orbit cases*, Proceedings of the 20th ISSFD, Annapolis, Septembre 2007

J. Fontdecaba, G. Métris, P. Gamet P. Exertier, *Solar radiation pressure effects on very high-eccentric formation flying.* Proceedings of 3rd Symposium on Formation Flying, ESTEC, Noordwijk, April 2008

J. Fontdecaba, P. Exertier, *Review of analytical studies of relative motions in flight formation*, Proceedings of SF2A 2006, Paris June 2006

J. Fontdecaba, G. Métris, P. Exertier, *The local orbital elements ; an alternative representation of relative motion.* Proccedings of SF2A 2007, Grenoble, July 2007

J. Fontdecaba, G. Métris, P.Exertier, *Formation Flying for Space Geodesy*, Proceedings of SF2A 2008, Paris, June 2008

C.3 Other publications

J. Fontdecaba, G. Métris, O. Laurain, M. Alvarado, *Study of onboard algorithms for absolute orbit propagation.* Final study report for Thales Alenia Space, August 2008

J. Fontdecaba, *Introduction la Mécanique Classique*, cours at Engineering School ESAIP, Grasse

C.4 Conferences

CCT-ORB: Formation Flying, Toulouse, October 2007

List of Figures

List of Tables

Bibliography

[1] M. Aguirre-Martinez, N. Sneeuw, Needs and tools for future gravity measuring missions, Space Science Reviews 108: 409-419, 2003

[2] A. Albertella, F. Migliaccio, F. Sans, GOCE: The Earth Field by Space Gradiometry, Celestial Mechanics and Dynamical Astronomy 83:1-15, 2002

[3] K. T. Alfriend, H. Schaub & D.-W. Gim, Gravitational perturbations, nonlinearity and circular orbit assumption effects on formation flying control strategies, AAS Guidance and Control Conference Breckenridge, CO, 2000

[4] M. Aguirre Martinez & N. Sneeuw, Needs and tools for future gravity measuring missions, Space Sciences reviews 108: 409-416, 2003

[5] K. Aksnes, Short-period and long-period perturbations of a spherical satellite due to direct solar radiation. Celestial Mechanics, No. 13 pp. 89-104, 1976

[6] G. Balmino, F. Perosanz, Comparison of geopotential recovery capabilities of some future satellite missions. Symp. of the I.G.C., Graz, Asutra, September 1994

[7] G. Balmino, Parametrage mixte des orbites des deux satellites de Grace, Note technique CNES, Novembre 2003

[8] J. D. Biggs & al., A search for invariant relative satellite motion, ESA/ESTEC - ACT Contract 18875/05/NL/MV, 2005

[9] A. Boutonnet, Deploiement optimal contraint et robuste de satellites volant en formations invariantes, Ph. D. Thesis, Toulouse, 2003

[10] D. Brouwer, Solution of the problem of artificial satellite theory without drag. The Astronomical Journal, no. 1274, 1959

[11] D. Brouwer & G. M. Clemence, Methods of Celestial Mechanics, Academic Press, 1961

[12] R. W. Bryant, The effect of solar radiation pressure on the motion of an artificial satellite, The astronomical journal, vol. 66, no. 8, october, 1961

[13] T. Carter & M. Humi, Fuel-optimal rendezvous near a point in general keplerian orbit, Journal of Guidance, vol. 10, pp. 567-573, 1987

[14] T. E. Carter, New form for the optimal rendezvous equations near a keplerian orbit, J. of guidance, vol. 13, No. 1, 1990

[15] S. Casotto, Position and velocity perturbations in the orbital frame in terms of classical element perturbations, Celestial Mechanics and Dynamical Astronomy, vol. 55, pp. 209-221, 1991

[16] S. Casotto, The mapping of Kaula's solution into the orbital reference frame, Celestial Mechanics and Dynamical Astronomy, vol. 55, pp. 223-241, 1993

[17] G. Colombo, System noise analysis of the dumbbell tethered satellite for gravity gradient measurements. Final Technical Report, NASA, 1979

[18] O. L. Colombo, The global mapping of gravity with two satellites, Netherlands Geodetic commission, Publications on Geodesy, vol. 3, num. 3, 1984

[19] M. K. Cheng, Gravitational perturbation theory for intersatellite tracking, Journal of Geodesy, vol. 76, pp 169-185, 2002

[20] W. H. Clohessy and R. S. Wiltshire, Terminal Guidance System for Satellite Rendezvous, Journal of the Aerospace Sciences, vol. 27, pp. 653-658, sept. 1960

[21] F. Deleflie, G. Métris & P. Exertier, Long period variations of the eccentricity vector valid also for near circular orbits around a non-spherical body, Celestial Mechanics and Dynamical Astronomy, vol. 94, pp. 83-104, 2006

[22] F. Deleflie, G. Métris & P. Exertier, An analytical solution of the Lagrange equations valid also for very low eccentricities: influence of a central potential, Celestial Mechanics and Dynamical Astronomy, vol. 94, pp. 105-134, 2006

[23] N. V. Emeljanov, A. A. Kanter, A method to compute inclination functions and their derivatives, Manuscripta Geodaetica, 14: 77-83, 1989

[24] J. Flury, R. Rummel, Future Satellite Gravimetry for Geodesy, Earth, Moon and Planets 94: 13-29, 2005

[25] P. M. Fitzpatrick, Principles of Celestial Mechanics, Academic Press, 1970

[26] P. Gamet, R. Epenoy & C. Salcedo, Simbol-X: A formation flying mission on HEO for exploring the Universe, 20th ISSFD, Annapolis, September 2007

[27] E. M. Gaposchkin, Smiths. Astr. Obs. Spec. Rep., 353, Cambridge, Mass., 1973

[28] J. L. Garrison, J.L. Gardner & P. Axelrad, Relative motion in Highly Elliptical Orbits, Paper No. AAS 95-194, Space Flight Mechanics Conference, Alburquerque, NM, Feb. 1995

[29] D-W. Gim & K. T. Alfriend, Satellite relative motion using differential equinoctial elements, Celestial Mechanics and Dynamical Astronomy, vol.92, no. 4, pp. 295-336, 2005

[30] H. Goldstein, Mecanique Classique, Presses Universitaires de France, 1964

[31] G. Gómez, M. Marcote, J. J. Masdemont & J. M. Mondelo, Zero relative radial acceleration cones and controlled motions suitable for formation flying, J. of the Astronautical Sciences, vol. 53, no. 4, pp 413-431, 2005

[32] G. E. Gullahorn, F. Fuligni, M. D. Grossi, Gravity gradiometry from the tetherd satellite system, IEEE Transactions on geoscience and remote sensing, vol. GE-23, no. 4 July 1985

[33] G. E. Gullahorn, Investigation of dynamic noise affecting geodynamics information in a tethered subsatellite, Final Report, NASA-CR-176031, 1985

[34] J.F. Hamel and J. Lafontaine, Linearized dynamics of formation flying spacecraft on a J2 perturbed elliptical orbit, AAS 07-301, 2007

[35] G. W. Hill, Researches on the Lunar theory, American Journal of Mathematics, vol. 1, no. 3, pp. 245-260, 1878

[36] G. Inalhan, M. Tillerson & J.P. How, Relative Dynamics and Control of Spacecraft Formations in Eccentric Orbits, Journal of Guidance, Control and Dynamics, vol. 25, pp. 48-59, 2002

[37] P. M. Kalaghan and G. Colombo, Gravity Gradient Determination With Tethered Systems, Alabama University, UAH/NASA Workshop on the use of a tethered satellite system p. 33-58, 2000

[38] C. D. Karlgaard, Second-order relative motion equations, Ph. D. Thesis, Virginia Polytechnic Institute, 2001

[39] C. D. Karlgaard & F. H. Lutze, Second order relative motion equations, Advances in the Astronautical Sciences, 109, pp. 2429-2448, 2002

[40] W. M. Kaula, Theory of Satellite Geodesy, Blaisdell Pub. Co. Walthan, Mass. USA, 1966

[41] J. Kim, Simulation study of a low-low satellite-to-satellite tracking mission, Ph. D. Thesis, University of Texas, 2000

[42] W. S. Koon, & al., 2001, J2 Dynamics and formation flight, AIAA 2001-4090, 2001

[43] R. Koop, Global gravity field modeling using satellite gravity gradiometry, Netherlands Geodetic Commision, Number 38, 1993

[44] J. Kostelecký, Recurrence relations for the normalized inclination functions, Bull. Astron. Inst. Czecholsl. 36: 242-246, 1985

[45] Y. Kozai, Effects of solar-radiation pressure on the motion of an artificial satellite, Smithsonian Astrophys. Obs. Spec. Rep. No. 56, 1963

[46] A. Labeyrie et al., Coherent arrays of separate optical telescopes in space: project TRIO, Proceedings Very Long Baseline Interferometry Techniques, CNES, Toulouse, 1982

[47] D. F. Lawden, Optimal trajectories for space navigation, Butterworth & Co. (Publishers) Ltd., 1963

[48] E. C. Lorenzini, G. E. Gullahorn, F. Fuligni, Recent developments in gravity gradiometry from the space shuttle borne tethered satellite system, Journal of Applied Physics, vol. 63, 1988

[49] R. Mackenzie & P. Moore, A geopotential error analysis for a non planar satellite to satellite tracking mission, Journal of Gedesy, 71: 262-272, 1997

[50] G. Métris, Analyse des perturbations dues à la gravité, cours d'été GRGS, Forcalquier, September 2002

[51] D. Mishne, Formation control of satellites subject to drag variations and J2 perturbations. J. Guidance, Control, Dyn. 27 : 685-692, 2004

[52] D. L. Richardson & J. W. Mitchell, A third order analytical solution for relative motion with a circular reference orbit. Journal of Astronautical Sciences 51, 1-21, 2003

[53] R. Rummel, Geoid and Gravity in Earth Sciences - An overview, Earth, Moon and Planets 94: 3-11, 2005

[54] M. Sabatini, R. Bevilacqua, M. Pantaleoni & D. Izzo, Periodic relative motion of formation flying satellites, AAS-AIAA Proceedings, Tampa, January 2006

[55] C. Sabol, C. A. McLaughlin & K.K. Luu, Meet the cluster orbits with perturbations of keplerian elements (COWPOKE) equations, 13th AAS/AIAA Space Flight Mechanics Meeting Ponce, Puerto Rico, 2003

[56] H. Schaub & K. T. Alfriend, J2 Invariant Relative Orbits for Spacecraft Formations, Celestial Mechanics, vol. 79, No.2, 77-95, 2001

[57] H. Schaub & K.T. Alfriend, Hybrid cartesian and orbit element feedback law for formation flying spacecraft, Journal of Guidance, Navigation and Control, vol. 25, pp. 387-393, 2002

[58] H. Schaub, Incorporating secular drifts into the orbit element difference description of relative orbits, 13th AAS/AIAA Space Flight Mechanics Meeting Ponce, Puerto Rico, 2003

[59] S. Schweighart & R. Sedwick, A perturbative analysis of geopotential disturbances for satellite cluster formation flying, IEEE Aerospace Conference Proceedings, Big Sky, pp. 10-17, 2001

[60] S. Schweighart, Development and analysis of a high fidelity J_2 model for satellite formation flying. Ph. D. dissertation, M. I. .T, June 2001

[61] P. Sengupta, S. R. Vadali & K. T. Alfriend, Second-order state transition for relative motion near perturbed, elliptic orbits, Celestial Mechanics and Dynamical Astronomy, vol. 97, pp. 101-129, 2006

[62] N. Sneeuw, Representation coefficients and their use in satellite geodesy, Manuscr. Geod. 17: 117-123, 1992

[63] N. Sneeuw, A major STEP for Geodesy, Report 1994 of the STEP Geodesy working group, ed. Rummel and Schintzer, GFZ Postdam, Germany, Nov. 1994

[64] N. Sneeuw A semi-analytical approach to gravity field analysis from satellite observations. Ph. D. Thesis. Technical University of Munchen, 2000

[65] N. Sneeuw, J. Flury & R. Rummel, Science requirements on future mission and simulated mission scenarios, on Future Satellite Gravimetry and Earth Dynamics, ed. Springer New York, 2004

[66] N. Sneeuw & H. Schaub, Satellite clusters for future gravity field missions, IAG Symposium 129, pp. 12-17, Springer Verlag, 2005

[67] B. D. Tapley & al., The gravity recovery and climate experiment: mission overview and early results, Geophysical research letters, vol. 31, May 2004

[68] B. .D Tapley & al. GGM02- An improved Earth gravity field model from GRACE, J. of Geodesy, vol. 79, September 2005

[69] M. Tillerson & J. P. How, Formation flying control in eccentric orbits, Proceedings of the AIAA Guidance, Navigation, and Control Conference, Montreal, 2001

[70] P.N.A.M. Visser, Low-low satellite-to-satellite tracking: a comparison between analytical linear orbit perturbation theory and numerical integration, Journal of Geodesy, vol 79, pp 160-166, 2005

[71] Yamanaka, & Ankersen, New state transition matrix for relative motion on an arbitrary elliptical orbit. Journal of Guidance, Control and Dynamics, vol. 25, no. 1, Jan-Feb. 2002

[72] C. A. Wagner, Improved gravitational recovery from a geopotential research mission satellite pair flying en echelon, Journal of Geophysical research, vol. 92, July 1987

[73] E. Wnuk, Tesseral harmonics perturbations for high order and degree harmonics, Celestial Mechanics, 44: 179-191, 1988

[74] E. Wnuk, I. Wytrzyszczak, The inclination function in terms of nonsingular elements, Celestial Mechanics, 42: 251-261, 1988

[75] E. Wnuk, The inclination functions for the high value of indices, Acta Astronomica, 38: 127-140, 1988

[76] E. Wnuk, J. Golebiewska, The relative motion of Earth orbiting satellites, Celestial Mechanics, 91:373-389, 2005

[77] E. Wnuk, J. Golebienska, Relative satellite motion in a formation, Advances in space research, 40 (2007) 35-42, 2007

[78] C. Xu, R. Tsoi & N. Sneeuw, IAG Proceedings, Springer, vol. 129, pp 36-41, 2005

[79] O. Zarrouati, Trajectoires spatiales, Editions Cepadues, 1987